NASA CONTRACTOR REPORT

NASA CR-186

STUDY FOR DEVELOPMENT OF ELASTOMERIC THERMAL SHIELD MATERIALS

by C. M. Dolan

Prepared under Contract No. NAS 1-3251 *by*
GENERAL ELECTRIC COMPANY
Philadelphia, Pa.
for

NATIONAL AERONAUTICS AND SPACE ADMINISTRATION • WASHINGTON, D. C. • MARCH 1965

STUDY FOR DEVELOPMENT OF

ELASTOMERIC THERMAL SHIELD MATERIALS

By C. M. Dolan

Prepared under Contract No. NAS 1-3251 by
GENERAL ELECTRIC COMPANY
Philadelphia, Pa.

for

NATIONAL AERONAUTICS AND SPACE ADMINISTRATION

For sale by the Office of Technical Services, Department of Commerce,
Washington, D.C. 20230 -- Price $4.00

FOREWORD

This report was prepared by the Aeromechanics & Materials Laboratory Operation, Re-entry Systems Department, General Electric Company, Philadelphia, Pennsylvania, under NASA Contract No. NAS 1-3251. The work was administered under the direction of the Langley Research Center--Structures Laboratory, National Aeronautics and Space Administration, with Mr. K. Wadlin as the Technical Monitor.

This report covers work conducted from 1 July 1963 to 1 June 1964.

This program was under the technical management of Mr. L. H. Shenker; Mr. C. M. Dolan was Technical Project Engineer. Others participating in the study and preparation of of this report were Messrs. J.S. Axelson, F.P. Curtis, R.L. Bierman, H.H. Edighoffer, M. Bennon, G.H. Thompson, K.J. Hall, R.A. Tanzilli, L. Cohen, B.H. Wilt, G. Catalano, F.H. Manning, R.C. Ziegler, R.H. Fuse, D.F. Block, C. Fehl, and Drs. R.A. Florentine and A.M. Melnick.

Each of the tasks in this study was subdivided into various phases. The program was reviewed with the technical monitor at the end of each phase. All material selections and program modifications were made by joint agreement. Technical visits were made with the technical monitor, Mr. K. Wadlin, 15 July 1963, at Langley; 8 October 1963, at Valley Forge; 22 January 1964, at Langley; and 8 April 1964, at Langley. The tests, results; and discussions of each sub-task have been reported in detail in the ten monthly status reports. This final report summarizes the efforts accomplished under each task.

ABSTRACT

Work was performed to a) define, evaluate, and demonstrate new concepts for an easier and more reliable manufacturing process for silicone elastomeric thermal shields, while maintaining high ablation performance and resistance to the general space environment, and b) define problems and conduct preliminary investigations of materials and methods leading to the development of shape stable elastomers for lifting re-entry vehicles.

The approaches to achieve an easier manufacturing process included investigation of resin systems, char improving additives, and physical reinforcement approaches. These materials and approaches were evaluated by consideration of manufacturing ease and by critical performance criteria of ability to withstand temperature cycling environment and satisfactory ablation performance. After various screening and evaluation phases, two material systems were selected, properties were generated, a thermo-structural analysis made, and a scale-up unit fabricated and thermal cycled. One of the material systems, a foamed phenyl silicone reinforced with aluminum silicate fibers in a discontinuous supporting matrix, met the performance criteria. The second material, a syntactic silicone foam filled with phenolic and silica microspheres in a discontinuous supporting matrix was used in a composite with an underlay of an unsupported foamed phenyl silicone. This formulation met the performance criteria except the extreme low temperature exposure in the scale-up thermal cycle.

Modifications of these materials were tested in an ablation environment simulating the re-entry conditions of a leading edge and control surface of a typical lifting re-entry vehicle. The materials exhibited high heats of ablation combined with minimum shape change to indicate feasibility for this application. In addition, studies were conducted for shield refurbishability, and fastening systems were defined for quick turn-around replacement.

TABLE OF CONTENTS

TABLE OF CONTENTS (Cont)

LIST OF TABLES

LIST OF TABLES (Cont)

1. INTRODUCTION

1. INTRODUCTION

The use of silicone elastomers as thermal shield materials for space vehicles has generated a great deal of interest for the following reasons:

1. Excellent potential mechanical compatibility with structures over a wide temperature range due to an extremely low glass transition temperature and good long time temperature capability.

2. Potential ease of manufacturing, leading to low cost of development and fabrication. Adaptability to design changes with inexpensive tooling and equipment.

3. Resistance to service damage that might occur during flight or prior to launch.

4. Resistance to micrometeorite damage.

5. Ease of repair.

6. Resistance to ground environmental factors including humidity, thermal cycling, erosion, fungus, vibration, shock, and aging.

7. Excellent resistance to radiation and other space environment conditions, including high potential for compatibility over the broad temperature range.

8. Capability of controlled density variability over a wide range permitting tailoring to a specific requirement.

9. Good insulating characteristics.

10. High temperature bond systems available, allowing fuller use of high temperature properties of substructure.

11. High heat of degradation for low flux-long term space vehicle re-entry, leading to an efficient low weight shield.

12. Adaptability to refurbishment for a multi-mission vehicle.

The use of phenolic-fiberglass honeycomb as a matrix for ablative material was originally proposed to improve the thermomechanical compatibility of the rigid ablators. The carryover of its usage in the early elastomer development was a natural result of the need to provide a usable material at the earliest date, as well as to improve char retention in the early formulations. The use of this honeycomb, in its present form, for an elastomeric shield material may be an unnecessary complication and, in fact, presents certain disadvantages both in performance and manufacturability:

1. The mechanical properties of the filled honeycomb system are dominated by the behavior of the honyecomb, and some of the physical advantages of the silicone elastomer system are lost.

2. The honeycomb system exhibits complicated bi-axial behavior which is difficult to characterize, analyze, and use in design. It has widely different properties in each honeycomb direction.

3. The coefficient of expansion of this Phenolic Glass honeycomb and of the filled honeycomb does not approach the coefficient of expansion of common substrates and has both positive and negative values depending upon the honeycomb direction. This could possibly be increasing the compatibility problem in some respects, instead of minimizing it.

4. In some of the filled honeycomb systems, it is difficult to achieve a reliable high strength bond between the elastomer cell filler and the honeycomb cell wall.

5. There may be a potential failure site at low temperature at the bond interface between adjacent layers of ribbon in the honeycomb. Such failures would propagate along the ribbon direction.

6. The honeycomb cells are somewhat difficult to fill reliably with the elastomer, particularly in a system where the honeycomb is initially hard bonded to a contoured structural substrate.

7. Honeycomb " saddlebacks" when bent in any direction. To make even a simple curved radius in a honeycomb segment, it must be heated for a short period at a relatively high temperature, formed immediately to the desired radius and cooled. This curvature can be made in this way only across the ribbon or tape direction and must be done correctly the first time. It can not normally be formed to complex curves or shapes. Even formed to a simple radius the honeycomb cell is strained in compression at the inner radius and in tension at the outer radius. This places built-in stresses on the weakest portion of the system, the adhesive bond of the ribbon.

Since one of the purposes of the honeycomb matrix utilized with an elastomer is to provide improved gross char structure and retention during re-entry, there are other methods and approaches possible to perform this function. These may eliminate the drawbacks of the honeycomb, result in an easier, more reliable manufacturing process, and provide the required thermostructural compatibility. This background provided the basis for the study to meet the initial objective.

One important area of application of ablation materials in general, and specifically elastomers, has not been exploited--the use of elastomers on lifting re-entry vehicles. Elastomers could be important in this advanced area not only for improved performance and reliability but for economic considerations. Based on the results of the initial study, the feasibility of using the higher performance formulations, with most emphasis on ablation performance with shape stability and shield replacement, was undertaken for the final phase of the study.

1.1 OBJECTIVES:

a. Define, evaluate, and demonstrate new concepts for an easier and more reliable manufacturing process for silicone elastomeric thermal shields, while maintaining high ablation performance (including resistance to aerodynamic shear) and resistance to the general space environment, in particular, low and high temperature exposure capability. Approaches other than the current phenolic-glass honeycomb shall be defined which still provide good char retention during re-entry and be capable of being bonded to typical substructure materials.

b. Define problems and conduct preliminary investigations of materials and methods leading to the development of shape stable elastomers for lifting re-entry vehicles. Chemical and physical additives in the elastomer system will be investigated to improve re-radiation capability and shape stability, with a goal leading to a refurbishable, moderate cost shield system for multi-mission vehicles.

The development work was divided into two primary phases, namely:

1 - New Concepts for Composite Synthesis Which Lend Themselves to Simple Fabrication Techniques.

2 - Preliminary Investigation of Shape Stable Elastomers for Lifting Re-entry Vehicles.

2. SUMMARY AND CONCLUSIONS

2. SUMMARY AND CONCLUSIONS

An easier fabrication technique was defined and demonstrated using a discontinuous matrix; the aluminum silicate fiber addition in the foamed phenyl silicone system improved its re-entry performance, and the low temperature cycling capability of the NASA 602 was significantly improved when used as a composite with an unsupported foamed phenyl silicone elastomer. Two systems were scaled-up with the ESM 1004B P-G-H/c-S surviving a $\pm 300^{\circ}F$ thermal cycle test and the composite system successful from $-275^{\circ}F$ to $+300^{\circ}F$.

The feasibility of using elastomeric shield materials for lifting re-entry vehicles was demonstrated by thermal tests under simulated re-entry conditions, by refurbishability studies, and by several quick-turn-around fastening techniques.

3. TASK 1 - NEW CONCEPTS FOR COMPOSITE SYNTHESIS WHICH LEND THEMSELVES TO PRACTICAL FABRICATION TECHNIQUES

3. NEW CONCEPTS FOR COMPOSITE SYNTHESIS WHICH LEND THEMSELVES TO PRACTICAL FABRICATION TECHNIQUES

The first phase of the program was based on studies previously carried out by NASA Langley, GE-RSD, and others; while considering the candidate resin systems, resin modifications, char improving additives, and physical reinforcement approaches. These materials and approaches were evaluated by consideration of manufacturing ease, ability to withstand temperature cycling environment, and satisfactory ablation performance.

All material and formulation selections were made jointly by the NASA technical monitor and the General Electric (GE) program personnel. Ablation performance of the candidates was compared to a group of existing silicone elastomeric systems in rigid phenolic-glass honeycomb matrices. The goal was to develop an elastomeric system which could be easily fabricated to complex curves and surfaces, which had equivalent or better ablation properties than the existing elastomeric systems, and which would retain structural integrity when fabricated on a typical structure and cycled between the temperature extremes expected in the space environment. The material systems started on a broad base and through various screening and selection phases resulted in the final systems.

3.1 SCREENING

The screening phase of this task involved the selection of the most promising combination of resin, resin modification, and physical reinforcement. The performance criteria were evaluated initially on three bases, (a) fabricability, (b) low temperature capability, and (c) heat of ablation.

All materials modifications were considered as to their ease of fabrication in the preparation of the evaluation samples while considering projected scale-up problems and possible approaches. The "Base Resin Systems" were evaluated for both low temperature capability and ablation performance. The standard formulations in honeycomb were tested first as points of base reference. The "resin modifications" and "additives" were initially screened on their effect on ablation performance. The "physical reinforcements" were screened on their low temperature capability performance. The best candidates were then selected in combined systems and evaluated for both ablation and cycling capability for the "Analysis and Preliminary Selection."

3.1.1 Low Temperature Capability - Plate Thermal Cycling

The sandwich configuration shown in Figure 1 was selected as a reasonable sample which, when soaked at low and high temperature conditions, would simulate the thermally induced stresses encountered in a cylindrical or frustum-shaped shield-structure system while minimizing the bending stresses. The 12-inch x 12-inch area was selected in relation to the 0.5-inch thickness to provide an approximate 6-inch x 6-inch test area of the shield material in the center of the specimen representing behavior free from edge effects. Shear effects on the bond system will also be evident but this configuration will not measure the direct tensile effect on the bond at elevated temperatures.

3.1.1.1 Test Conditions and Methods

Thermocouples were placed in the sample as shown in Figure 2.

A small hole was drilled through the shield material to the aluminum plate. Thermocouples were inserted so the thermocouple heads touched the bond line. The hole was then filled with the shield material formulation and cured in place.

The specimens were programmed by step-wise temperature changes in the air-circulating chamber cooled by liquid nitrogen injection. Sufficient time was allowed at each temperature level to ensure soaking of the entire sandwich specimen as monitored by two embedded, copper-constantan thermocouples. This soak period was at least fifteen minutes. Forty-degree fahrenheit temperature increments were used in the non-critical temperature region and ten to twenty-five degree increments in the more critical temperature range.

Materials failure, as evidenced by surface discontinuities, was monitored by resistance measurements of a painted silver circuit on each face of the sandwich. The test was considered completed when a discontinuity was obtained or when the soak condition of $-300^{\circ}F$ was reached. If a sample successfully completed the low temperature soak, the sample was then soaked at $+300^{\circ}F$.

The results of the thermal cycle tests on all the initial materials are listed in Table 1.

The Phenolic-Glass honeycomb support used in the series of reference materials (w) has been shown, as predicted, to be a limiting factor in the low temperature capability of the systems. In every case in the (x) series, the low temperature capability was greatly improved when discontinuous types of reinforcement were used. It became evident that the Phenolic -Glass honeycomb was a restrictive factor in that it controlled the thermomechanical behavior of the system and, therefore, the desirable elastomeric properties of the base resins were not utilized. However, the elimination of this rigid matrix was not sufficient, in itself, to assure low temperature performance. When this restriction was removed, the relative low temperature capability of the base resin systems became significant. The phenyl silicones (ESM 1001 P and ESM 1011 P) appeared to have a distinct advantage over the dimethyl type (ESM 1001) and others tested when compared with similar matrix systems. Low temperature capability of the system, then, appeared to be affected by both the elimination of the rigid matrix and by the low temperature capability of the elastomeric filler (the temperature at which the elastomer exhibits a drastic increase in modulus).

3.1.1.2 Results of Tests and Selection of Materials

The results of these tests were reviewed on October 8, 1963, at Valley Forge with K. Wadlin, the NASA technical monitor. The following six material systems, which combined cycling capability and promising performance from the ablation screening tests, were jointly selected for further testing in a "Plate" thermal cycle environment. The results of these tests are listed in Table 2 and comments on the thermal cycle test of these materials are as follows:

1. ESM 1011 P-G-H/c-S (RTV-560 Bond)

Slight resistance changes were noted at -200°F. Examination at -200°F showed hair line cracks appearing on the printed circuit material. Although this resistance change did not indicate a material failure, its result was different in character than that seen in previous runs on ESM material at General Electric. Further examination of the panel at -300°F and room temperature showed no gross evidence of failure.

2. ESM 1001 P-G-H/c-S (RTV-560 Bond)

No failure noted down to -300°F. (Initial Run). This panel was further cycled under the following schedule:

+ 70 to -300°F
-300 to + 70°F
+ 70 to +300°F
+300 to + 70°F
+ 70 to -240°F
-240 to +300°F
+300 to + 70°F
+ 70 to -300°F
-300 to + 70°F

There were no failures noted throughout this cycle.

3. NASA 602 G-H/c-S (RTV-560 Bond)

The RTV-560 bond was selected because of its low temperature properties and its compatability with the NASA base resin system.

Initial hair line cracks on the circuit material were noted at -95°F. This was indicated by a slight change in the monitored resistance measurements.

Severe cracking occurred at -150°F. The cracks were of the type shown in Figure 3.

Sectioning of the panel after tests revealed no bond failures.

4. ESM 1004A P-G-H/c-S (RTV-560 Bond)

The following cycle was carried out:

+ 70 to -300°F
-300 to + 70°F
+ 70 to +300°F
+300 to + 70°F
+ 70 to -300°F
-300 to + 70°F

No failures were noted throughout this cycle.

5. ESM 1001 P-Asb-H/c-S (RTV-560 Bond)

No failures were noted down to -300°F.

No failures were noted at +300°F.

6. NASA 602 Asb-H/c-S

A change in resistance was noted at -100°F. Examination of the panel at this temperature showed hair line cracks in the circuit material. Severe cracking occurred at -180°F. The failures were of the type described in item 3.

Sectioning of the panel after test revealed no bond failure.

The Phenolic Glass Honeycomb was cut through its thickness so that the honeycomb tape was completely discontinuous at each cell (Figure 4).

Because of its flexibility, the asbestos honeycomb was unable to be cut in more than one direction. In earlier tests, the mode of failure was along the tape at the bond between individual cells; therefore, the direction of cut when using asbestos honeycomb was across the tape (Figure 5).

This direction of cut also allows for contouring to cylindrical shapes.

3.1.1.3 Discussion of Results

During the testing of both NASA 602 formulations (1) in Split Phenolic Glass H/c and (2) Split Asbestos H/C, resistance changes were noted at approximately the same temperature, -95 to -100°F. Although complete cracking did not occur at this temperature, indications were that a change was taking place. Original plate thermal cycling of NASA 602 G-H/c formulation showed a failure at -120/140°F when the matrix was rigid intact H/c. No significant improvement was made by using split or discontinuous matrix systems of Phenolic Glass (failure temperature = -150°F). A slight improvement was achieved when using the more flexible asbestos H/c (failure = -180°F).

This resistance change was also noted in ESM 1011 Phenolic Glass H/c although no drastic failures were noted down to -300°F or at +300°F.

An additional sample was used to define further the significant contributing factors leading to low temperature capability. Specifically, is low temperature capability a function of the base resin or its physical form (syntactic versus free foam)? A thermal cycle panel was prepared using the RTV-560 base resin filled with 15.4 percent syntactic fillers consisting of silica Eccospheres and phenolic Microballoons at a 3 to 2 ratio in a split Phenolic Glass honeycomb. The sample successfully survived the ±300°F thermal cycle, indicating that the base resin and not the physical form of the foam is the significant contributing factor (along with the discontinuous matrix) for low temperature capability.

The two final scale-up candidates were selected - ESM 1004B P and NASA 602 G-H/c-S/ESM 1001 P composite system.

The NASA 602 G-H/c-S system demonstrated consistent superiority in the various ablation tests but did not meet the low temperature cycling criteria. Therefore, a composite system was fabricated with NASA 602 G-H/c-S overlayed on an unsupported ESM 1001 P foam at a ratio of 3 to 1, in an attempt to increase the thermal compatibility of the NASA 602 G-H/c-S system. Property determinations were also made on the free foam underlay material for the later trade-off analyses which included this composite. However, before properties were generated on the underlay material, a plate thermal cycle specimen was made and evaluated to measure the effectiveness of this composite.

The composite sample of NASA 602 G-H/c-S over a free foam underlay, at a ratio of 1 to 1, was successfully cycled between $\pm 300^{o}F$. No failures were noted throughout this cycle. The resistance measurements versus temperature are shown in Figure 7. However, relatively large differences were noted in the degree of contraction of the NASA 602 G-H/c-S, aluminum, and ESM 1001 P, even at $-150^{o}F.$, as illustrated in Figure 6. This may have been due to the difference in the two composite materials in their transitional temperature from ductile to brittle behavior. The ESM 1001 P underlay continued to strain at temperatures significantly below the transitional temperature of the NASA 602 G-H/c-S material.

Although the NASA 602 G-H/c-S material with ESM 1001 P underlay successfully survived a $\pm 300^{o}F$ range on a plate thermal cycle, this did not assure a $\pm 300^{o}F$ capability on a full size vehicle for the following reasons. The shear lag relief of the ESM underlay on a 12-inch test panel relieves the tensile strain in the NASA 602 G-H/c-S material. To obtain the same strain relief on a large structure in the hoop direction, the unsupported foam would have to compress sufficiently to reduce the tensile strain in the NASA 602 G-H/c-S material to the same level as in the test panel. Also, in the meridional direction, the strain levels in a large structure would be similar to those in the test specimen only if the frustum section were 12 inches long. Further analysis using the properties of the two materials was necessary to determine the low temperature capability of this system on a full size vehicle. This analysis is described in Section 3, paragraph 3.2.2.1.

3.1.2 Specific Heat Determinations

Early evaluation of elastomeric shield materials showed a dependence of mechanical behavior at low temperatures upon physical transitions in the polymer. Although several thermoanalytic techniques and mechanical tests can measure this phenomena, the continuous specific heat measurement was selected in an attempt to correlate transitions with thermal cycle capability. If successful, this method could be used as a future tool in assessing the low temperature capability of a resin system. Glass transitions (second-order transitions) are normally characterized by an abrupt change in specific heat which is equivalent to the slope of a curve representing accumulative heat capacity versus temperature. Other phase transitions ("crystallizations", "crystal melting") are characterized either as endothermic or exothermic peaks in the specific heat versus temperature curve or as dips and peaks in the

curve of accumulative heat capacity versus temperature curve. The specific heat experiment was applied to the six final candidate formulations.

3.1.2.1 Test Method

The specific heat experiment consisted of an adiabatic calorimetry system in which a guard heater is maintained at the same temperature as the specimen/specimen holder system to minimize heat loss by conduction and convection from the specimen. A vacuum environment is employed to further reduce heat losses. (Initial cooling of the system below -250°F is accomplished quickly with liquid nitrogen.) Heat is metered into the specimen and holder by maintaining constant voltage and current across a resistance heater (wire). A record of specimen temperature versus time is obtained which, after proper calibration of specimen holder characteristics, can be converted to a curve of accumulative heat input to the specimen versus temperature. The specimens measured 2.5 inches x 2.5 inches x (approx.) 0.25 inch and were "sandwiched" by the two halves of the specimen holder. Specimens weighed between 12 and 30 grams. The MC_p (product of mass times specific heat) of the specimen holder was at least ten times that of the specimen. The heating rate approximated 2°F per minute.

3.1.2.2 Test Results

The accumulative heat input versus temperature curves for ESM 1001, ESM 1001 P, ESM 1011 P, DC 325, NASA 602, and NASA 182 elastomers are shown in Figures 8 through 14. These curves exhibit unexpected behavior in that many dips, peaks, and slope changes occur. A single consistency can be found to apply to all of the curves; a significant endothermic phase change takes effect at -50°F to -40°F for all six elastomers. ESM 1001 exhibited the least complex curve. At approximately -190°F, an abrupt change in slope occurs, characteristic of a glass transition (Tg). At -40°F, a major endothermic reaction occurs, characteristic of a crystalline melting point (Tm). Between the temperatures of -190°F and -40°F, the other five materials exhibit erratic exothermic phenomena (particularly ESM 1001 P) as determined from the observation that little heat input was required to raise the temperature significantly. The second run on ESM 1001 P showed that almost no heat input was required to raise the temperature of the specimen from -170° to -50°F. The experiments, in general, did not show clear definition of the glass transition temperature, although Tg appears to be approximately the same for ESM 1001, ESM 1001 P, ESM 1011 P, and DC 325 at about -190°F. NASA 182 and NASA 602 both exhibit a possible double endotherm at -65° and -40°F.

3.1.2.3 Discussion

The major emphasis related to this experimentation was to approximate transition temperatures of the elastomers for subsequent evaluation of their effects upon mechanical and thermal properties and upon the pertinent applications. Initial results indicated that the technique employed had considerable promise for accomplishing this purpose and for measuring the thermal effects and behavioral aspects involved. However, determination of mechanical behavior accompanying the physical phenomena must be determined by other means. For example, both ESM 1001 and ESM 1001 P exhibit their glass transitions at -170° to -190°F and crystalline melting at -40°F. However, mechanically, ESM 1001 P is flexible

down to its glass transition, but ESM 1001 stiffens just below its crystalline melting point and is found to be "hard" at -90°F. Thus ESM 1001 P, which contains a phenyl modification of the basic dimethyl silicone contained in ESM 1001, is not affected mechanically by the crystallization phenomena whereas ESM 1001 is very much affected. The crystallization behavior is also accompanied by significant changes in specific volume which is detrimental, in the case of low temperature compatibility of ESM 1001, due to simultaneous stiffening. Further experiments are therefore required to complete the study of the criticality of transition behavior of each elastomer (i.e., correlation with low temperature mechanical compatibility tests, expansion behavior, etc.).

3.1.3 Ablation Tests

3.1.3.1 Test Facilities

3.1.3.1.1 Torch

In this equipment, propane gas (flame temperature 2300°F) was burned at controlled pressure in a Meker burner, mixed with a controlled volume of air, and passed through an insulated 1-1/2-inch copper pipe against the surface of the material. The heating profile was varied by changing the sample distance from the exit nozzle of the pipe. Backface temperatures were monitored continuously with a thermocouple. The device was operated at ambient pressure. The heating rate of the equipment was varied in the range of 18 - 21 BTU/ft^2 sec. A 1-inch diameter copper calorimeter was used to calibrate the equipment for any particular set of runs.

3.1.3.1.2 Hypersonic Arc Tunnel

A general description of the Hypersonic Arc Tunnel Facility follows:

(a) Hypersonic Arc Tunnel (s):

Power Supply: 500 KW, Rectified AC

Ballast Resistors: Water cooled metal tubes, variable in minimum increments of 0.065 ohm to a maximum resistance of 1.300 ohms.

Arc Heater: Tandem Gerdien configuration. Graphite electrodes: divided air flow so that carbon contamination is prevented from entering test gas.

The facility has a maximum measured enthalpy capability of 17,000 BTU/lb. It is capable of broad variation in operating conditions which are governed by several controllable parameters:

1. Delivered Power:
   By altering ballast resistance

2. Mass flow:
   By manual operation of throttling valves from high pressure air supply

3. Hardware configuration:

By interchanging plenum chambers of different inside diameters

By interchanging swirl plates of different inside diameters

By interchanging nozzles of different throat diameters and cone angles

All variables described are altered in incremental steps. Conditions during a given run are held at a nominally constant value.

A few typical operating conditions which have been achieved are summarized in Table 3.

In addition to stagnation models (cylindrical, conical, spherical), the facilities have been used for testing wedges, inclined plates (with a distributed heat transfer rate across the surface), and a few composite structures of irregular shape. These models are supported at the exit of the conventional conical nozzle. Specimens have been tested for times approaching 20 minutes. A novel configuration also employed is a rectangular nozzle,the side walls of which incorporate test specimens. The rectangular nozzle provides very low heating rates under non-stagnation conditions. Run time capability exceeds 20 minutes.

For the screening ablation phase of this program, rectangular specimens were used with the test specimens incorporated as the side walls of the rectangular nozzle. The heating rate was 2 - 7 BTU/ft^2 sec with an enthalpy ratio, (h_s/RT_o), of 400 and aerodynamic shear of 0.2 - 0.5 lb/ft^2. The gas enthalpy was 12,000 - 13,000 BTU/lb.

The test time was 1200 seconds. The reported data includes heat of ablation in BTU/lb and backface temperature rise. All models were tested at a thickness corresponding to a standard lb/ft^2.

3.1.3.1.3 NASA Arc Jet

The 2500-KW Arc Jet can be operated with nozzles of 12, 6, 4, 2, 1.5, and 1.0-inch-diameter and heat transfer rates on a 3-inch flat-face from 10 to 450 BTU/ft^2 sec, depending on the flow condition and nozzle diameter with enthalpies from 500 to 4000 BTU/lb. The Mach number will range from 0.02 to 1.6.

3.1.3.1.4 MALTA Facility

Pit No. 1 at the Malta Test Station employed a rocket motor with a 5-inch exit diameter shockless nozzle, designed to produce parallel exhaust flow at a Mach No. of about 2.45. The facility was equipped with all the instrumentation and apparatus required to record the engine operating conditions. Each test was run under the following environmental conditions.

Oxygen to Fuel Ratio	2.10
Total Chamber Pressure	300 psia
Total Chamber Temperature	5800^{o}F
Enthalpy Ratio h_s/RT_o	88 (est.)
Mach No.	2.45

a. Test Model

The test specimen was an 18-degree wedge made of molded phenolic-nylon. The candidate elastomeric materials were bonded inserts on the face of the wedge. A static pressure tap and copper calorimeter slug were provided at the wedge face to measure the environmental conditions. At a 0-degree angle of attack, the heat flux was 110 BTU/ft^2 sec with an aerodynamic shear of 10 lb/ft^2.

b. Test Procedure

The model was installed so that the centerline of the model and engine were aligned. The nose of the model was located approximately two inches downstream of the nozzle exit. The motor was started and brought to a stabilized condition before the motor was gimballed onto the model, and the model exposed for 10 seconds.

3.1.3.2 Formulations

The formulations listed in Table 4 were initially screened in the Torch and Hypersonic Arc Facilities.

The formulations were selected on the following basis. Since the reinforcing matrix selection was most dependent on thermal cycle performance, possible filler combinations were evaluated for effect on ablation performance. In order not to confuse performance effects, a single base system was selected and all possible filler systems evaluated at the same concentration level. Performance differences were then used along with cycling and fabrication to select the next series of system screening specimens.

3.1.3.2.1 Results

The ablation results of screening formulations in the Propane Torch Test 20 - 22 BTU are given in Table 5.

3.1.3.3 Hypersonic Arc Tunnel Test Results

The performance parameters used to evaluate the material were the following: (1) back-face temperature, (2) heat of degradation based on total degradation depth, and (3) heat of ablation based on weight loss. The heat flux averaged 3.4 BTU/ft^2 sec over the face of the specimen. The heats of ablation were calculated from the weight losses and are indicative of the ablation efficiency per pound. There are significant differences between weight loss and insulation characteristics and these differences and similiarities between resin systems and filler types were carefully analyzed to assure the selection of the optimum base resin-filler combinations.

The sample size was based on the space available in the rectangular nozzle which was 4.5 inches wide and 4 inches long. The samples were fabricated so that two samples would be placed side by side, thereby providing a direct comparison of performance. The heat flux was determined to be 3.4 BTU/ft^2 sec, by a series of calorimeters. The run time

was fixed by the arc tunnel capability which was close to the typical re-entry time that was being simulated.

The performance of the materials were rated on heat of degradation and on heat of ablation. Heat of degradation is based on the amount of virgin material remaining. Heat of ablation is based on the amount of material lost in the ablation process. Cold wall heat fluxes were used to calculate both of these values.

The results of these tests are reported in Table 6.

3.1.3.4 NASA Arc Jet Results

The control materials were fabricated in the laboratory and shipped to NASA-Langley for testing. All samples were in the continuous phenolic-glass honeycomb matrix. The results were supplied by NASA-Langley and are tabulated in Table 7.

3.1.3.5 Comparison of Ablation Results

The rating of the materials on an effective heat capacity basis varied with the thermal environment. This was indicated by superior performance obtained for NASA 602 G-H/c with respect to NASA 182 G-H/c in all the GE and NASA facilities except the GE Hypersonic Arc Tunnel where NASA 182 G-H/c performed better. The chars on the NASA formulations were carbonaceous and powdery in the GE facilities while those on the ESM formulations were carbonaceous and hard. In the NASA Langley facility, the chars on all the materials were glassy in appearance.

3.1.4 Material Selection

In assessing the relative merits of the various matrices, resins, and fillers in meeting the overall objectives of ablation performance, fabricability, and thermal cycle capability, the seven material systems and tests listed in Table 8 were jointly selected for further evaluation in the screening phase of the program to select the three final candidates.

The LTV 602 resin system was selected as representative of the syntactic foam approach and was compatible with the phenyl silicone elastomeric bonding system. The phenyl silicones RTV-560 and RTV-511 were selected for improved low temperature capability. The RTV-511 appeared to have greater insulating capability. The split matrices were used in all cases for both fabrication and thermal cycling capability. The asbestos matrix was used since it might have greater system insulating capability. The filler systems incorporated both the standard asbestos fiber, the standard phenolic Microballoon/silica Eccosphere composite, and the aluminum silicate fiber which was the only filler which showed a distinct possibility for improved performance. The combinations were further selected to show relative comparative performance for each of the formulation variables.

3.1.5 Additional Ablation Tests

The formulations selected were prepared and tested, with the following results.

3.1.5.1 Laboratory Torch

Duplicate samples of the seven candidate formulations listed in Table 9 were tested in the laboratory torch at a heating rate of 18 BTU/ft^2 sec. The evaluation criteria was the time necessary to have a backface temperature rise of 200°F. The backface temperature was also measured at the end of a thirty-minute exposure. It appeared that, for similar type materials, density was the largest contributing factor to backface temperature rise performance in this facility. The test was essentially a transient method of measuring thermal conductivity. The test also indicated that insulation performance using the split Phenolic Glass honeycomb may be better than the split asbestos honeycomb, and that a layer of unsupported free foam below the reinforced ablation surface may substantially improve the transient insulating properties of the system. A properly designed composite system of this type could have the highest overall efficiency in meeting all the thermal, mechanical, and ablation requirements.

3.1.5.2 NASA Arc Jet

These seven candidate materials were also fabricated and sent to NASA -Langley for testing. The results are shown in Table 10.

3.1.5.3 Hypersonic Arc Tunnel Results - 3.4 BTU/ft^2 sec

The final test phase of the program in the GE Hypersonic Arc Tunnel examined samples of eight materials. Specimens were weighed and profiles were taken both before and after test. The profiles were obtained with the universal measuring apparatus in the RSD Thermophysics Laboratory. Five readings of the final dimensions were taken along the center line of each specimen and average values were used in the subsequent data reduction. When there was clear evidence of serious material degradation below the char layer, a dimensional change based on full depth of degradation was used to evaluate ablation performance. Performance was evaluated on each of two bases: total mass loss from a specimen and total change to the virgin material-degraded material interface.

The specimens, mounted in the side walls of a rectangular nozzle, were subjected to non-stagnating high enthalpy air flow of approximately 13,500 BTU-lb. The measured cold wall heat rate to the specimens was a nearly constant 3.4 BTU/ft^2 sec. The tests were 1200 seconds in duration. Each specimen was equipped with a thermocouple affixed to its back face. The time temperature history was recorded during the entire course of each test. The results are shown in Table 11.

The eight materials selected for evaluation of ablation characteristics at the low flux level of 3.4 BTU/ft^2 sec. were rated on the basis of weight loss and amount of degraded material. Four of the materials tested were essentially a repeat of previous formulations. In general, the materials did not show good repeatability. Either the weight loss was significantly different or the amount of degraded material had changed. The four repeat specimens were compared to the previous tested samples and the following observations made.

NASA 602 G-H/c-S	Slightly less char than before Sub layer not as discolored
ESM 1001 P-G-H/c-s	Char very similar to before but degraded depth about one half of previous sample
ESM 1004A P-G-H/c-S	Char and degradation similar to previous sample
ESM 1011 P-G-H/c-S	Char and degradation similar to previous sample

The following conclusions were drawn:

1. The low flux level results in a small weight loss and degradation depth, making measurements of both these quantities difficult to assess with the accuracy desired.

2. The nature of the materials are such that swelling of the char layer and virgin material make physical measurement of the char-virgin material interface difficult to measure.

3. The ESM 1004A P-G-H/c-S continues to demonstrate better ablation performance than the standard ESM 1001 P-G-H/c-S at low flux levels.

3.1.5.4 Hypersonic Arc Tunnel Results - 40 BTU/ft^2 sec

The eight materials selected for the final test phase were evaluated for ablation characteristics at a medium flux level of 40 BTU/ft^2 sec in the GE-SSL Hypersonic Arc Tunnel. These were rated on the basis of amount of degraded material. The specimens were fabricated as elliptical specimens and were oriented at an angle of attack of 50 degrees. The projected area of the model face is two inches in diameter. The heat flux varied over the surface of the model as shown in Figure 15. The flow is subsonic attached flow having a shear force of 0.25 lb/ft^2. Arc operating conditions were the same as used in the low flux runs, i.e. h_S = 13,500 BTU/lb, P = 0.05 mm Hg in the tunnel. A five-inch exit diameter nozzle was employed and the model was centered within the flow from the nozzle. The heats of degradation were calculated on three measurements taken along the centerline of the model and utilized local cold wall heat fluxes at those points. The leading and trailing edges of the model were excluded in the calculations because the char depth varied considerably in those areas.

The NASA 602 G-H/c-S and NASA 602 Asb-H/c-S performed better than the other materials in this environment both from the standpoint of higher heat of degradation and lower backface temperature. The results are shown in Table 12.

3.1.5.5 Malta Rocket Engine Facility Pit No. 1 Results

The eight selected materials were fabricated into strips 1/2 inch wide, 1/2 inch deep, and 5 inches long. These strips were bonded to the face of a 4 inch wide, 30-degree included angle, two-dimensional wedge which had a 0.75-inch nose radius. Previous testing with this type of wedge in the 5 inch diameter Pit No. 1 engine gave a cold wall flux of 150 BTU/ ft^2 sec and a shear force of 8 lb/ft^2 when the side of the wedge was inclined to the flow at a 10-degree angle of attack. This represented the upper limit of environmental conditions to which these materials might be subjected.

The specimens were located so that the NASA 602 G-H/c and ESM 1001 P-G-H/c-S would be at the centerline of the flow where the flow was most uniform. Starting from these specimens, the others were placed so as to change only one parameter at a time, where possible. The final order is shown in Table 13 where the degradation depths are shown along with the heats of degradation. These values were taken 2-1/2 inches from the leading edge of the specimen. Heat fluxes were reduced about 15 percent from the centerline of the model to the edge of the outer specimen due to a velocity gradient over the face of the model. The model, after test, is shown in Figure 16.

The other side of the wedge also contained the same specimens. The heat flux was higher--775 BTU/ft^2 sec and the shear force was higher--35 lb/ft^2. All of the specimens ablated away completely except ESM 1004A P-G-H/c-S. The higher shear forces present on this side, allowing for somewhat reduced conditions at the edge, indicated better shear resistance of the char for this aluminum silicate filled formulation.

The results indicated that the ESM 1004A P-G-H/c-S performed the best in this flux and shear environment.

3.2 FINAL CANDIDATE MATERIAL SELECTION

This completed the ablation tests for the screening phase of Task 1. On Jan. 22, 1964, the GE program representatives met with the NASA technical monitor, K. Wadlin, reviewed the data and jointly selected the final three candidate materials for this Task. Mechanical, thermal, and additional ablation data were generated for the trade-off study towards selecting the final materials system for scale-up and thermal cycle. The final candidate materials were the NASA 602 G-H/c-S, the ESM 1001 P, and the ESM 1004B P. The NASA 602 G-H/c-S formulation had shown consistently high ablation performance throughout all the tests. The incorporation of this filler in a split honeycomb matrix did not significantly improve its low temperature capability. However, when used as an ablation overlay on a free foam phenyl silicone system, it appeared that this deficiency might be eliminated. In this case, the underlay would act as a compressible bond system while still providing ablation protection. The addition of aluminum silicate fibers in the foamed phenyl silicone system had so improved the char strength and stability and ablation performance that this formulation was also selected. The data was generated on this formulation in its unsupported form to provide a candidate that was significantly different in its compositional form. It still was necessary to determine whether the unsupported material would perform well under the high range of interest of re-entry aerodynamic shear.

3.2.1 Data Generation on Final Candidates

The final ablation testing was conducted in the NASA-Langley Arc Jet. Although the mechanical and thermal property data were generated on the foamed phenyl silicone formulation with 6 percent aluminum silicate, ESM 1004B P, the ablation models contained samples at 6 percent, ESM 1004B P, and 12 percent, ESM 1004A P, filler concentration to evaluate this difference.

3.2.1.1 NASA Arc Jet Ablation Results

The NASA arc jet ablation results are shown in Table 14.

3.2.1.2 Mechanical Properties

The three candidate elastomeric materials were tested to develop trends of mechanical properties and thermal expansion with temperature variation. The properties of tension, compression, tensile-shear, and linear thermal expansion were measured on specimen configurations representative of behavior in an ablation shield application. The experimental results support previous observations of the effects of transitional characteristics upon physical behavior of the resin systems. The two ESM formulations showed significant mechanical stiffening in the glass transition region of approximately -180°F; NASA 602 G-H/c-S shows this stiffening at about -90°F, the end of the crystallization region of this class of silicone resins. Double lap shear (tensile-shear) tests almost duplicated the tensile tests relative to ultimate strengths, supporting the consideration that this experiment primarily evaluates tensile behavior of an elastomeric material system.

3.2.1.2.1 Experimental Techniques

Tensile "dog-bone" specimens with cross-sections of 1.0 inch x 0.5 inch were used to represent circumferential and longitudinal loading in a heat shield application. At +300°F, a "sandwich-type" tensile specimen of 6-inch x 6-inch cross-section and 0.25 inch thickness was tested to simulate radial stresses in a shield application. Most tensile tests were performed between room temperature and -280°F.

Double lap shear specimens (tensile-shear) were tested between -300°F and +300°F.

Compression specimens measuring 1 inch x 1 inch x 1 inch were tested between room temperature and +300°F to represent circumferential and longitudinal loading in a shield. ESM 1001 P and ESM 1004B P did not exhibit failure prior to deflecting the specimen twenty-five per cent. NASA 602 G-H/c-S was tested and did exhibit compressive failure prior to twenty-five percent deflection. ESM 1001 P was also tested in compression at -130°F and -160°F in thin-sheet configuration (6 inch x 6 inch x 0.25 inch) to simulate radial stresses relative to the shield application.

All tests were performed on an Instron testing machine utilizing a crosshead travel rate of 0.02 inch/minute, approximating realistic strain rates. Temperatures were obtained in an air-circulating chamber using sufficient soaking time to ensure isothermal conditions. Extensometers were used for tensile strain measurements and for strain of

"sandwich-type" specimens. Crosshead movement records were sufficient for measuring compressive strain at elevated temperatures.

Thermal expansion tests were performed in an MTI dilatometer at a heating rate of 1°F/min. The specimens, 2 inches x 0.5 inch x 0.5 inch, were cooled rapidly to -300°F, allowed to come to thermal equilibrium and then put on the 1°F/min heating ramp to +300°F. Temperature was measured by a thermocouple imbedded directly in the specimen.

3.2.1.2.2 Test Results

Tables 15 and 16 summarize the tensile data obtained for the three materials. Tables 17 through 19 list tensile-shear results. Tables 20 and 21 summarize all compression data. Figures 17, 18, and 19 show change in length versus temperature (linear expansion) for ESM 1004B P, NASA 602 G-H/c-S and ESM 1001 P.

It should be noted that in heating any one of the elastomeric formulations from a soak condition of -300°F, expansion characteristics of a brittle elastomer are exhibited through the glass transition temperature and up to the beginning of crystalline effects (approximately -90°F to -70°F). Thereafter, very high expansion characteristics are evidenced by the steep slope of the $\Delta L/L$ versus temperature curve. This latter expansion rate is typical of the rubbery behavior of elastomers. The crystalline phenomenon involves an ordering of polymer molecules with an accompanying decrease of volume (increase in density). Crystallinity does not necessarily coincide with sharp changes in mechanical properties as exhibited by the difference in mechanical transition temperatures between ESM formulations and NASA 602 G-H/c-S. Polymer structure controls the mechanical response to transition behavior.

3.2.1.3 Thermal Properties

Thermal conductivity, specific heat, and TGA data were generated on the candidate materials. The results are shown in Tables 22, 23, and 24 and in Figures 20, 21, and 22.

3.2.1.3.1 Thermogravimetric Analysis (TGA)

Samples of the candidate materials were heated to 1000°C at a linear rate of 150°C/hr. in a non-oxidizing atmosphere (nitrogen). The results show that ESM 1001 P and 1004B P are much more thermally stable at temperatures above 350°C than NASA 602.

The Chevenard thermobalance was used to heat the samples up to 1000°C at a linear rate and to record the residual weight continuously with time. An independent measurement of the specimen block temperature verified the linearity of the heating rate. Specimen configurations consisted of 100 milligrams of tiny slivers cut from sheets of the elastomers. As the samples were heated, dry nitrogen was passed through the furnace chamber. Flow rates were adjusted to provide a non-oxidizing atmosphere and to remove volatile products of polymer degradation. The results are shown in Table 22.

The ESM 1001 P and ESM 1004B P behaved very much alike using the TGA technique. The major weight loss for these two materials occurred between 300 - 650°C. A wide temperature

interval is indicative of a complex degradation reaction sequence. Any apparent differences from 650°C onward can be asscribed to the fillers used in ESM 1001 P and ESM 1004B P.

NASA 602 was quite atypical when compared to ESM 1001P and ESM 1004B P. There was a relatively narrow range (350 - 450°C) where the major portion of the decomposition took place. A relatively clean-cut decomposition mechanism can be expected from this material. Since NASA 602 contains 15 percent organic filler and is low temperature vulcanized, breakdown of the phenolic Microballoons and incomplete cross-linking can account for most of the degradation taking place in such a short temperature interval.

3.2.1.3.2 Thermal Conductivity

All samples were 2.5 inches x 2.5 inches x 0.25 inch with the heat flow parallel to the 0.25-inch thickness dimension. Thermal conductivity was measured over the temperature range 100°F to 600°F. The measurements were made on a Dynatech Comparative Thermal Conductivity Instrument, TC-1000, which has an accuracy of ±5 percent, in the following manner: the sample of unknown conductivity was sandwiched between two identical heat meters of known thermal conductance. The sample and heat meters were, in turn, held between a heater and a fluid-cooled heat sink. Thus, the test section consisted of a stack containing, in vertical order from the top, the heater, a heat meter, the sample, a second heat meter, and, finally, a heat sink. During the test the heat flowed from the heater assembly through the stack to the heat sink. The surface temperatures were measured for each heat meter and for the sample. Since the conductance was known for the heat meter, this together with the temperature measurements provided the means of establishing the heat flux through the heat meters and, in turn, through the sample. The thermal conductivity of the sample was determined by knowing the heat flux through the sample, the thickness of the sample and the temperature drop across the sample.

The thermal conductivity coefficients of both ESM formulations decreased with increasing temperature while the NASA 602 G-H/c-S coefficient remained constant.

3.2.1.3.3 Specific Heat

All samples were 2.5 inches x 2.5 inches x 0.25 inch consisting of the elastomeric material without the supporting matrix. Measurements were made over the temperature range -200°F to +400°F. The measurements were made on a Dynatech Automatic Continuous Specific Heat Instrument (SHC series) which has an accuracy of ±2 percent from -250°F to +200°F and ±5 percent from +200°F to +600°F. The data were taken by automatically thermally isolating a test specimen, applying an accurately measured quantity of thermal energy, and recording the functional relationship between the temperature response of the sample and the quantity of energy added. Once the sample was inserted into the instrument, it was not touched until the test was completed.

These specific heat determinations, along with those reported in Figures 8 through 14, detected a transitional phase change at about -40°F. (This coincides with the change in shape of the thermal expansion coefficient curves.) The NASA 602 formulation experienced creep behavior during the specific heat measurements which led to a permanent shape change after measurement.

3.2.2 Trade Off Study and Final Selection

3.2.2.1 Structural Comparison of Elastomeric Heat Protection Systems

Three elastomeric heat protection systems were compared.

ESM 1001 P, ESM 1004B P, and NASA 602 G-H/c-S/ESM 1001 P composite.

The shell, to which the heat protection systems were attached, was twenty inches in diameter and one-tenth of an inch in thickness. Both steel and aluminum shells were analyzed. The heat protection systems were 5/8-inch thick. Note that the NASA 602 G-H/c-S material was one-half inch thick with 1/8-inch of ESM 1001 P underlay. See Figure 23.

The ESM 1001 P was evaluated as a control material.

To calculate the thermal stresses induced in the composite cylindrical shells described above, the following equation was used.

$$T_p = \frac{(\alpha_p - \alpha_m)\,\Delta T\, R}{\dfrac{R^2(1-U_p)}{E_p t_p} + \dfrac{R^2(1-U_m)}{E_m t_m} + \dfrac{t_B}{E_B}} \cdot \frac{R}{t_p} \qquad (1)$$

This equation was for thin shells of elastic isotropic materials where:

α_p = shield mean coefficient of thermal expansion = in/in/^oF

α_m = sub-strate mean coefficient of thermal expansion = in/in/^oF

ΔT = temperature change from stress free state = ^oF

R = radius to outer surface of sub-structure = inches

u_p = shield Poisson's ratio

E_p = shield elastic modulus = psi

t_p = shield thickness = inches

u_m = sub-structure Poisson's ratio

E_m = sub-structure elastic modulus = psi

t_B = bond thickness = inches

E_B = bond elastic modulus = psi

t_m = sub-structure thickness = inches

When analyzing the NASA 602 G-H/c-S/ESM 1001 P heat protection system, the ESM 1001 P underlay was treated as a soft bond. Therefore, the t_B/E_B term, in Equation (1) was for ESM 1001 P.

Then, analyzing the ESM heat protection systems, there is no soft bond and $t_B = 0$; therefore, $t_B/E_B = 0$.

To account for the variation of material properties with temperature, the stresses were calculated in intervals. The plots of stress versus temperature were then obtained by superposition of the stresses from the several intervals.

3.2.2.1.1 Discussion and Conclusion

The stresses in NASA 602 G-H/c-S, ESM 1004B P and ESM 1001 P heat shield materials were also calculated for a steel substructure. The stress reversal was not seen here. In the ESM 1004B P system, there was a stress reversal from tension to compression. This was due to the fact that the $\Delta L/L$ curve for the substrate, crossed over the $\Delta L/L$ curves for the heat shields. Tensile failure of the shield at -280°F was, therefore, not probable. The ESM 1001 P developed a tensile stress of 308 psi at -280°F. With an ultimate tensile strength of 1400 psi, the ESM 1001 P should have an adequate safety margin.

The stresses in NASA 602 G-H/c-S, ESM 1004B P, and ESM 1001 P heat shield materials were also calculated for a steel substructure. The stress reversal was not seen here. This was due to the fact that the $\Delta L/L$ curve for the substrate did not cross over the $\Delta L/L$ curves for the heat shield materials. The margins of safety (MS) based on ultimate tensile strength were:

ESM 1004B P $\quad MS = \frac{1540}{72} - 1 = 20.1$

NASA 602 G-H/c-S/ESM 1001 P $\quad MS = \frac{1680}{163} - 1 = 9.2$

ESM 1001 P $\quad MS = \frac{1400}{486} - 1 = 1.89$

ESM 1001 P-G-H/c-S would develop stresses similar to those developed in ESM 1001 P; however, margins of safety with ESM 1001 P-G-H/c-S would be somewhat lower because of its slightly lower ultimate strength.

Therefore, though the ESM 1001 P and NASA 602 G-H/c-S/ESM 1001 P heat protection systems have positive safety margins at -280°F, the ESM 1004B P system has a higher structural margin of safety.

3.2.2.2 Ablation

The NASA 602 G-H/c-S/ESM 1001 P composite performed very well, as expected, in the two flux-shear levels of the NASA-Langley arc jet test. The unsupported ESM 1004B P aluminum silicate fiber addition performed well at the lower shear level but performance fell off drastically at the higher shear condition in the Langley arc jet. Therefore, the unsupported 1004B P did not meet the total ablation performance criteria.

3.2.3 Final Material Selection

The NASA 602 G-H/c-S/ESM 1001 P composite appeared to meet the selection criteria. It had performed well in all ablation environments. Although not as simple to fabricate as the ESM systems, it could be easily fabricated using the split honeycomb matrix. Although it appeared to be capable of surviving the thermal cycle environment, the margin of safety was not as high as the ESM system. On the other hand, the foamed, aluminum silicate fiber filled phenyl silicone, ESM 1004B P, met all the criteria with higher confidence margins except the ablation performance under the higher shear level. It had been demonstrated in the earlier tests that this resin system had shown good performance over the complete range of flux and shear conditions when in the split honeycomb matrix. From past experience with mechanical data generation on the ESM 1001 P system, there is very little difference mechanically whether the material is in the split honeycomb matrix or unsupported. Therefore this system would also meet the performance criteria for scale-up and thermal cycle selection.

Since both systems were different and met the performance criteria, it was agreed to test both systems in the scale-up and thermal cycle test. By fabricating the composite shield over the nose radius and the upper portion of the skirt section, leaving a gap, and fabricating the ESM 1004B P-G-H/c-S over the remainder of the skirt section, both materials could be evaluated in the thermal cycle environment.

3.2.3.1 Fabricability

Throughout the program the ease of fabrication was evaluated in the preparation of screening formulations for test models. Discontinuous honeycomb matrix was used for all samples. Rigid honeycomb "saddlebacks" when bent in any direction and could not be formed to complex curves and shapes. Foamed silicone in the discontinuous matrix (ESM-1000 series) acted much like a rubber blanket and readily conformed to contoured surfaces. The system still retained the original function of the matrix, to aid in the resistance to aerodynamic shear forces. When using syntactic foam materials, pre-forming of the honeycomb matrix over the desired curved surface was necessary before filling and curing. After curing the parts were removed from the mandrel and machined. Final machining for all formulations was accomplished by using cup shaped grinding wheels on either a Bridgeport mill or lathe. In the final contouring of the scale-up structure the same type of cup shaped grinding wheel was employed on a boring mill.

3.2.3.2 Scale-Up 602 G-H/c-S/ESM 1001 P Composite

In the fabrication of the full scale unit with NASA 602 G-H/c-S/ESM 1001 P composite material, the following approaches were necessary.

To achieve an adequate bond, the composite system had to be precisely matched and fitted to the structure surface. If higher bonding pressures were used to deform this comparatively inflexible shield material to match the tolerance irregularities of the structure, significant stresses could be induced in the shield. This could partially be relieved by using a higher thickness percentage of the flexible underlay in the shield system.

An 8-inch diameter base, sphere-cone configuration of the composite formulation was fabricated in the laboratory to define the approach to full scale fabrication. The following general procedure was followed:

(1) A 12-inch disc of tri-directional split Phenolic Glass honeycomb was cut and primed (Figure 24)

(2) Two triangular wedges were removed to allow for conforming to shape.

(3) The NASA 602 formulation was prepared (Figure 25). The disc was supported by open cell urethane foam and the formulation troweled into the cells. The urethane foam acted as an air release and allowed the honeycomb to be completely filled without the entrapment of air. Examination of a section of this filled material revealed air and void free cells.

(4) The urethane foam was then used as bleeder material and a vacuum bag technique employed (Figure 26).

(5) The bag material and components were pulled into place by applying vacuum at a slow rate.

(6) The entire unit was then cured at 150°F (29-inches Mercury) for five hours.

Visual examination of the finished part revealed a void free cap conforming to the mandrel configuration.

This system was then successfully applied to the fabrication of the full scale unit.

The skirt section of the composite material was fabricated in four 16.5-inch x 6.0-inch sections. The slit, primed honeycomb was positioned slit side down over a curved (10-inch radius) perforated steel sheet and held in place with nylon cord.

The NASA 602 material was troweled onto the honeycomb until the material was forced completely through the honeycomb cells and perforated steel sheet.

The mold was transferred to a circulating air oven and cured at 150°F for 16 hours, then post cured at 225°F for 5 hours.

After curing, the excess material was carefully removed from both surfaces of the curved panel. No voids were apparent on examination of the cross-section of the shield segments.

The ESM 1001 P material was foamed in open trays to a thickness of 1.5 inches. After cure and post cure the material was slit to 0.125-inch thick sheets.

The sheet was then bonded* to the NASA 602 G-H/c-S material to form the composite shield. Final machining resulted in a composite shield of the dimensions NASA 602 G-H/c-S, 0.375 inch/ESM 1001 P, 0.125 inch.

The composite sections were then tailored to fit the structure and bonded* using vacuum bag techniques at 115°F for five hours.

ESM 1004B P-G-H/c-S

The ESM 1004B P-G-H/c-S was prepared in flat sheets, machined to a thickness of 0.060 inch on a "Bridgeport" mill, cut to configuration, and bonded to the lower portion of the structure using vacuum bag techniques. The final thickness of 0.50 inch was machined on a boring mill. The unit was completed and ready for application of the "break" printed circuit and associated instrumentation for the thermal cycle test.

3.2.3.3 Thermal Cycle

3.2.3.3.1 Test Setup and Procedure

The test structure was instrumented with painted conductive silver grids on each panel to detect any cracking which might occur (Figures 27 and 28) and copper-constantan thermocouples were distributed over the inner surface of the aluminum substructure to monitor temperature during the cycle. The arrangement of the instrumentation on the structure is also shown on Figure 27. In addition to the thermocouples on the substructure, three thermocouples were arranged outside the test structure inside the test chamber to monitor air temperature. The thermocouples and the painted circuits were all monitored on a single Minneapolis-Honeywell, 20-point strip chart potentiometer recorder. The temperature chamber employed liquid nitrogen for the temperatures below ambient. The 20 channels recorded included the following:

7 channels - Thermocouples on the structure.
3 channels - Thermocouples to monitor chamber temperature.
1 channel - Ice bath thermocouple reference.
9 channels - Painted circuit crack sensors.

The thermal cycle employed is shown on Figure 29 and represents the average readings of thermocouples 2 and 6. The points at which cracks occurred in the various shield sections are indicated on Figure 29 also. Painted circuits, numbers 2 and 4, were damaged during installation in the test chamber and did not provide test data.

3.2.3.3.2 Test Results

The temperature of the structure was reduced from an ambient of 74°F to -150°F at a rate of approximately 2°F/minute, at which point conductive circuit No. 1 indicated a failure (Figure 30). At this point, the structure was examined and a crack was visible on the cap extending from the mating line (1) at the base, through the center, and approximately 1/3 down the opposite side (2).

At this point, shrinkage was noted in the NASA material similar to that demonstrated on the flat thermal specimens.

---

*Bond material = RTV 560 + 0.5 percent Thermolite 12.
cure = 8 hours at 130°F

The test was continued. Temperature was held at -150°F for thirty minutes then reduced to -200°F. At this point, the crack propagated to the opposite mating line (3). Temperature was held at -200°F for thirty minutes.

The temperature was then reduced to -250°F and held for thirty minutes and the structure examined visually through a window in the test chamber. No significant changes were noted. All circuits remained intact. The unit was then slowly brought back to room temperature overnight by closing the liquid nitrogen supply to the closed chamber.

The chamber was opened the following morning and the unit examined at room temperature conditions. The crack in the nose cap had closed and was hardly visible. The test was continued and the temperature reduced to -250°F at an approximate rate of 1°/minute (a slower rate than planned due to a malfunction of chamber equipment). Circuits No. 2 and No. 4 became inoperative during this period when the solder connections of the leads to the painted circuit failed. The test was continued and the temperature reduced to -275°F. At this temperature, Circuit No. 5 opened and a crack was detected on one of the NASA 602 G-H/c-S/ESM 1001 P composite skirt panels. The temperature was held at -275°F for 15 minutes and then reduced to -300°F. At -296°F, Circuit No. 3 opened and cracks were noted in the NASA 602 G-H/c-S. All circuits on the ESM 1004B P-G-H/c-S material were still intact, indicating no failures. The temperature was held at -300°F for thirty minutes then elevated to room temperature at approximately 2°F/minute.

Examination of the structure showed crack failures throughout the NASA 602 G-H/c-S material in both the cap and sheet sections. There was no evidence of failure in the ESM 1004B P-G-H/c-S material section. All cracks were completely closed at room temperature.

The temperature was increased to +300°F at 2°F/minute. At 200°F, bulging of the shield around the cracks was noted. The temperature was held at 300°F for 30 minutes, then allowed to return slowly to +85°F. At this point, the chamber was opened and the unit examined.

3.2.3.3.3 Observation

After the 300°F cycle, the cracks were open at room temperature, and are shown in Figure 31.

3.2.3.3.4 Discussion

The unit was thoroughly examined. The nose section and skirt of the composite contained several large cracks which extended through both the NASA 602 G-H/c-S and ESM 1001 P underlay to the structure. At room temperature, the larger cracks are open to a width of approximately 0.125 inch. Many smaller cracks are visible and randomly located throughout the cap and skirt sections. These do not extend throughout the entire thickness but only through the NASA 602 G-H/c-S material. They remain essentially closed at room temperature. The shield areas around the main cracks which bulged when the shield was in compression during the high temperature cycle were generally unbonded along the length of the cracks. The NASA 602 G-H/c-S/ESM 1001 P skirt panel which had the least number of voids in the bond area at the ESM 1001 P structure interface failed at the lowest temperature (-296°F).

The ESM 1004B P-G-H/c-S skirt section showed no defects. All areas were completely bonded.

The inability to achieve a complete uniform bond in the composite shield sections may be due to the following reasons:

The sections were dry fitted at room temperature, but the bond was cured at +115°F. In spite of the vacuum bag pressure, the sections may have expanded sufficiently to pull away from the structure in localized areas leaving unbonded pockets. The material sections were pre-formed using the structure as a mandrel. The final shield may not have been bonded onto the structure in the exact location of fabrication and the thickness of the underlay was insufficient, with the fairly inflexible NASA 602 G-H/c-S shield, to take up the difference in tolerances using vacuum bag pressure.

The thermal cycle test indicated that the ESM 1004B P-G-H/c-S will successfully survive a ±300°F thermal cycle when bonded to an aluminum structure. The thermal stress analysis indicated that ESM 1004B P-G-H/c-S shield system had the largest margin of safety at the low temperature extremes. The thermal cycle test also showed that the NASA 602 G-H/c-S, with an under layer of ESM 1001 P, can withstand temperatures as low as -275°F. As indicated in the analysis and substantiated in the test, the composite shield material has greatly improved the low temperature capability over the original, high ablation performance, NASA 602 G-H/c formulation.

4. TASK 2 - PRELIMINARY INVESTIGATION OF SHAPE STABLE ELASTOMERS FOR LIFTING RE-ENTRY VEHICLES

4. TASK 2 - PRELIMINARY INVESTIGATION OF SHAPE STABLE ELASTOMERS FOR LIFTING RE-ENTRY VEHICLES

Modifications were made to the base systems of the successful formulation and fabrication approaches defined in Task 1 to optimize performance for shape stable and minimum shape change compositions for thermal shield and control surfaces over a 20-minute exposure in the 0 - 160 BTU/ft^2 sec heating range. Fastening systems and other considerations were investigated for field replacement of shields.

4.1 SHAPE STABLE MATERIALS SELECTION

Based on the Task 1 effort and other related studies, three material systems were selected for shape stability and ablation evaluation under simulated conditions:

1. 10.1 percent aluminum silicate fibers
   1.0 percent asbestos fibers
   0.2 percent glass fibers

   in the foamed phenyl silicone (RTV-560) base resin (density 30.0 lb/ft^3)

2. 16.0 percent graphite fibers
   3.9 percent asbestos fibers
   0.8 percent glass fibers

   in the foamed phenyl silicone (RTV-560) base resin in a split Phenolic Glass honeycomb matrix (density 68.8 lb/ft^3)

3. Same as item 1 but in a split Phenolic Glass honeycomb matrix.

These formulations were selected, along with other key requirements, on their performance in the higher shear, ablation tests in the Malta Rocket and the NASA-Langley facility. The RTV-560 was used for its low temperature capability with a ductile to brittle transition temperature of -180^{o}F. The foamed system was selected for the available density control, where higher density materials may be advantageous as surface overlays to minimize shape change. The split honeycomb matrix provided char retention capability while eliminating the specific application problems of a rigid honeycomb matrix over multicurved surfaces. The aluminum silicate fibers most drastically improved ablation performance over the entire heat flux and shear regime. (The material was evaluated both with and without the supporting matrix, since the performance was sufficiently improved by the addition of these fibers that in many stations of a lifting re-entry vehicle, the supporting matrix would not be necessary.) A graphite fiber filled formulation was also selected for shape retention studies and although it was not selected as a continuing candidate in the Task 1 study because of its relatively higher thermal conductivity, was applicable here because of its superior shape stability. Graphite fiber filled formulations could be used as overlay materials on low density free-foam composites (as in the case of the NASA 602 G-H/c-S/EMS 1001 P composite in Task 1) to lower backface temperature response.

4.1.1 Malta Pit No. 1 Rocket Exhaust Tests

The graphite fiber filled formulation was selected for this evaluation on the basis of the following comparative ablation tests which were conducted by General Electric prior to this study. Ablation models of ESM formulations were tested in the GE Malta Pit No. 1 Rocket Exhaust facility under varying heat flux and shear conditions. Molded Phenolic Nylon was used as a reference material in these tests. In Test No. 1, ESM 1001 G-H/c and ESM 1001A G-H/c (with twice the normal concentration of asbestos fibers) were tested. In Test No. 2 the ESM was the graphite fiber filled, Shape Stable Material No. 2 except that it was in a rigid rather than a split phenolic-glass honeycomb matrix.

4.1.1.1 Test Facility

Pit No. 1 at the Malta Test Station employs a rocket motor with a 5-inch diameter shockless nozzle designed to produce parallel exhaust flow. Each test was run under the following environmental conditions:

Oxygen to fuel ratio	2.10
Total chamber pressure	300 psia
Total chamber temperature	5800°R
Enthalpy ratio (h_s/RT_o) est.	88
Mach No.	2.45

The test model was a 9-degree wedge of molded Phenolic Nylon with the ESM specimen bonded flush with the surface on half of each side of the face of the wedge. A static pressure tap and copper calorimeter slug were inserted on the Phenolic Nylon side of each wedge to measure the environmental conditions.

4.1.1.2 Test Procedure

Each model was installed so that the centerline of model and engine were aligned. The nose of the model was located approximately two inches downstream of the nozzle exit. The motor was started and brought to a stabilized condition before the motor was gimballed onto the model. The model was exposed for 10 seconds. The models were oriented at varying angles of attack to produce the range of heat flux and shear conditions. The angle of attack was the angle between the flow and the surface of the model.

4.1.1.3 Test Results

The results of these tests are shown in Tables 25 and 26.

4.1.1.4 Discussion

The heat of degradation of the ESM 1001 G-H/c, with the normal concentration of asbestos fibers, was not as high as the Phenolic Nylon control sample over the range of test conditions. When the asbestos fiber concentration was doubled and the density increased, the performance of the ESM was improved at the lower flux and shear conditions. The performance crossover with the reference Phenolic Nylon occurred somewhat above a heat flux of 374 btu/ft^2-sec and a shear level of 35.3 lb/ft^2. At the highest flux and shear condition with an angle of attack of 27 degrees, there was a significant decrease in the ESM 1001 A G-H/c performance.

In the case of the graphite fiber filled ESM formulation in test No. 2, the performance crossover occurred somewhat above a heat flux of 1075 btu/ft^2-sec and a shear level of 43 lb/ft^2. Thus the graphite fiber filled formulation was selected as a test material in the shape stable material study since it demonstrated improved ablation performance and lower mass loss at the higher flux and shear levels.

4.2 SIMULATION ABLATION TESTS

The test model configuration was based on the heat fluxes that occur on a typical lifting re-entry vehicle that requires about 1300 seconds to re-enter. The study, from which the heat fluxes were derived, was based on the use of an elastomeric shield material. The cold wall heat fluxes are for the maximum heating case using a trip Reynolds number of 100,000.

The stagnation heat fluxes were calculated for a vehicle leading edge radius of approximately one half foot. Peak heating for this location reached $\dot{q}$ = 105 BTU/ft^2 sec with a time integrated heating of 50,000 BTU. Peak heating half way back on the vehicle reached a $\dot{q}$ = 15 BTU/ft^2 sec with a time integrated heating of 14,000 BTU. This heating would be for the lower surface of the vehicle. The upper surface has a peak heating of about one quarter of that on the lower side. Correcting the fluxes to hot wall would result in a 15 percent to 20 percent reduction over most of the trajectory.

Previous tests in the program have been performed at the flux levels which fit those that would occur on a lifting re-entry vehicle. Since one of the more important aspects of this type vehicle depends upon the shape stability, we obtained time integrated heating fluxes at two locations where the heat flux is relatively high and where shape change is more likely to occur. These two regions are the leading edge and the lower surface of the vehicle. The test conditions listed in Table 27 were used and are compared to the typical case: time at 150 seconds; altitude 217,000 feet; M = 22.

The test configuration was a two dimensional model having a nose radius of 0.75 inch and a local body angle of 65 degrees to the flow field. The model was 2 inches wide and had the same blockage as the elliptical models used in previous tests. The nose region had the reinforcing matrix oriented in line with the flow, and the 65 degree body surface would have the reinforcing matrix perpendicular to the flow as indicated. Backface temperature was measured at two locations. Suitable back and side thermal protection was used to eliminate conduction paths to the backface of the model. Tests were conducted in the Hypersonic Arc

Tunnel at the same enthalpy and pressure level used in previous Task 1 tests. All three materials selected for evaluation in Task 2 were tested in this model configuration.

A test model of material No. 3 is shown before and after test in Figures 32 and 33. This was typical of the three test models. Shape measurements and backface temperature responses were made at several locations along the body. Char measurements, relative heats of degradation, surface temperature, and backface temperature response are shown in Table 28. Relative heats of degradation were based on the cold wall heat flux as determined by a calorimeter model and were calculated with the following equation:

$$H_d = \frac{\dot{q}t}{\rho x}$$

where: $\dot{q}$ = heat flux
t = run time
ρ = density
x = total degradation

Heats of degradation at stations other than the stagnation point were somewhat inconsistent, due to separation of the flow along the model surface. The swelling of the material in the ablation environment compensated for the material loss and resulted in a minimum shape change. Although all formulations showed adequate shape stability, the aluminum silicate filled formulations would provide more efficient selections due to their higher heats of ablation and lower backface temperature response.

4.3 COMPOSITE SYSTEMS

Several approaches were examined for combining shape stability with efficient backface temperature response. These included elastomeric pillar bonding systems, density variations through the shield, and overlays on low density insulating foams, forming composites.

Laboratory samples were prepared defining the fabrication process with the elastomeric pillar bonding system. This system forms an insulating air gap at the bond line and the apparent modulus of the bond can be changed by varying the size and spacing of the pillars. A forming mold was fabricated consisting of an 1/8-inch aluminum plate with 1/8-inch holes, countersunk on the top surface, on 3/8-inch centers. RTV-511 was selected as the pillar material since it was a better insulator than the iron oxide filled RTV-560. The RTV-511 was poured into an open pan mold to a height of 1/8-inch. When the perforated aluminum mold was then pressed down into the RTV-511, the elastomer was forced through the countersunk holes. A thin film of RTV-511 was formed on the surface. When this material was cured and removed from the mold, the individual pillars were attached to the surface film. This skin was then bonded to samples of Shape Stable Material (Item 3 - Section 4.1), with a thin layer of RTV-511. An alternate pillar system was also fabricated in the same manner using a blowing agent in the elastomer to form foamed pillars. This system would have additional insulating value but would not have the strength of the solid pillar system. Fabricability was demonstrated, but no tests were made on the pillar system.

Attempts were made to increase the insulation properties of the shield system by varying the density through the shield thickness. Samples of Shape Stable Material (Item 3-Section 4.1) were fabricated by anchoring the split honeycomb to the base of the mold during the foaming and curing step in the process. The mold surface restricted the degree of foaming of the material adjacent to the mold. This restriction resulted in a layer of increased density at the mold surface. This higher density layer would subsequently become the outer surface of the shield. Although this procedure did vary the density through the shield thickness, the variation was difficult to control and samples could not be made with repeatable consistency.

The most efficient system involved the use of the shape stable material over a low density insulating foam, forming a composite material. This system, developed in this section, was also incorporated, evaluated, and is fully reported in the Task 1 study involving the NASA 602 G-H/c-S/ESM 1001 P composite. While in Task 1 the composite was used to increase low temperature capability, the same composite fabrication approach was applicable to shape stable compositions in maintaining minimum backface temperature response. The ablation test results, using low density foams to form composite samples, are shown in Tables 9, 10, 11, 12, and 13. There was a lowering of backface temperature response for the ESM 1001 P-G-H/c-S when used with the lower density ESM 1001 P in a composite material. In addition to improve thermal compatibility and ease of fabrication, the low density insulating underlay provides additional re-entry thermal protection.

4.3.1 Ablation Tests

4.3.1.1 Torch

The following tests were conducted to demonstrate the effectiveness of the composite approach in reducing backface temperature response. Screening studies were conducted in the laboratory propane torch on samples of Shape Stable Material #1 and #2 and with composites of #2 with two levels of lower density, foamed RTV-560 as underlay materials. Material #2 was selected since it had a relatively high density and with the addition of graphite fibers would have relatively high thermal conductivity. This test was designed to demonstrate the effectiveness of the composite concept with any shape stable material of higher density and/or thermal conductivity.

The test samples were fabricated from the following formulations:

Sample No.	Material
#1	Shape Stable Material #1
#2	Shape Stable Material #2
#3	Composite - Shape Stable Material #2/foamed RTV-560, density 27 lb/ft^3, containing 4.3 percent asbestos fibers and 0.9 percent glass fibers
#4	Composite - Shape Stable Material #2/foamed RTV-560, density 43 lb/ft^3, containing 4.3 percent asbestos fibers and 0.9 percent glass fibers

The thickness of Shape Stable Material #2 was three times the thickness of the low density underlay material in each of the composite samples. This thickness ratio had been selected with the technical monitor, in both Task 1 and Task 2, as representative of the relative shield thicknesses required for ablation and for insulation. Each of the four test samples were fabricated to a thickness corresponding to an overall weight of 3 lb/ft^3.

The samples were tested in the Propane torch facility under the same conditions described in Section 3.1.3.1.1. The equipment was calibrated with a copper calorimeter. Backface temperatures were continuously monitored by a thermocouple. The time in minutes required to reach a backface temperature rise of 200°F was used as the evaluation criterion. The results are shown in Table 29 .

As expected, Sample #1, with the lowest overall density, reached the backface temperature limit in the longest time. The test time for Sample #2 material was increased when used as a composite with the 43 lb/ft^3 underlay in Sample #4. The test time was further increased when the 27 lb/ft^3 underlay was used in composite Sample #3. The results in this screening facility indicated an improvement in backface temperature capability of high density, shape stable compositions when used as a composite with a low density underlay.

4.3.1.2 Additional Simulation Ablation Tests

Based on the results of the propane torch tests, a model was prepared of composite Sample #3 for the simulation ablation test described in Section 4.2. From this test, a quantitative comparison was made on the backface temperature response of Shape Stable Material #2 with and without (Section 4.2) an insulating composite underlay.

Composite Sample #3 had a thickness of 1.19 inches of Shape Stable Material #2 over 0.348 inches of the27 lb/ft^3 foamed underlay at the stagnation point of the model. The material thicknesses at stations #1, #2, and #3 along the face of the model were 0.750 inches and 0.210 inches for the Shape Stable Material #2 and the low density underlay respectively. The test conditions were:

Run No.	Volts	Amps	Power (KW)	P_p* (psig)	Surface Temp (K^o)	Run Time (sec)
114	390	680	264	6.5	—	500

Post test char depths, degradation measurements and heats of degradation are shown in Table 30. The backface temperature response over the test time is illustrated in Figure 34. In both Table 30 and Figure 34 the results from the previous simulation ablation test on Shape Stable Material #2 are shown for comparison. The backface temperature response for the composite model, consisting of Shape Stable Material #2 with a 27 lb/ft^3, foamed underlay was approximately one-half as great as the backface temperature response of Shape Stable Material #2 for the same test time and conditions.

*Pp = Plenum Pressure

4.4 REFURBISHABILITY STUDIES

Several panels of elastomeric shield material were exposed to the laboratory propane torch (used in Task 1, ablation screening study) at a heat flux of 21 BTU/ft^2 sec for periods of thirty minutes. The resultant char was then physically removed for the refurbishability study in the following manner. After exposure, the sample was allowed to cool to room temperature and the char removed by grinding with a high speed drill equipped with an aluminum oxide bit. This was accomplished easily while producing an abundant amount of char dust. As soon as the underlying virgin material is reached the dusting ceases, thus acting as a built-in stop sign. After the surface was vacuumed, a sheet of elastomeric material was bonded to this surface to achieve original shield thickness. After three or four heating cycles on refurbished shields, there was no noticeable deterioration to the uncharred virgin material and there was no increase in the degradation rate or char depth of the shield material. By stocking panels of shield material of varying thicknesses, quick turn-around, on site refurbishments can be made without requiring elaborate tooling.

4.5 SHIELD FASTENING STUDIES

Three shield fastening systems were selected from the screening study for data generation. Bond-shear measurements were made on all three systems over the temperature range, 75^{o}F to 250^{o}F.

4.5.1 Loop and Pile Method

Loop and pile fastening methods (Figure 35) are usually associated with fabric fastening but may be applicable to attaching elastomeric shields. The loop and the pile may be bonded to either attachment surface and the shield may be attached to the structure with slight pressure on the shield which knits the pile into the loop. The shield material is easily removed or replaced by peeling but has good potential tensile and shear strength. There are no cure cycles or bonding problems involved if the system meets the design requirements. Fabrics such as glass may also be substituted for nylon, thus increasing the temperature capability of the bond line.

4.5.2 Perforated Interface

A second method of attaching a shield to a structure yet allowing easy removal involves placing a perforated interface of unbondable material, such as Teflon coated glass, between the shield and the structure (Figure 36). The shield is applied by coating the structure with bonding material, and the perforated Teflon coated glass cloth is rolled onto the structure. A thin coat of bonding material is then applied to the shield which in turn is bonded to the structure over the perforated scrim. The bond is achieved through the perforations and is similar to a series of spaced pillars. The shield can be easily removed after flight by peeling the Teflon-coated cloth. Glass scrim cloth and aluminum foil may be substituted for the perforated Teflon-coated fabric in the bond line.

4.5.3 Nut and Bolt Type Fastening

Samples were made using ESM 1001 P-G-H/c-S. An 0.008-inch epoxy-glass laminate was bonded to the attachment side of the pre-machined shield material to provide some rigidity (Figure 37). A plug was then cut through the shield with a diameter slightly larger than the Nylon washer used in the system. A section of this plug-cylinder was cut and a hole, the diameter of the Nylon bolt, drilled through the center of this circular section. This section was then bonded in the plug hole flush with the glass laminate at the attachment surface. A flat-headed, primed bolt and washer was inserted through the plug hole from the outside shield surface and bonded with the washer flush with the top surface of the bonded section. The remainder of the initial plug was then rebonded into the original plug hole. The shield was then attached through the bolt and nut into pre-drilled holes in the structure. This method lends itself to easy application and removal of pre-assembled panels, however, holes must be drilled in the skin of the structural material.

4.6 ADDITIONAL FASTENING AND REMOVAL METHODS

Two additional methods of shield attachment and removal were studied in the laboratory: the expandable bumper gasket and chemical shield removal.

4.6.1 Expandable Bumper Gasket

The expandable gaskets of silicone rubber are prefabricated, bonded to the shield, and the shield attached by pushing the bumper sections into the holes in the structure (Figure 38). This method also presumes that holes may be drilled in the structure.

4.6.2 Chemical Shield Removal

The investigation was made on removal of the normal bond system using solvent systems which would hopefully attack the primer at the surface of the structure. The attack on the bond was very slow using conventional solvents, such as toluene and xylene, and, at best, produced only a swelling of the silicone bond material. After the bond system was additionally cured through exposure to repeated thermal cycles, the bond became increasingly resistant to solvent attack. Chlorinated hydrocarbons, which form the base of many commercial resin strippers, were also tried. They also swelled the bond material but it was difficult to restrict their action and these solvents had a tendency to migrate to surrounding areas where attack may not be desired. The use of chlorinated hydrocarbons also presents a toxicity problem. Although the primer did not appear to be attacked in these cases, the use of toluene or xylene sufficiently softened the bond so that the shield could be removed from the structure using bladed knives and rotating brushes. These tools would be fabricated from materials which are softer than the structural metal, to prevent damage to the surface of the structure.

4.7 BOND-SHEAR TEST

Lap shear tests were run on the three selected attachment systems at 250°F, 200°F, 150°F, and 75°F as shown in Figure 39. The results are shown in Table 31.

The shear capabilities of all three fastening systems are adequate to meet the general load requirements for lifting re-entry vehicles. The "dressmakers" Nylon loop and pile was used to show feasibility of the concept. In an actual application, where bond capabilities would be required for higher bond temperature limits, high temperature Nylon (Nomex) or inorganic fibers would be used.

The strength of the Teflon coated glass system can be design controlled to requirements by varying the perforation size and spacing.

Although the stress capability of the nut and bolt system is more than adequate, there might be a tendency for a flexible shield to buckle between attachment points during high temperature exposure. This would be a definite drawback in the use of this system.

Shields can, of course, be bonded normally to the substructure with the elastomeric adhesive and removed with a "putty knife" type scraper at the bond line.

4.8 GENERAL CONCLUSIONS

This study has completed another step in the development and application of silicone elastomer thermal shields. The use of a discontinuous, supporting matrix in the system, as compared to a rigid, Phenolic Glass honeycomb, has minimized the fabrication and bonding problems to typical vehicle configurations. The incorporation of aluminum silicate fibers into the material has improved the performance of the system so that the reinforcing matrix may be entirely eliminated except in those areas of maximum expected re-entry heat flux and aerodynamic shear. Composite systems have been fabricated to achieve a more efficient shield system, from a weight basis, while meeting expected design criteria. Finally, the feasibility of using the silicone based elastomeric systems to meet the requirements for lifting re-entry vehicles has been demonstrated.

5. ILLUSTRATIONS AND TABLES

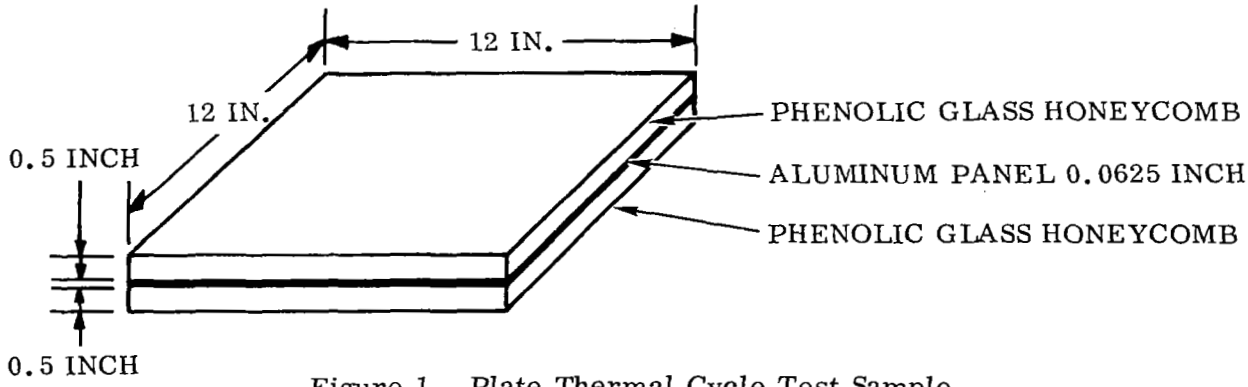

Figure 1. Plate Thermal Cycle Test Sample

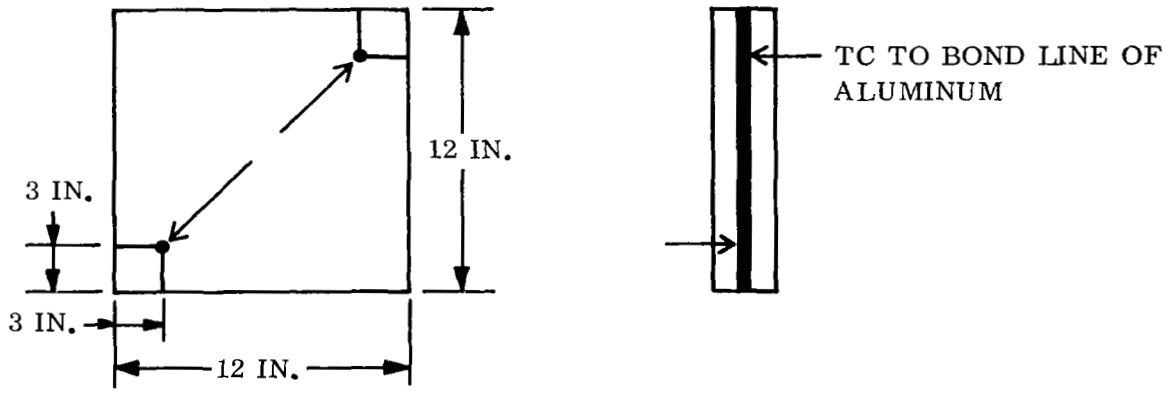

Figure 2. Thermocouple Placement - Plate Thermal Cycle Test Sample

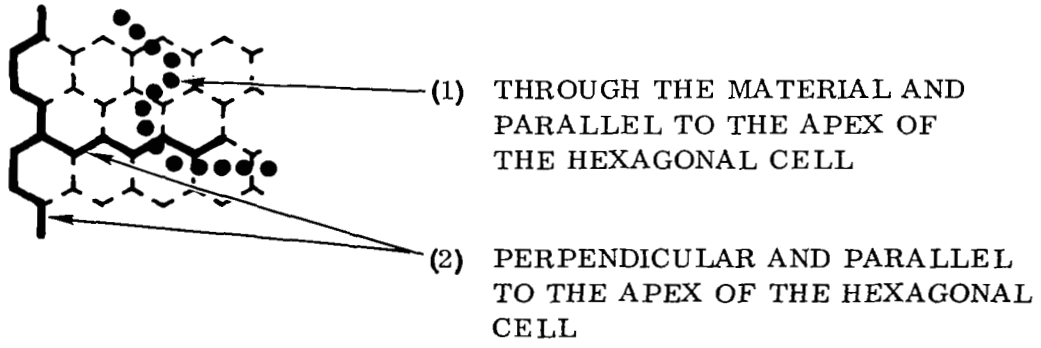

Figure 3. Failure Modes in Plate Thermal Cycle Tests

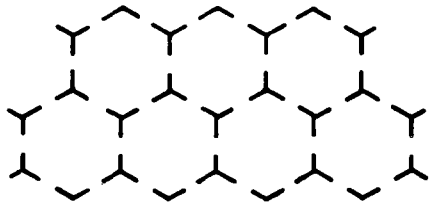

Figure 4. Splitting Pattern of Phenolic-Glass Honeycomb

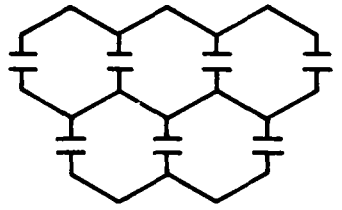

Figure 5. Splitting Pattern of Asbestos Honeycomb

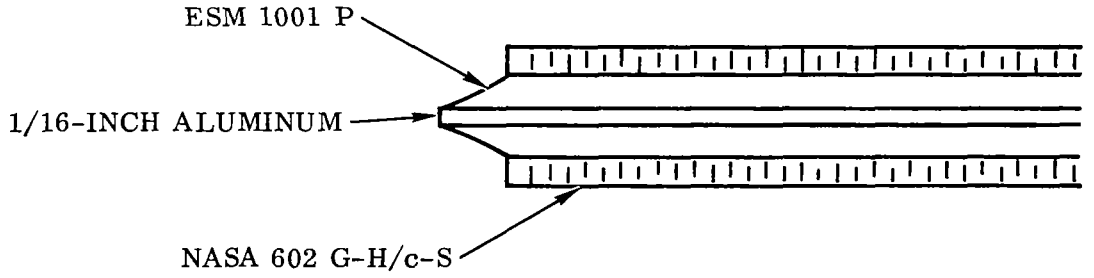

Figure 6. Behavior of NASA 602 G-H/c-S — ESM 1001 P Composite at Low Temperatures in Plate Thermal Cycle Test

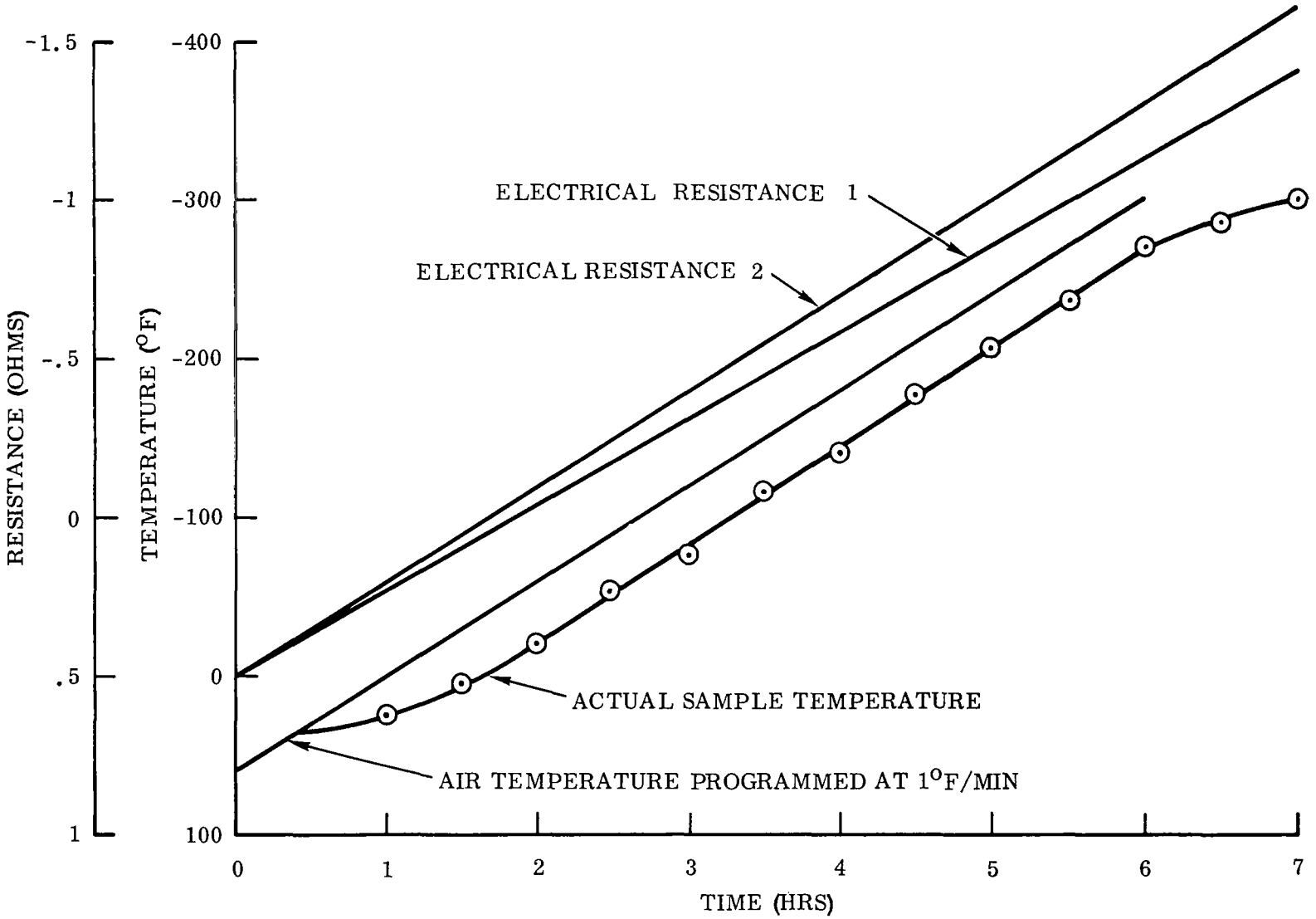

Figure 7. Resistance Change versus Temperature on Monitor Circuit During Plate Thermal Cycle Test of NASA 602 G-H/c-S/ESM 1001 P Composite

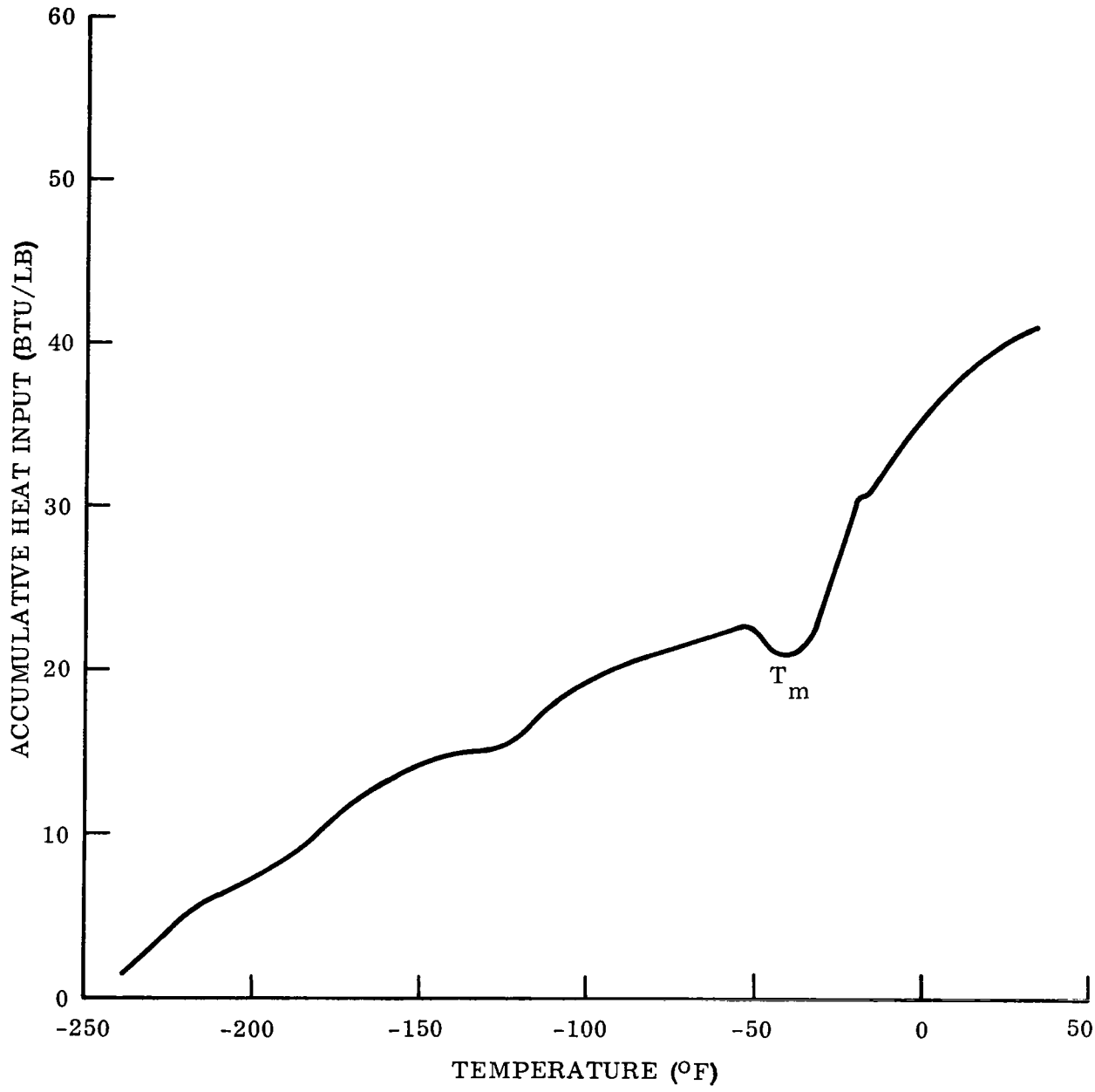

Figure 8. Continuous Specific Heat Measurement of DC 325 Elastomer

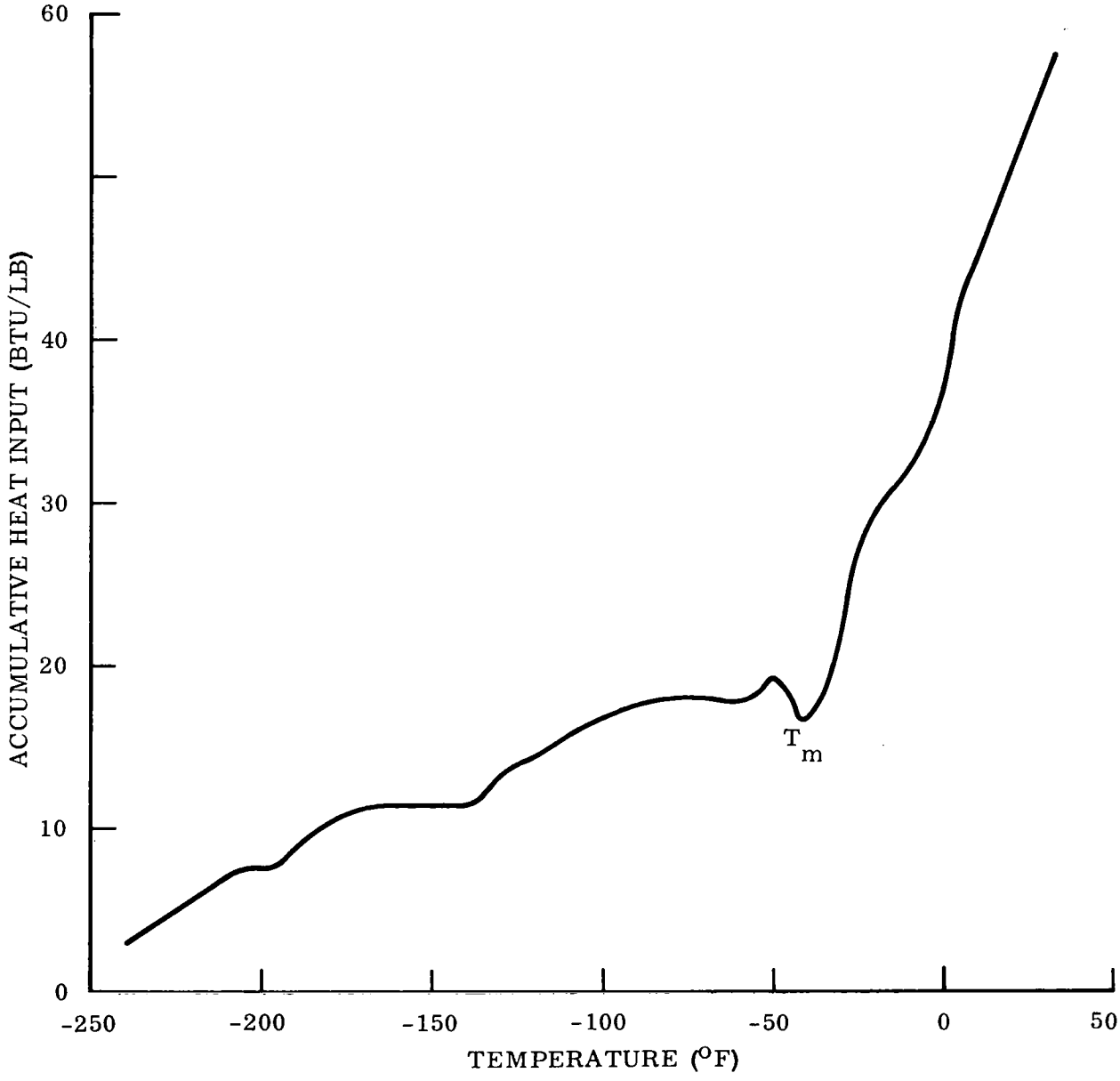

Figure 9. Continuous Specific Heat Measurement of NASA 182 Elastomer

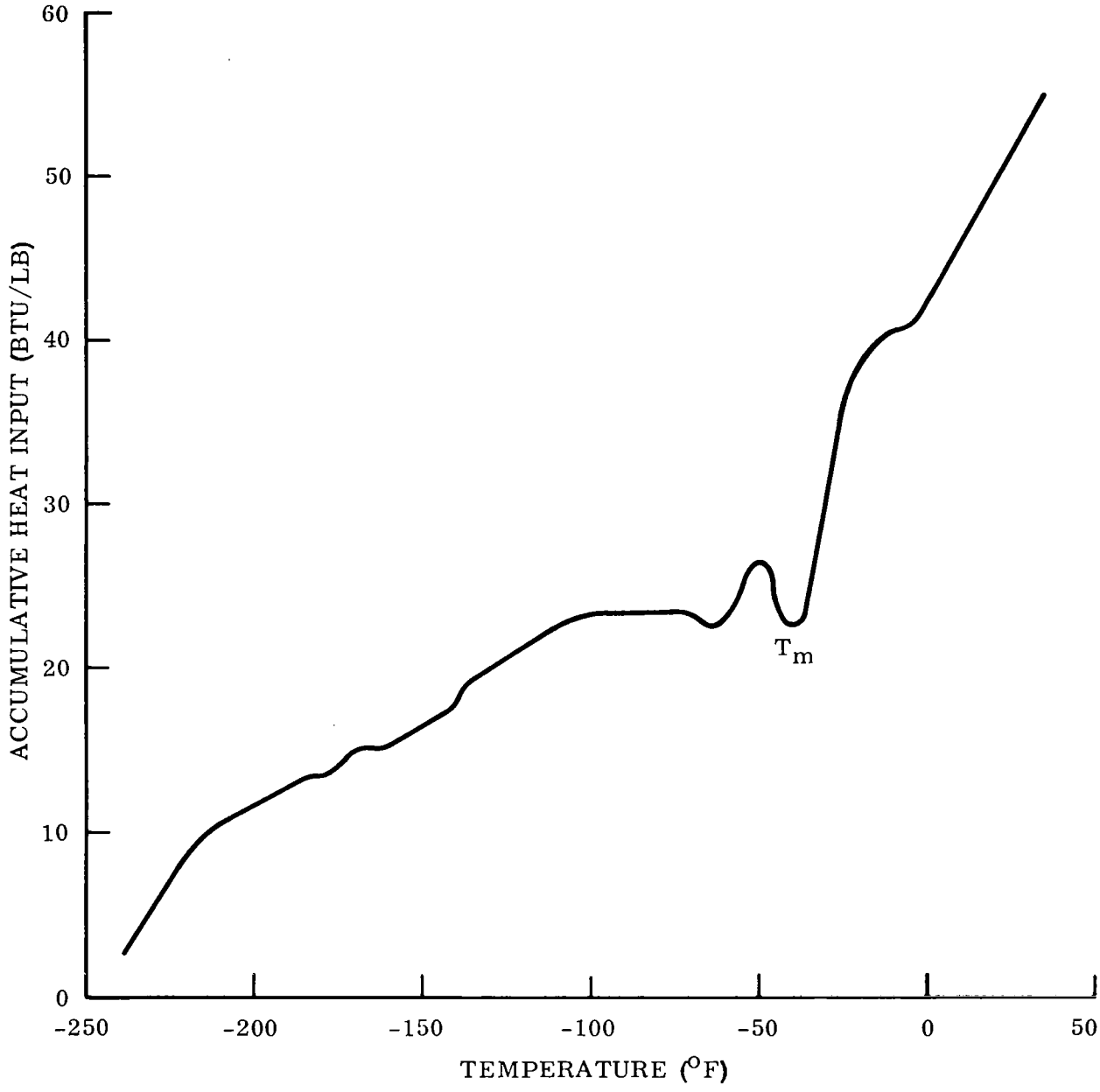

Figure 10. Continuous Specific Heat Measurement of NASA 602 Elastomer

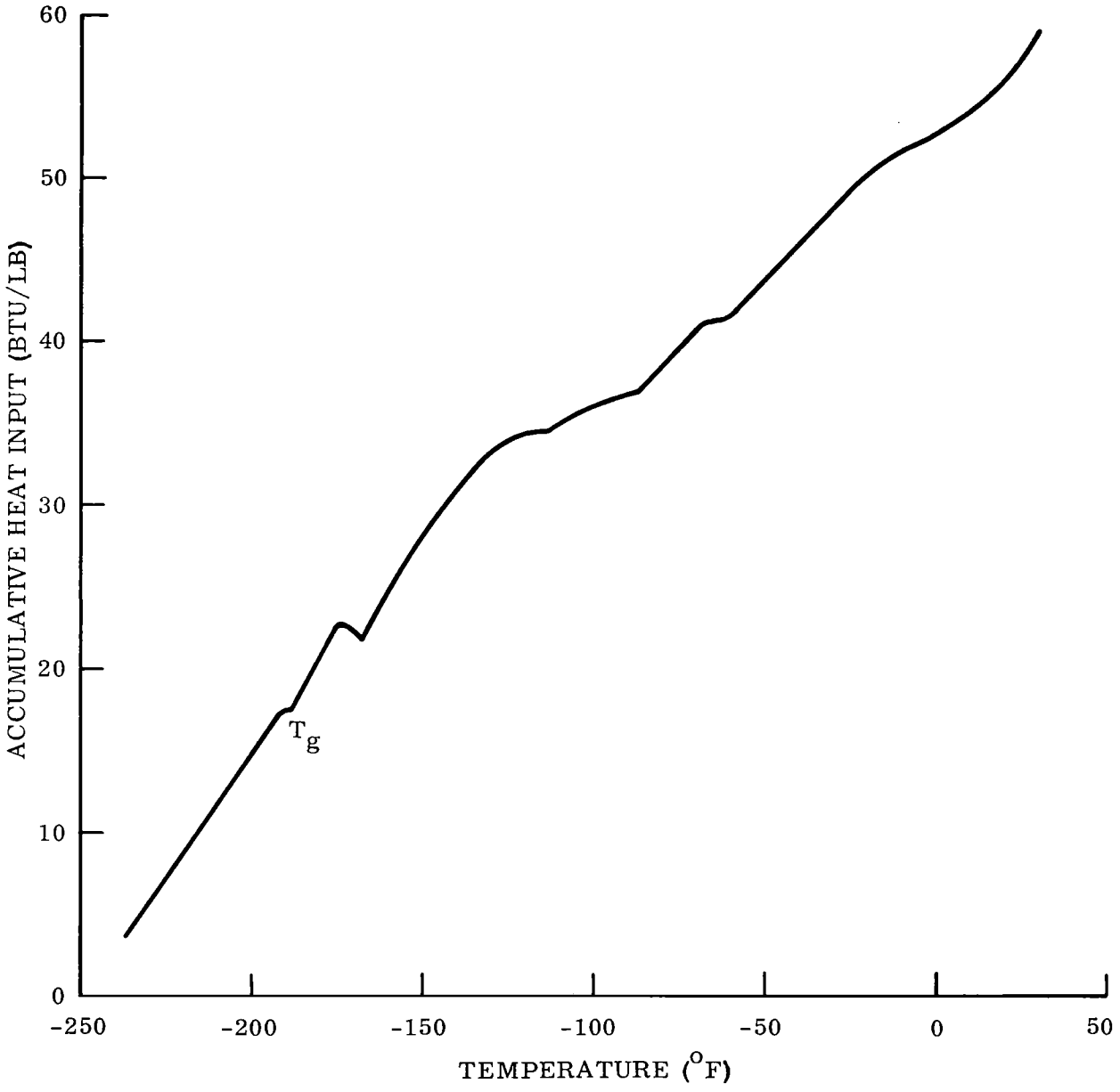

Figure 11. Continuous Specific Heat Measurement of ESM 1011 P Elastomer

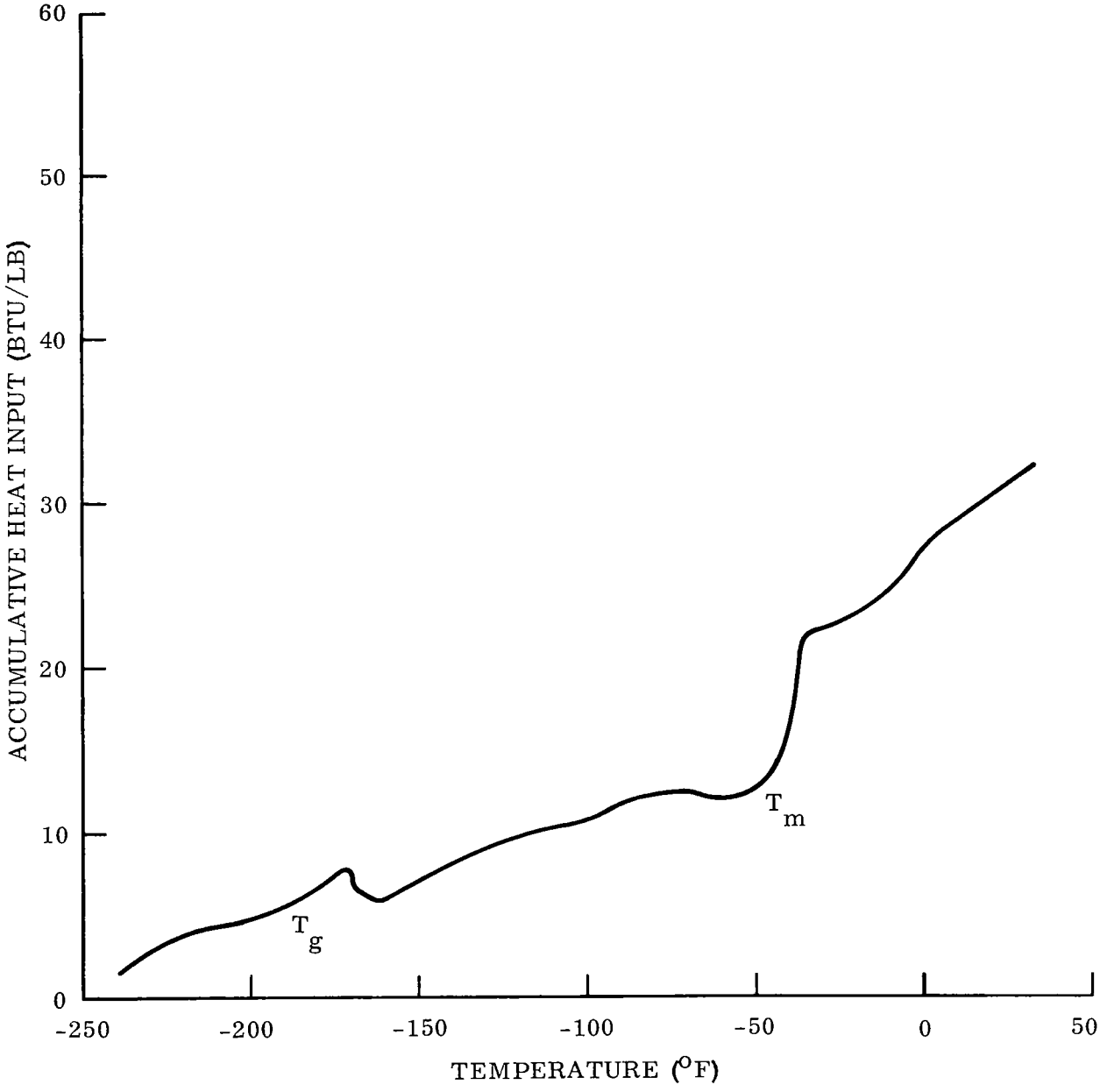

Figure 12. Continuous Specific Heat Measurement of ESM 1001 P Elastomer (First Run)

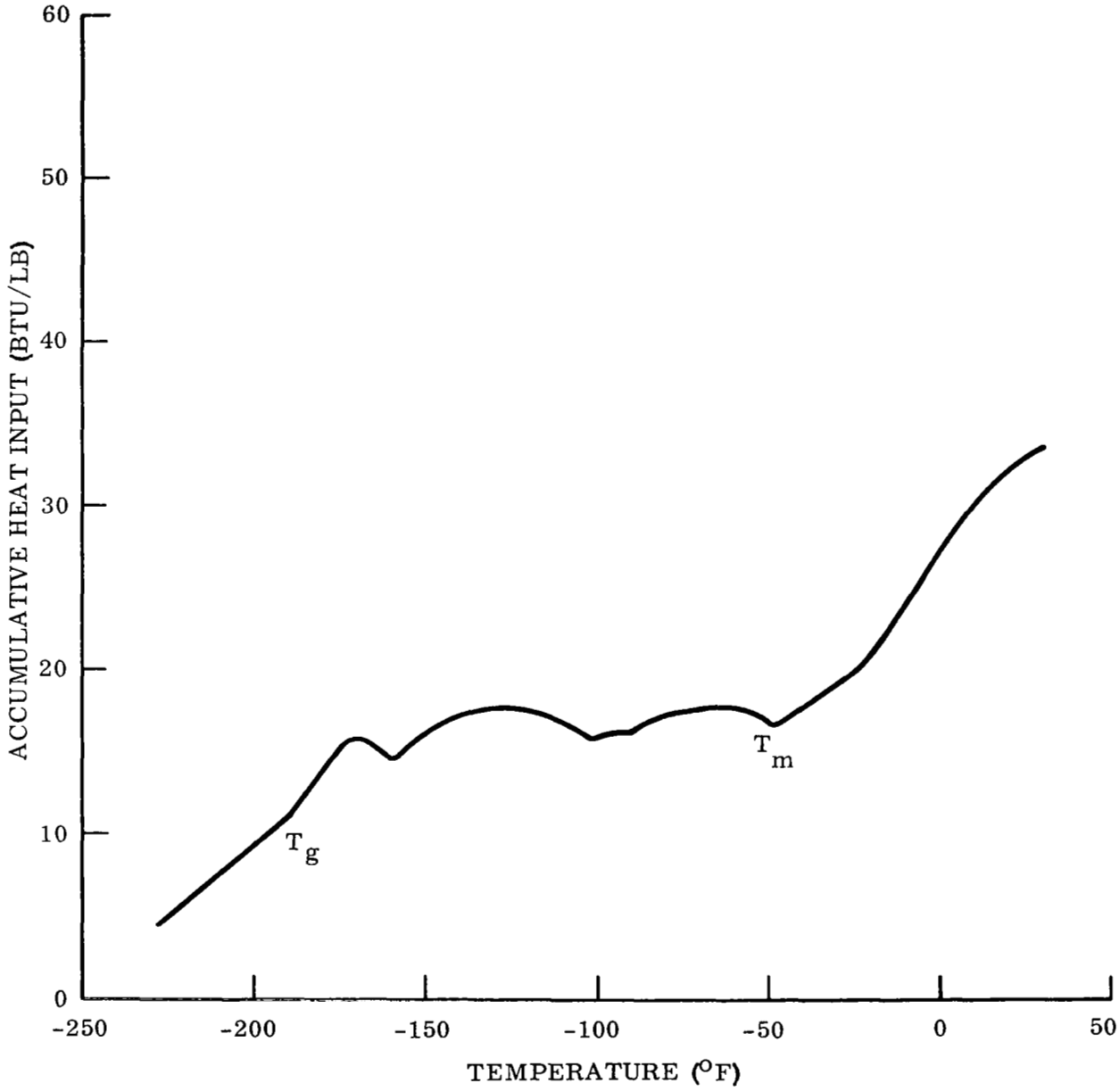

Figure 13. Continuous Specific Heat Measurement of ESM 1001 P Elastomer (Second Run)

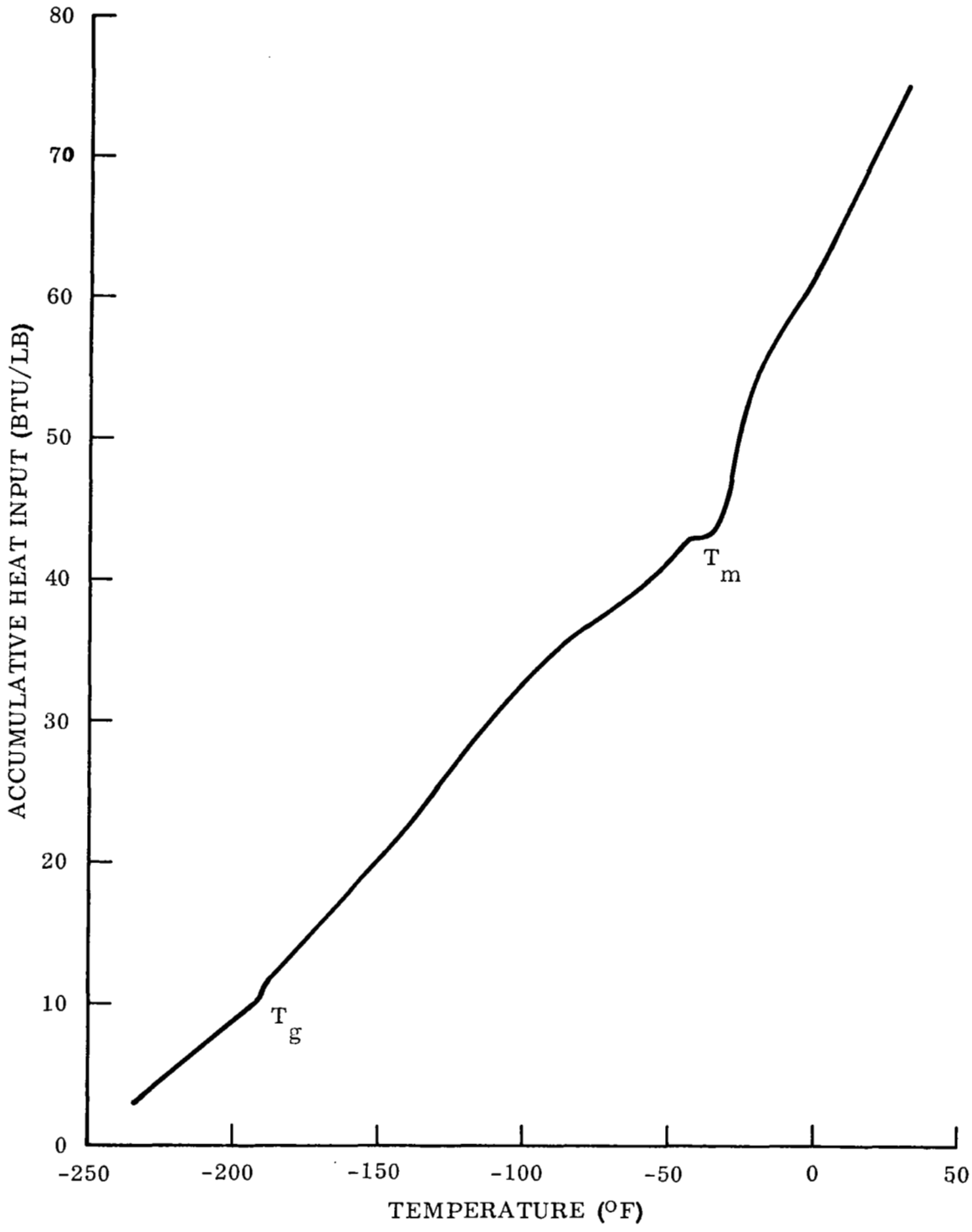

Figure 14. Continuous Specific Heat Measurement of ESM 1001 Elastomer

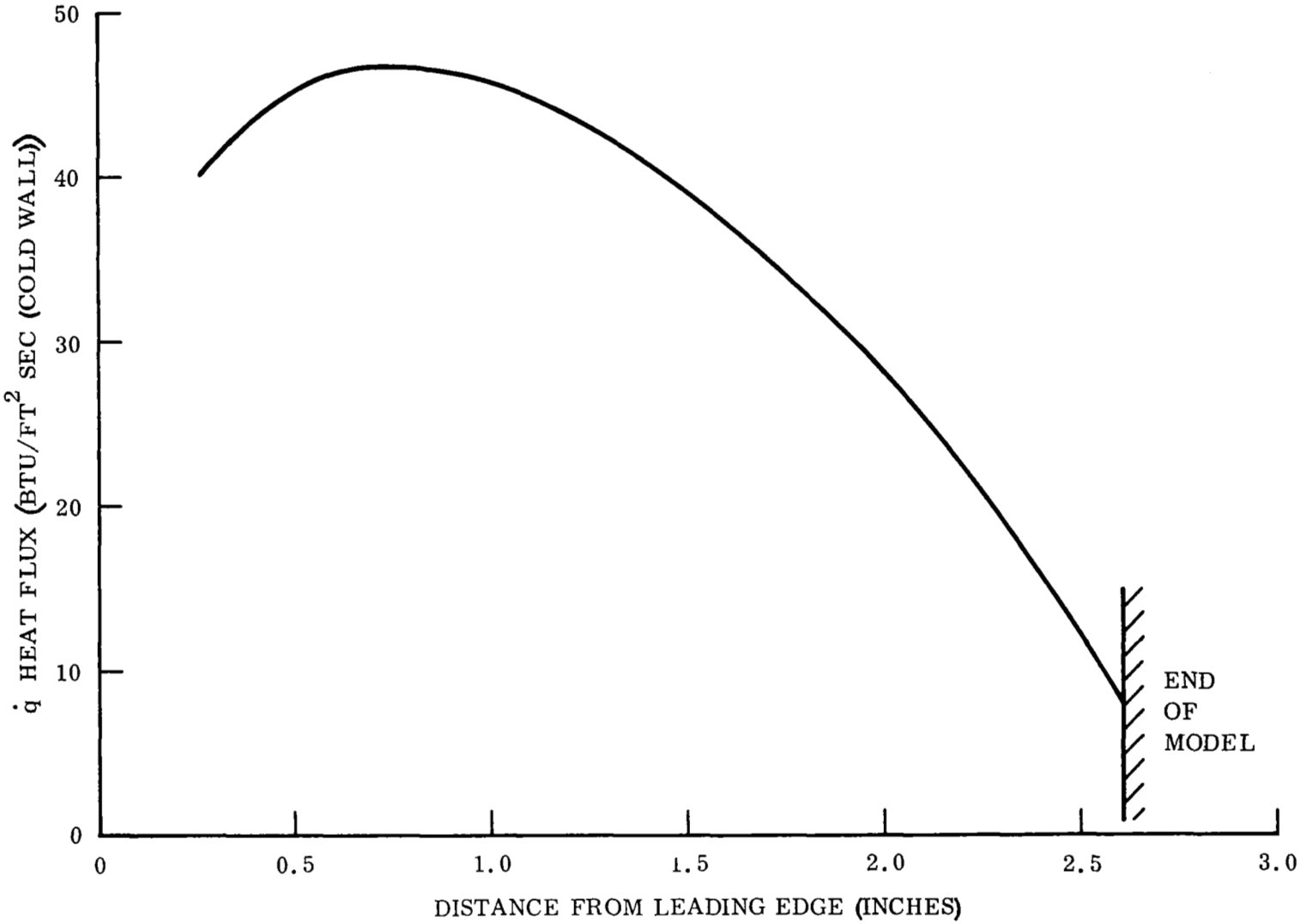

Figure 15. Heat Flux Distribution on the A-40 Ablation Model

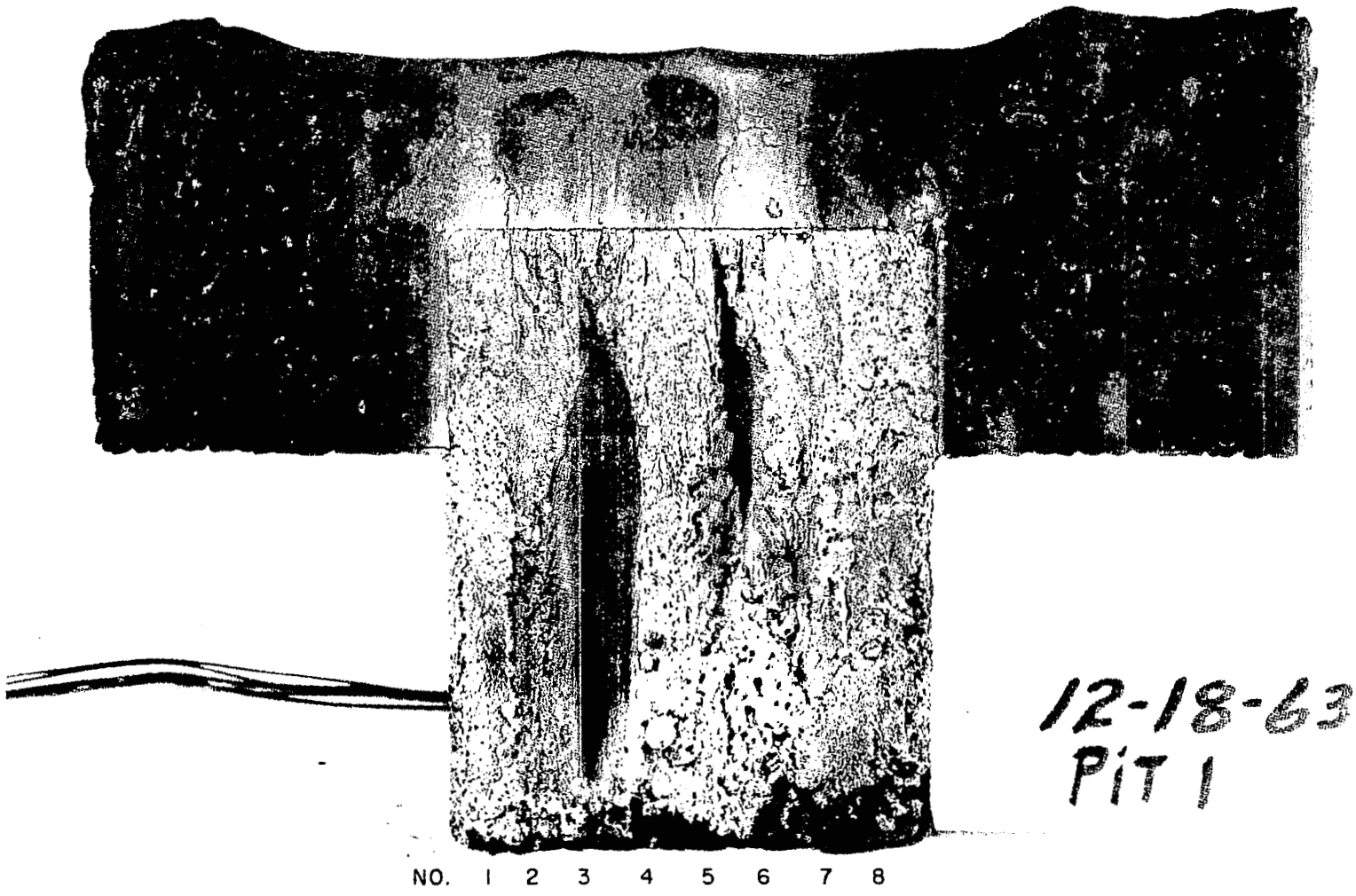

Figure 16. Malta Rocket Engine Pit #1 Model - After Test

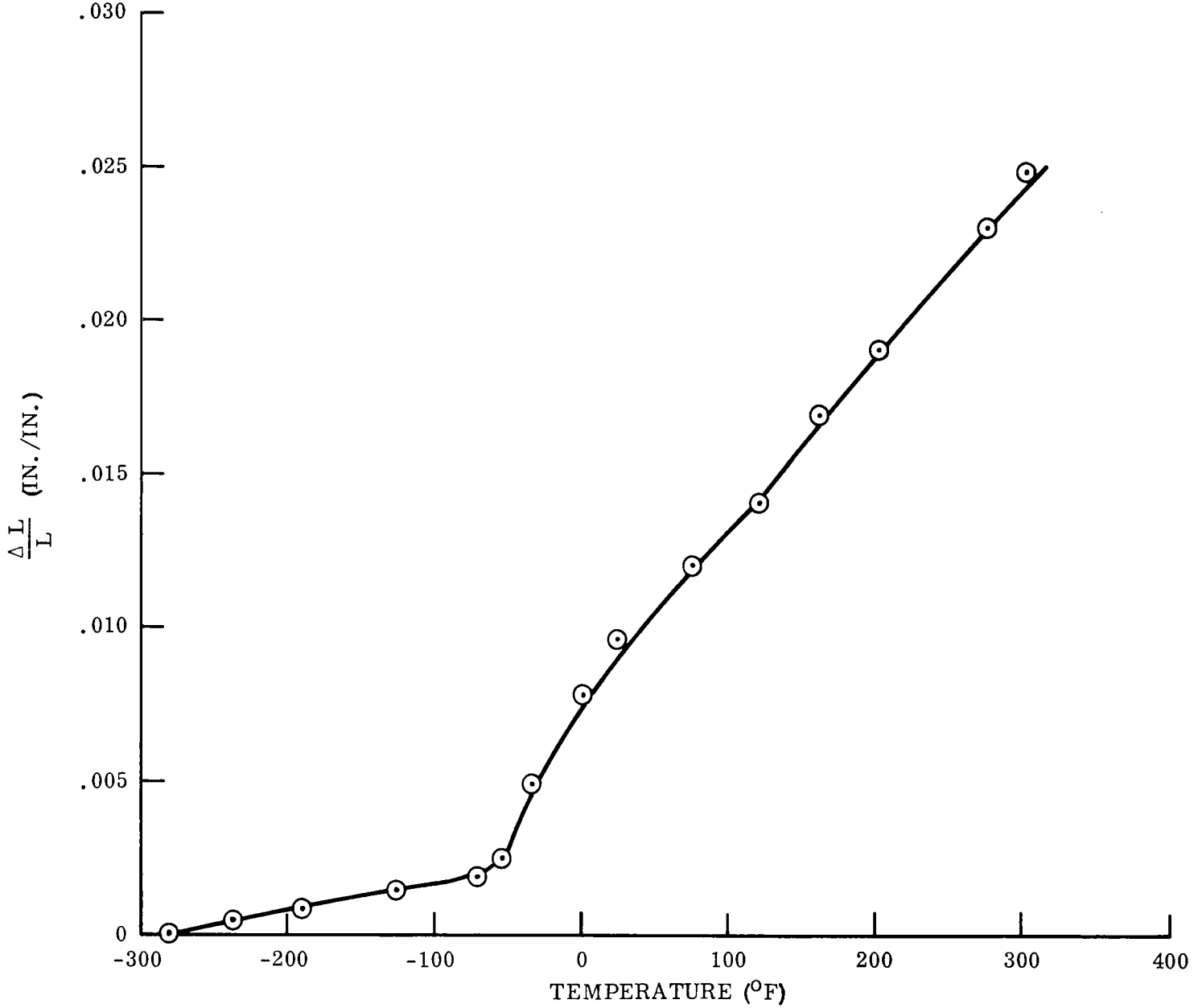

Figure 17. Thermal Expansion - Δ L/L versus Temperature NASA G-H/c-S

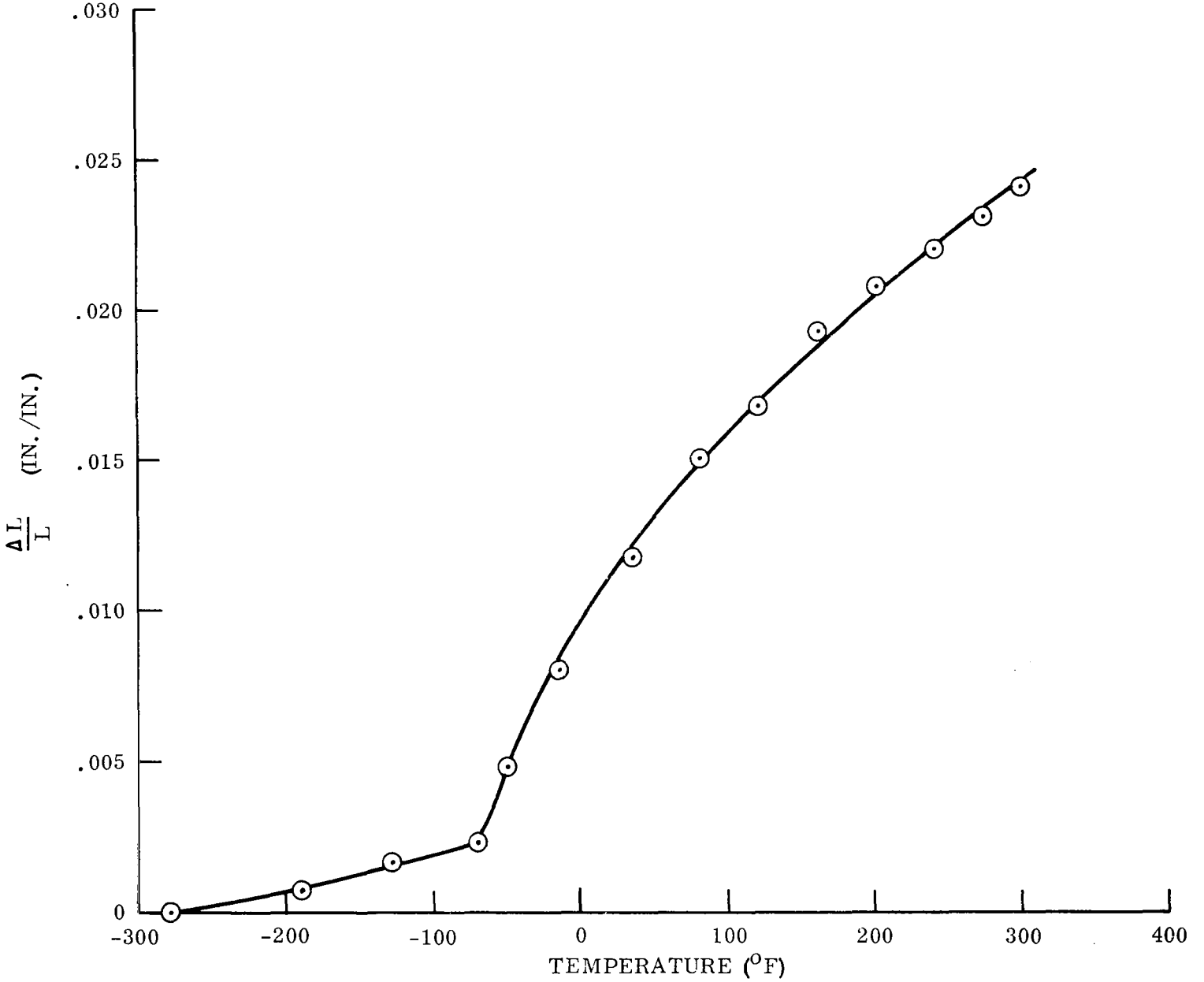

Figure 18. Thermal Expansion - Δ L/L versus Temperature ESM 1004B P

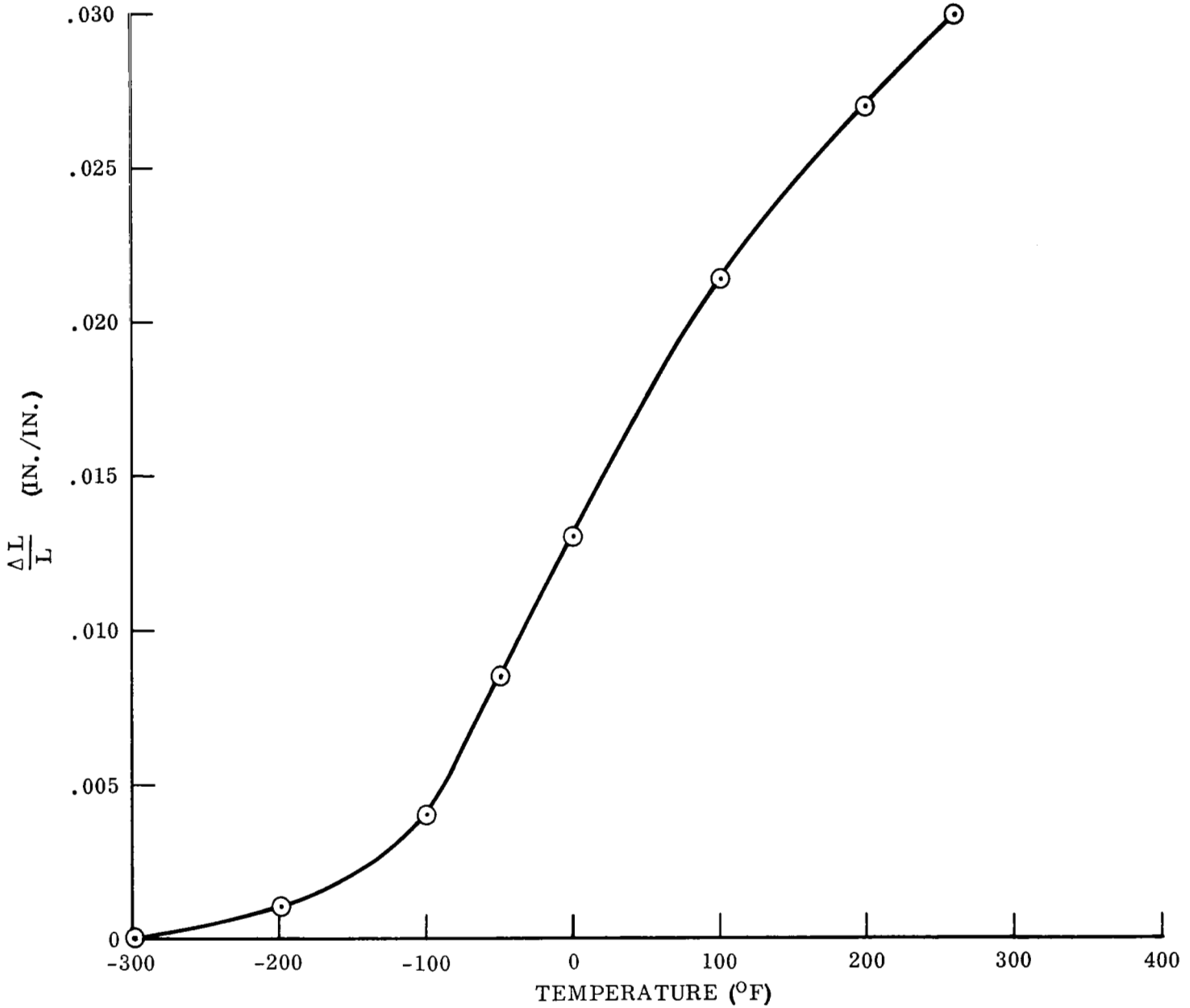

Figure 19. Thermal Expansion - Δ L/L versus Temperature ESM 1001 P

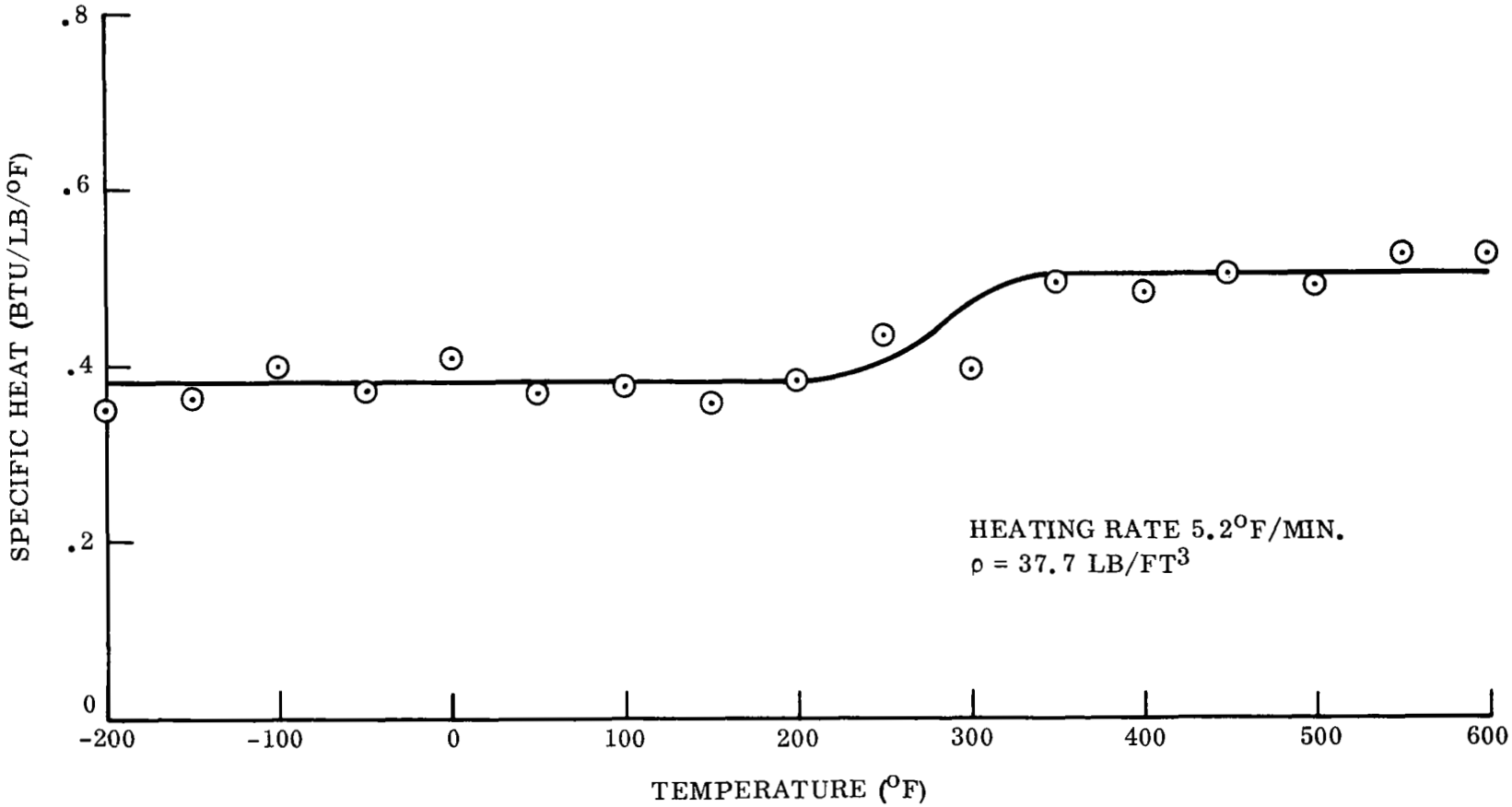

Figure 20. Specific Heat of ESM 1001 P

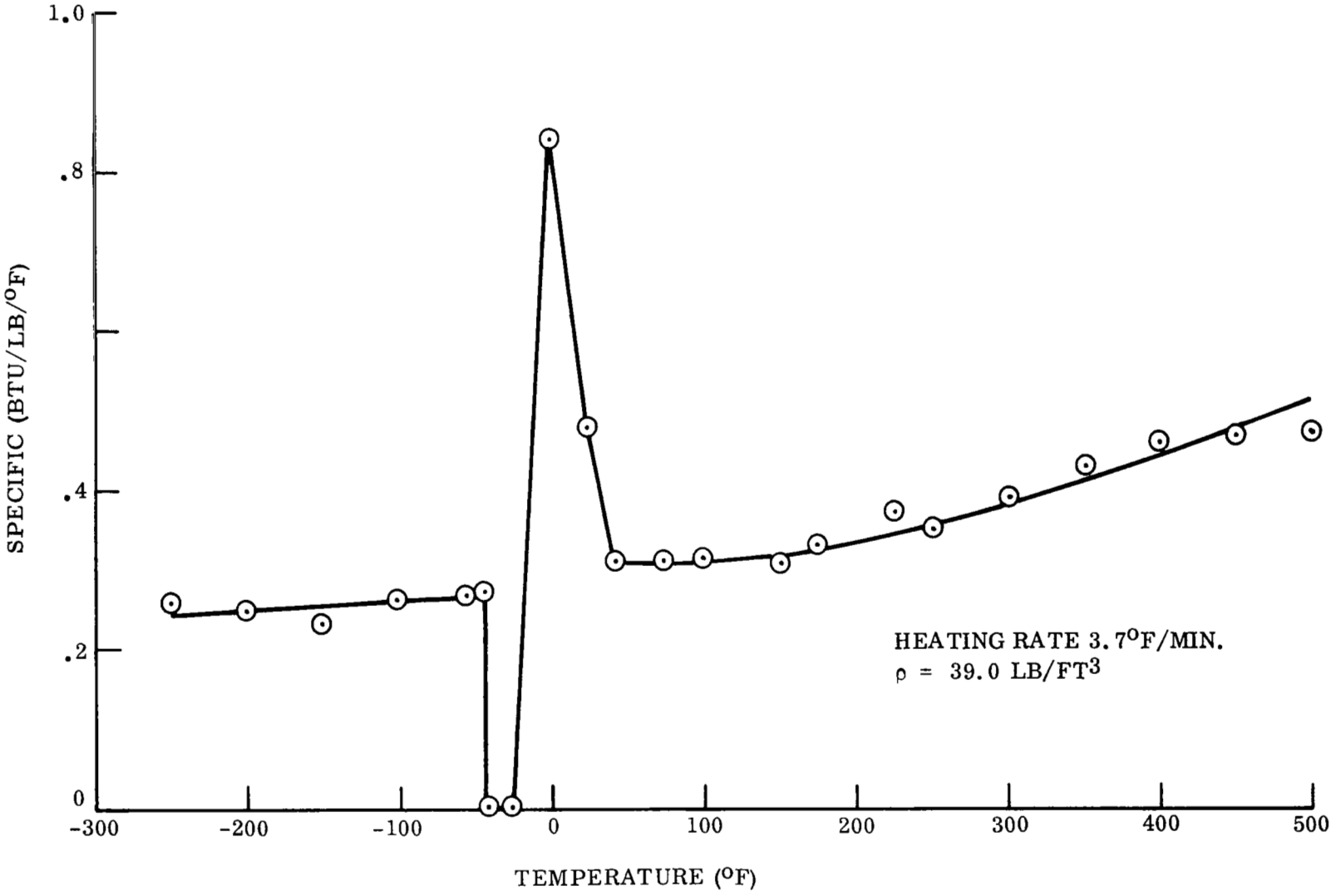

Figure 21. Specific Heat of ESM 1004B P

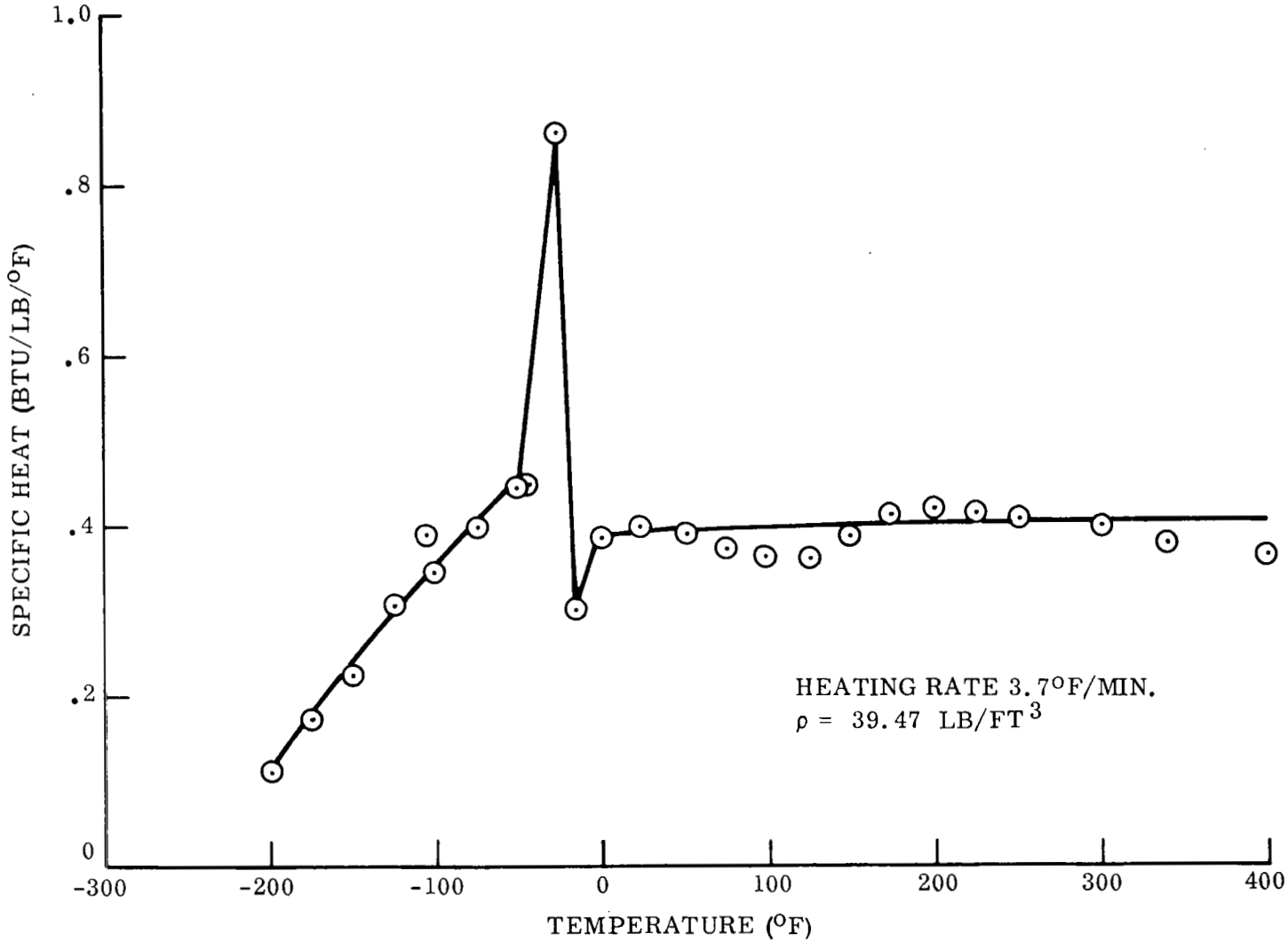

Figure 22. Specific Heat of NASA 602

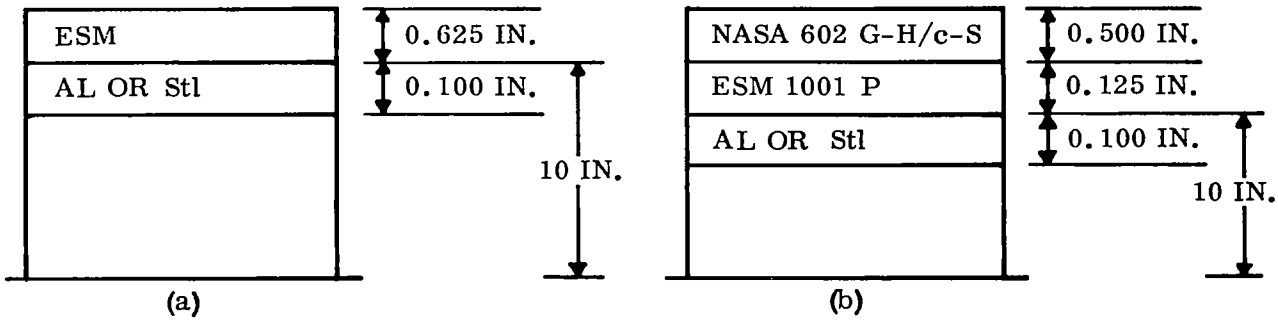

Figure 23. Structural Analysis Configuration

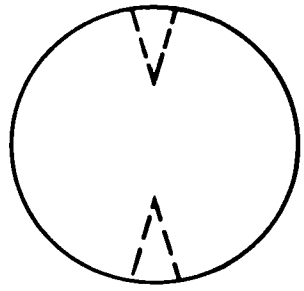

Figure 24. Scale-Up Fabrication of NASA 602 G-H/c-S - ESM 1001 P Composite

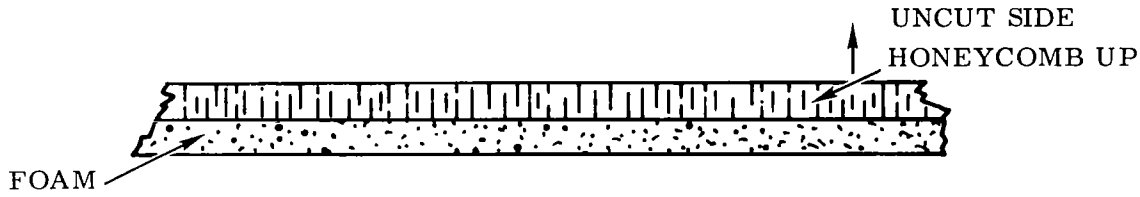

Figure 25. Scale-Up Fabrication of NASA 602 G-H/c-S - ESM 1001 P Composite

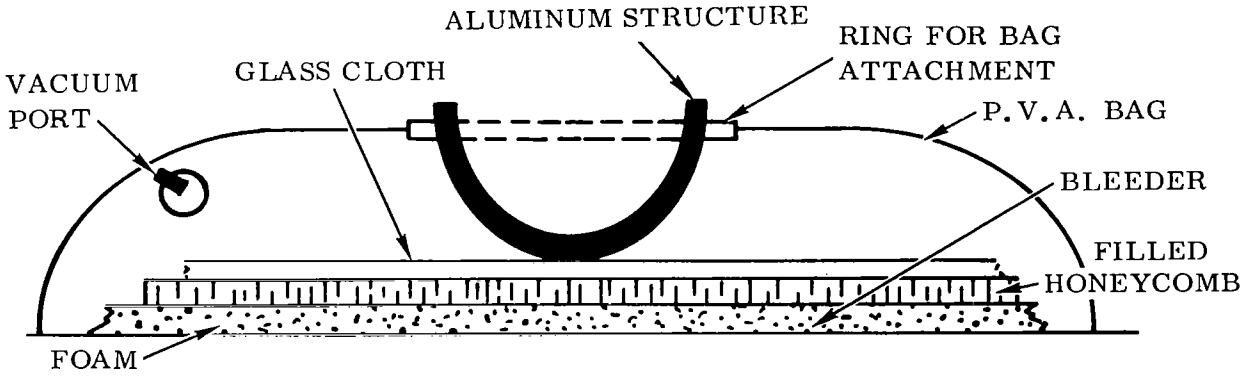

Figure 26. Scale-Up Fabrication of NASA 602 G-H/c-S - ESM 1001 P Composite

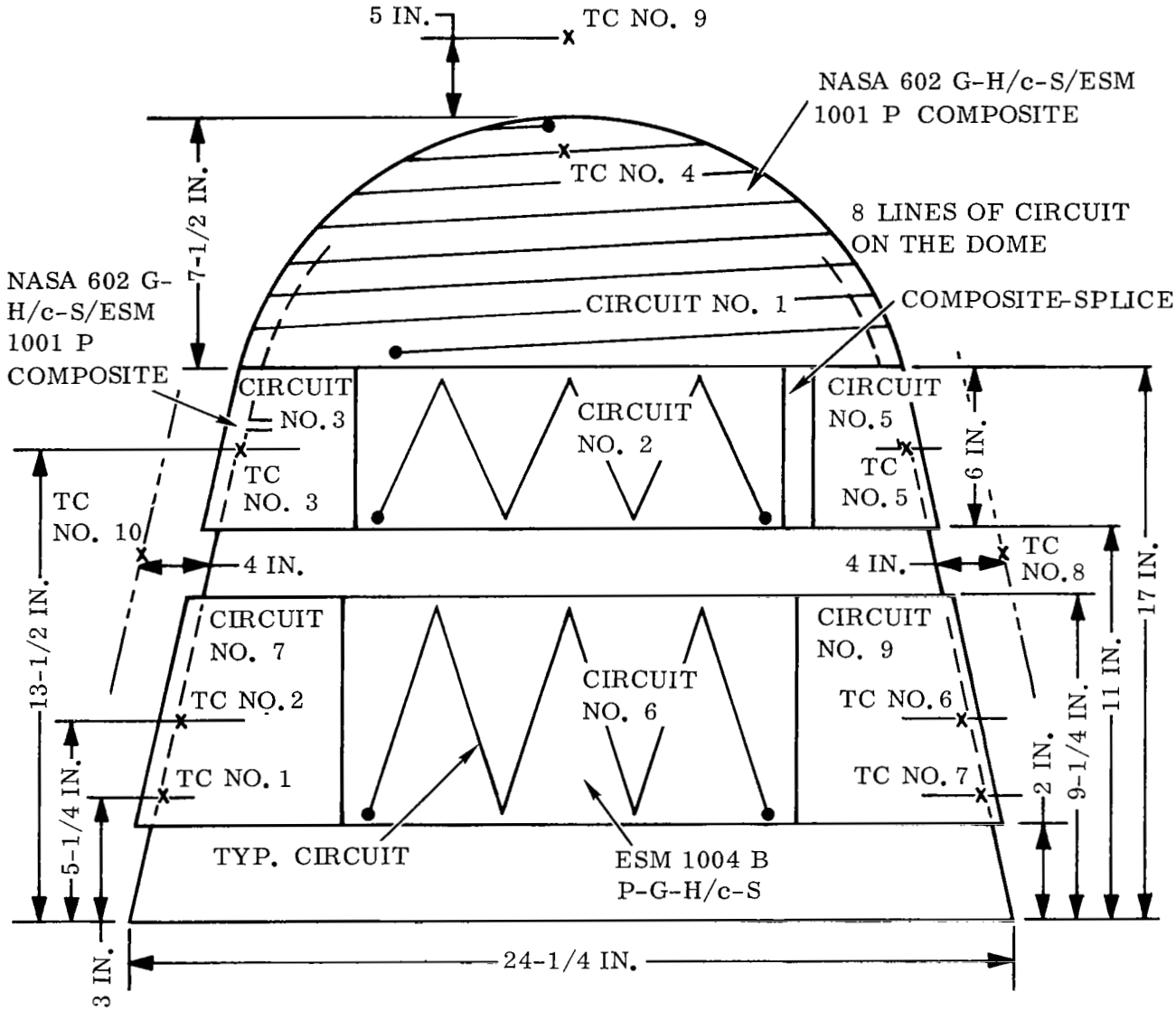

NOTES

1. CIRCUIT NO. 4 IS 180° FROM NO. 2.
2. CIRCUIT NO. 8 IS 180° FROM NO. 6.
3. TC NO. 3 DIRECTLY BEHIND THE COMPOSITE-SPLICE, ATTACHED INSIDE STRUCTURE.
4. TC NO. 1, 2,AND 3, ARE IN LINE ATTACHED INSIDE STRUCTURE.
5. TC NO. 5, 6,AND 7,ARE IN LINE AND 180° FROM TC NO. 1, 2, AND 3, INSIDE.
6. TC NO. 4 TOP DOME, INSIDE.
7. CIRCUIT NOS. 1, 2, 3, 4, AND 5 ON NASA 602 G-H/c-S COMPOSITE, CIRCUIT NOS. 6, 7, 8, AND 9 ON ESM 1004B P-G-H/c-S.

Figure 27. Instrumented Thermal Cycle Unit

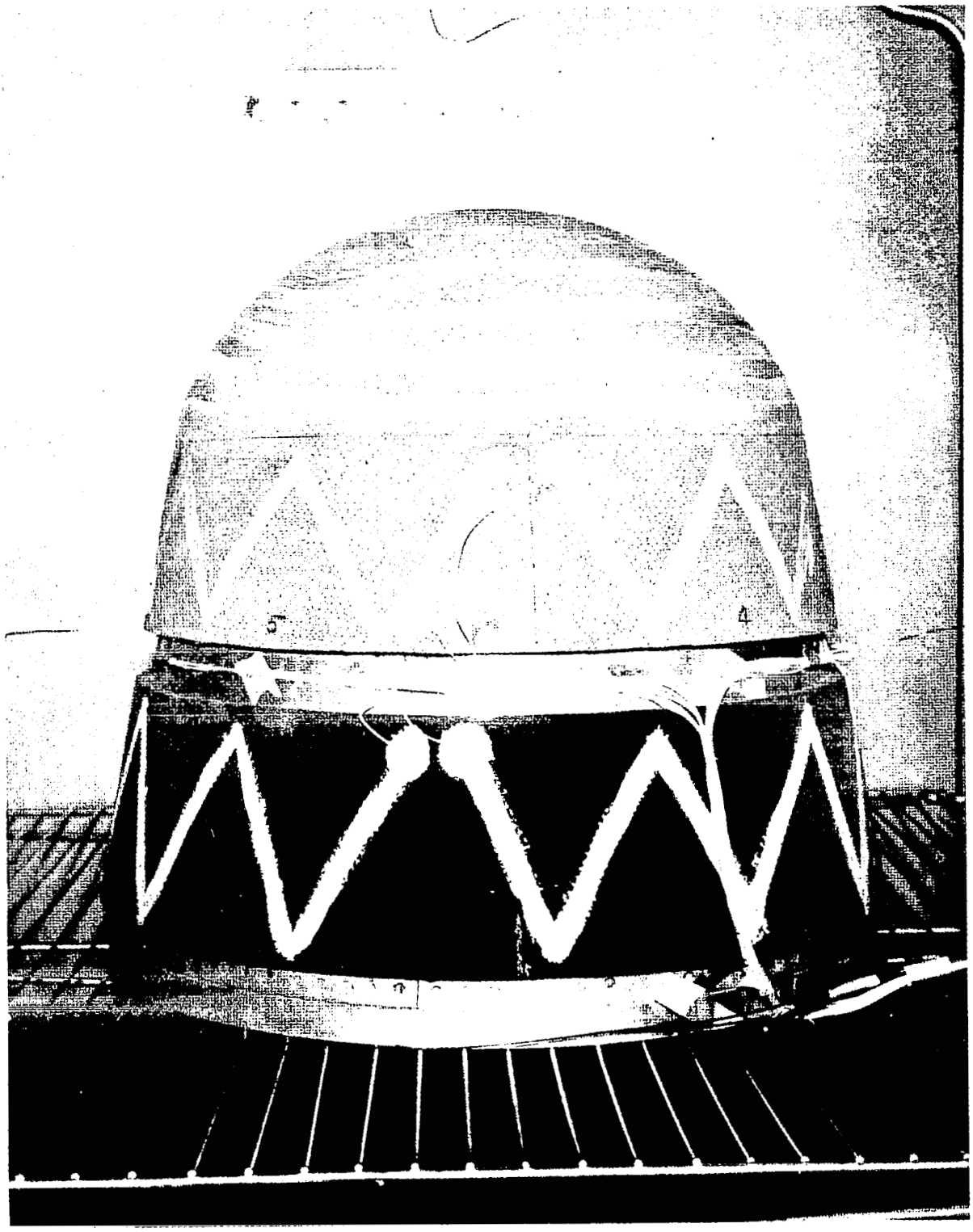

Figure 28. Instrumented Thermal Cycle Unit

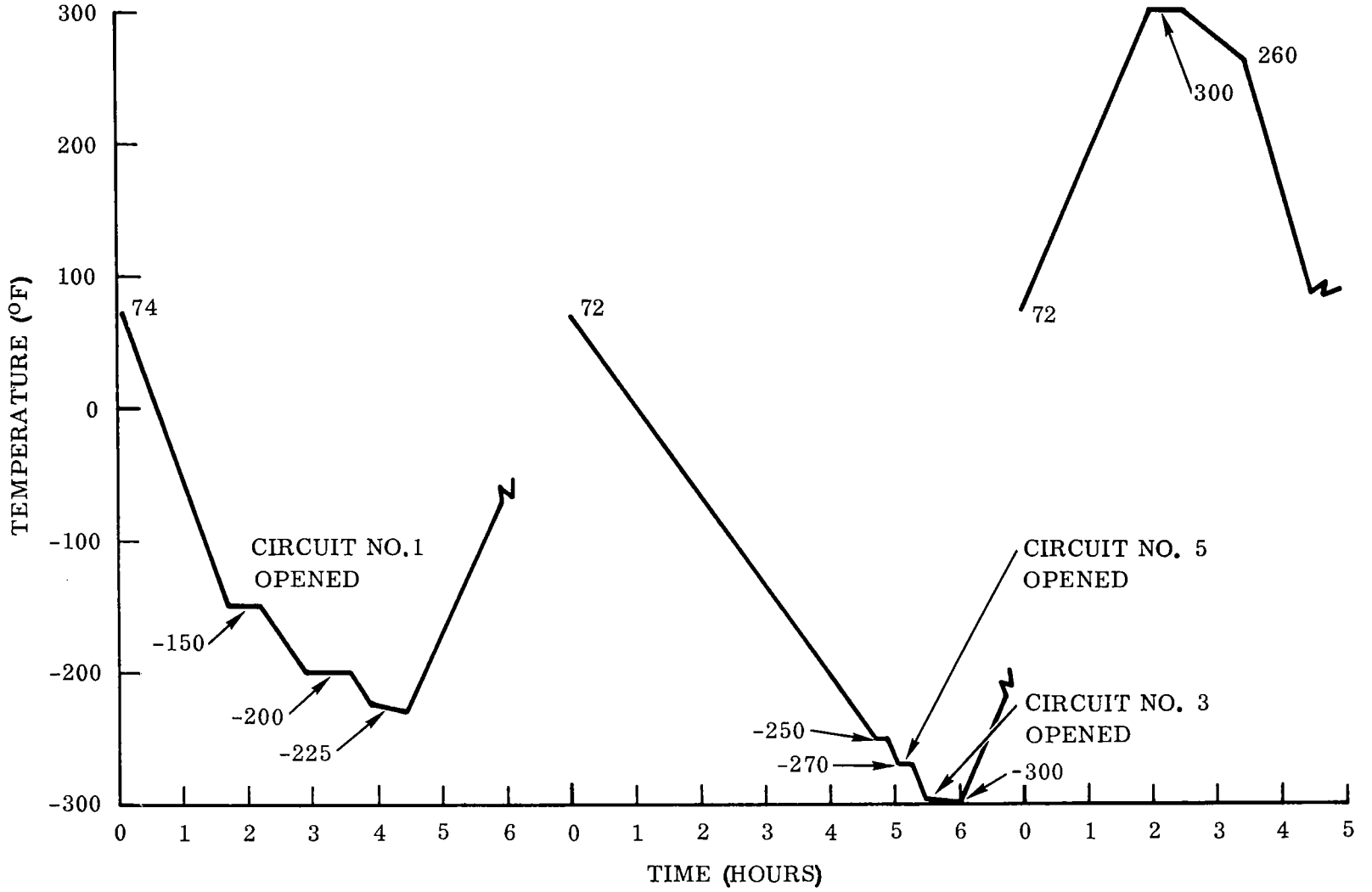

Figure 29. Thermal Cycle

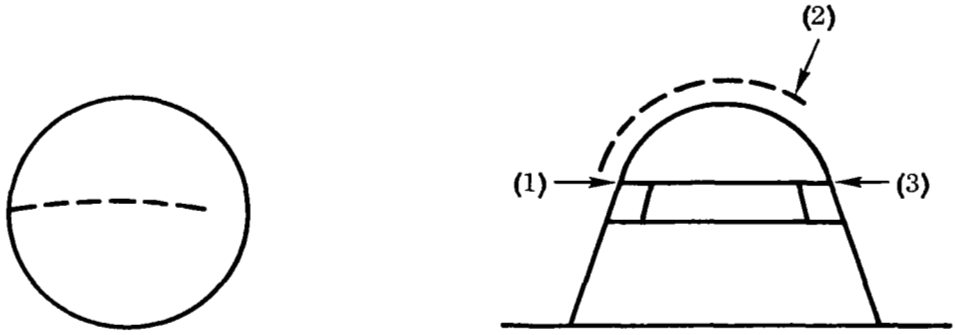

Figure 30. Location of Cracks in Thermal Cycle Unit

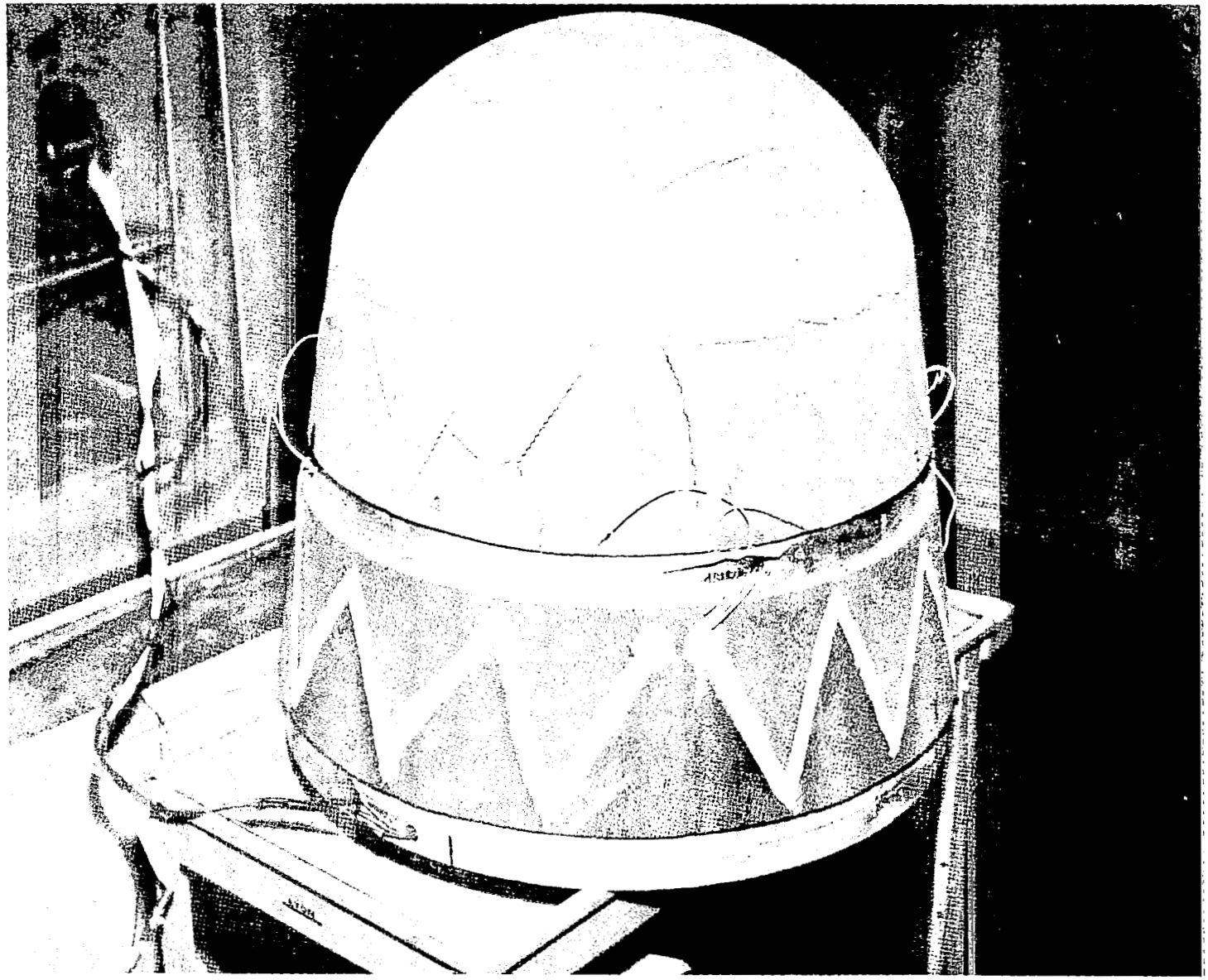

Figure 31. Thermal Cycle Unit After Test

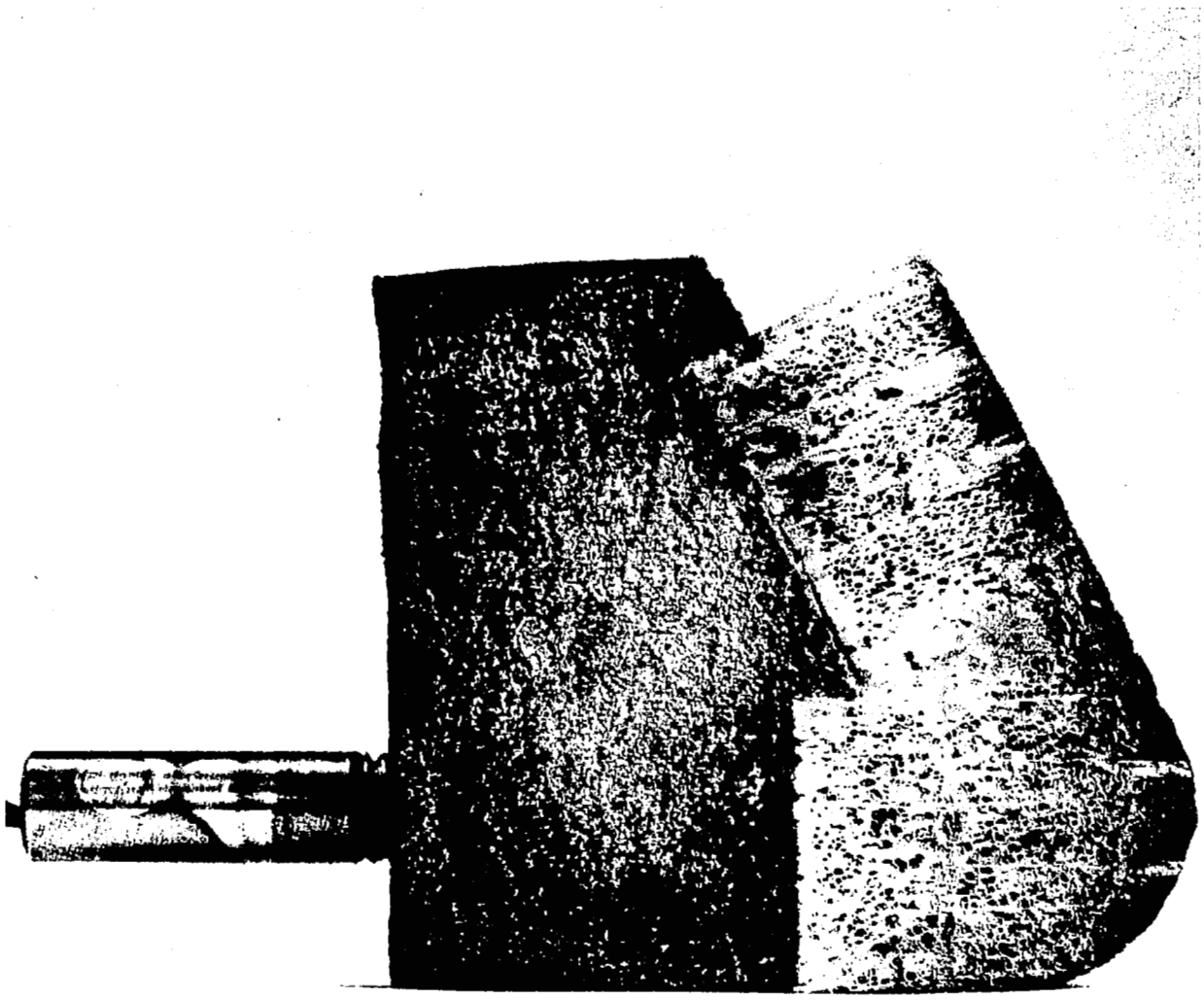

Figure 32. Shape Stable Silicone Material No. 3 - Ablation Model - Before Test

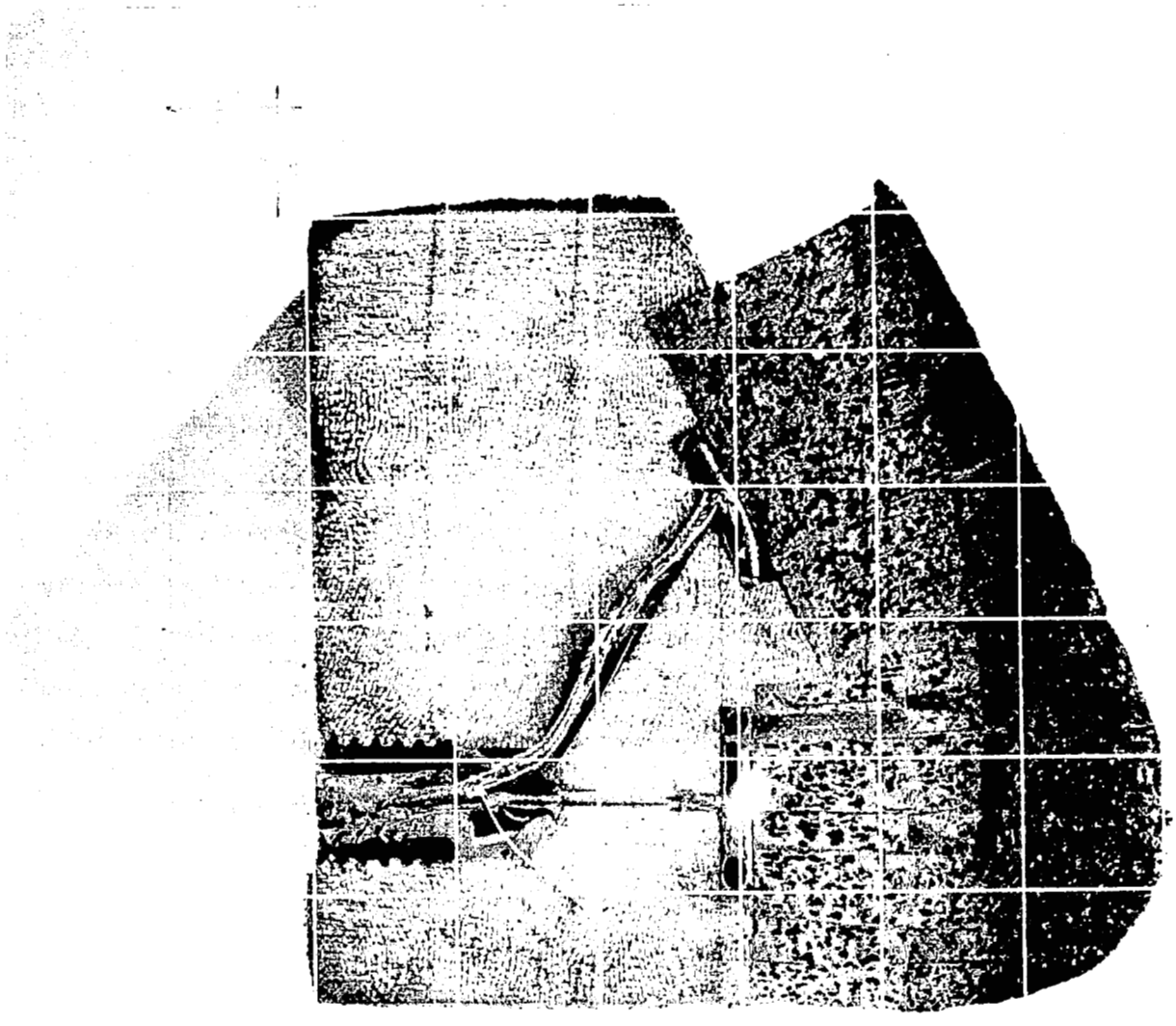

Figure 33. Shape Stable Silicone Material No. 3 - Ablation Model - After Test

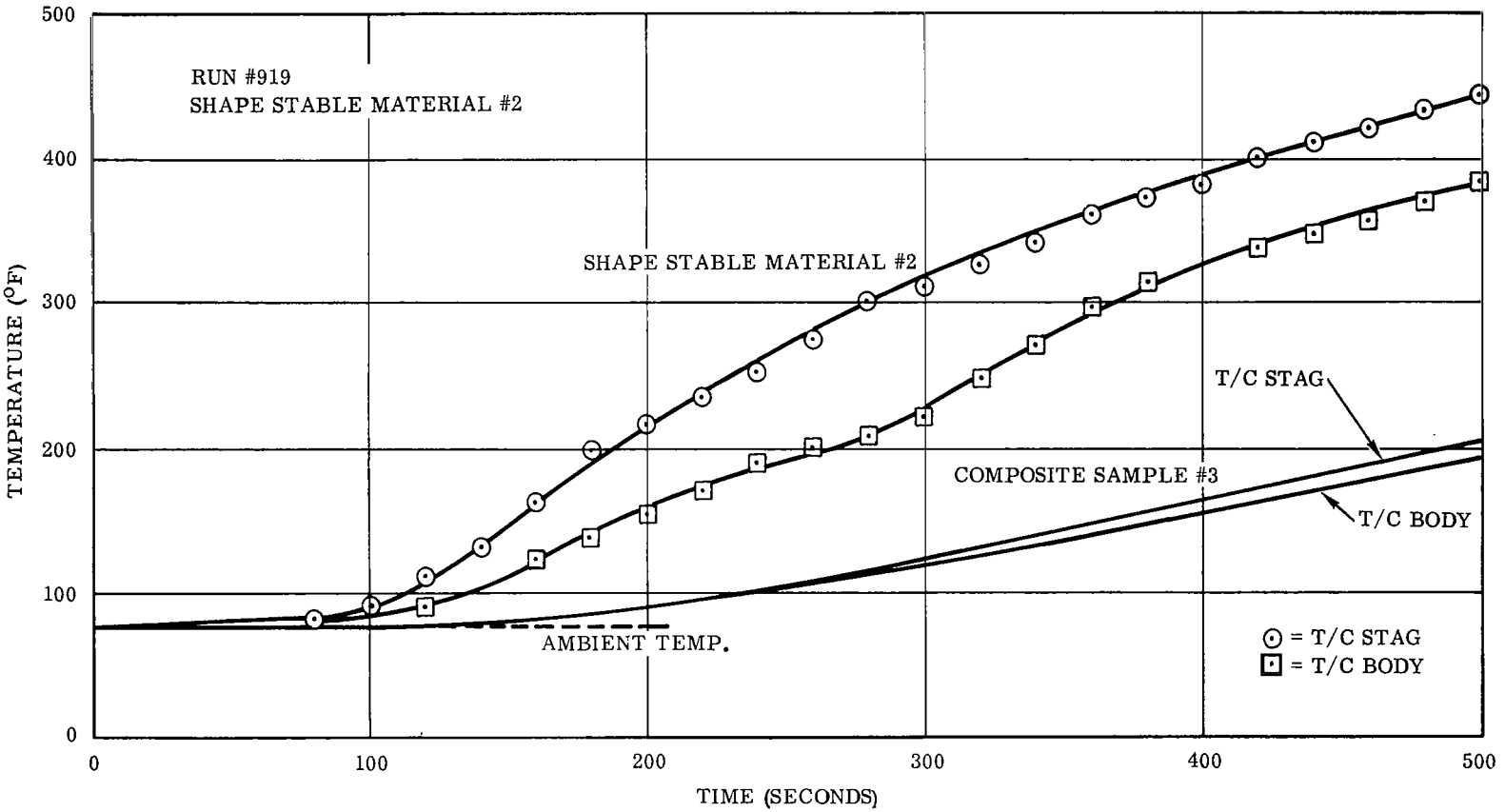

Figure 34. Backface Temperature of Composite Sample #3 In Simulation Ablation Test

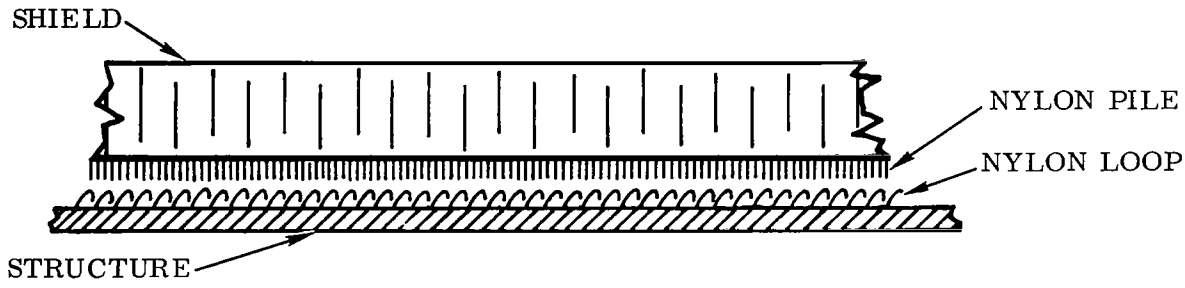

Figure 35. Illustration of "Loop and Pile" Fastening Method

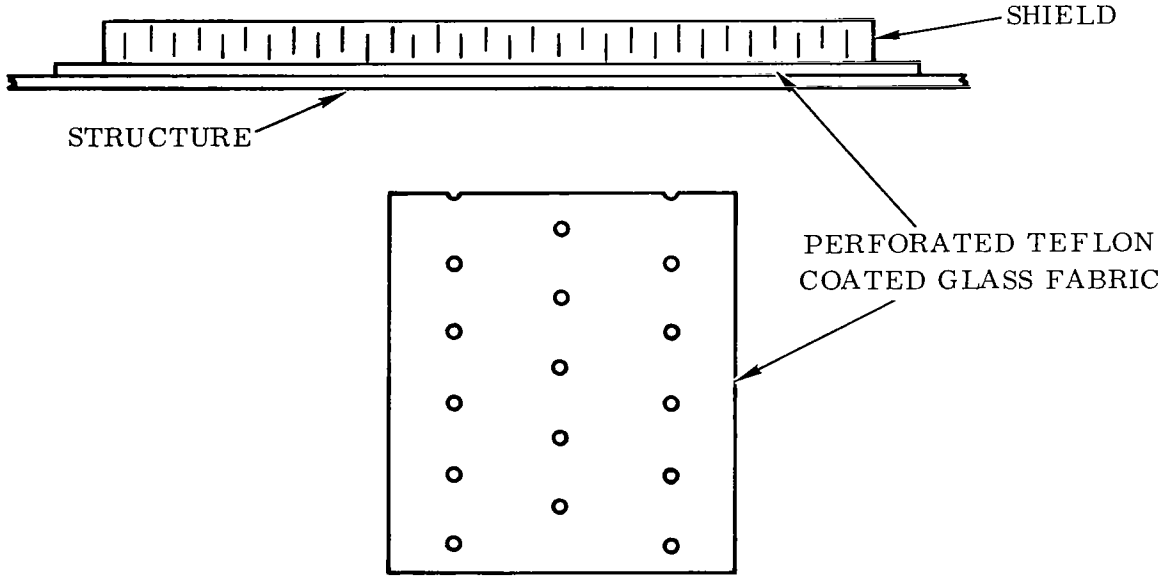

Figure 36. Illustration of "Perforated Interface" Fastening Method

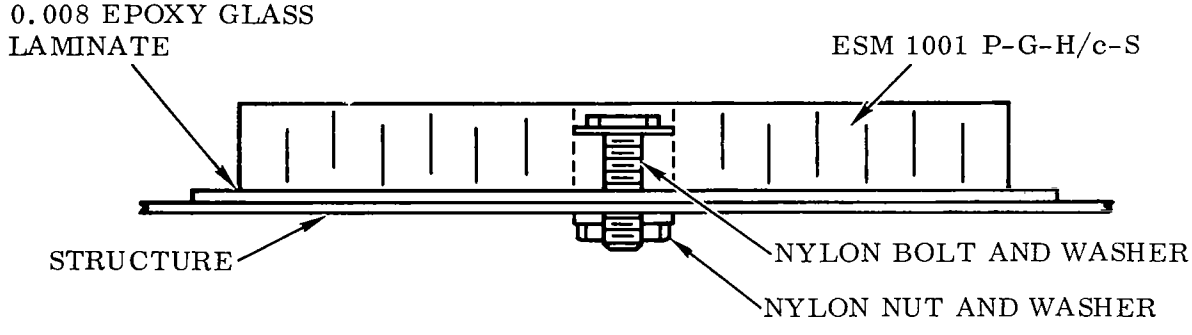

Figure 37. Illustration of Nut and Bolt Type Fastening

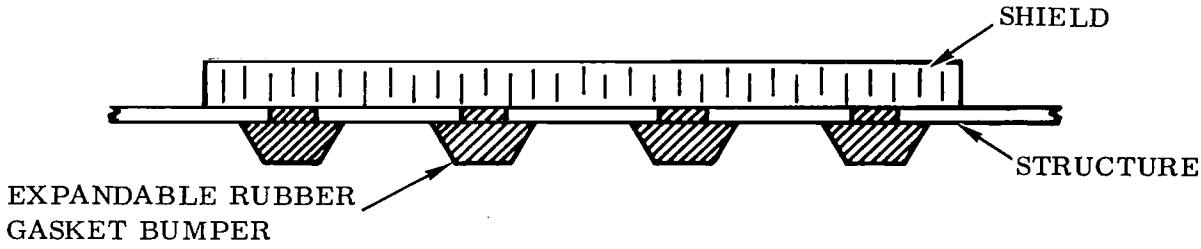

Figure 38. Illustration of "Expandable Bumper Gasket" Fastening

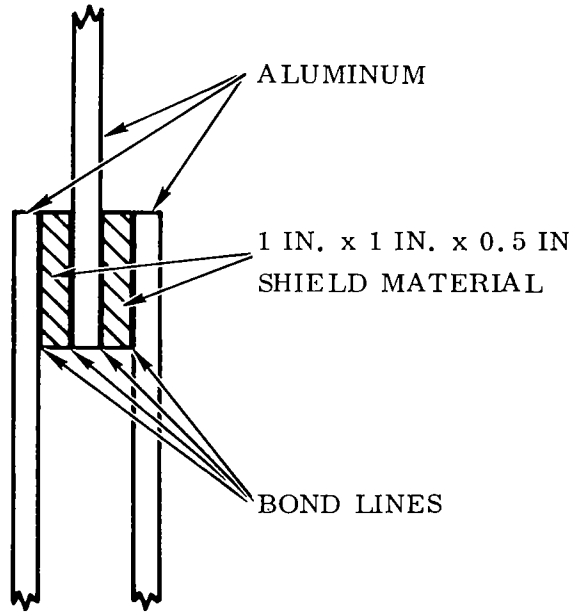

Figure 39. Bond-Shear Test Sample Configuration

TABLE 1

PLATE THERMAL CYCLE TEST RESULTS

	Resin	Bond	Failure °F
(w)	1. ESM 1001-G-H/c	HT 424	-150
	2. ESM 1001-G-H/c	B.E. (RTV-560)	-150/-200
	3. ESM 1001P-G-H/c	HT 424	-300
	4. ESM 1001P-G-H/c	B.E.	-250/-275
	5. DC 325-G-H/c	HT 424	-120/-140
	6. NASA 602-G-H/c	HT 424	-110/-150
	7. NASA 182-G-H/c	B.E.	-115
	8. ESM 1001-G-H/c-S	B.E.	-170
(x)	1. ESM 1001P	B.E. (RTV-560)	-300***
	2. ESM 1001P-G-H/c-S	B.E.	-300***
	3. ESM 1001P-Asb-H/c-S	B.E.	-275
	4. ESM 1001P (Flex. Glass H/c)	B.E.	Not Run
	*5. ESM 1001P**(Disconnected P-G Pillars)	B.E.	-300***
	6. ESM 1001P (Glass Cloth Laminate)	B.E.	-300***
	7. ESM 1011P-G-H/c-S	RTV 511	-300***

*Number 5 (x) was subjected to a more stringent thermal cycle after successfully completing the standard cycle to -300°F. The sample was allowed to return to room temperature then dropped to -240°F and held for 16 hours. Returned to room temperature then to +300°F returned to room temperature then dropped to -300°F and back to room temperature.

**Same as split H/c except twice as much Phenolic Glass removed in cutting process.

***No Failure

TABLE 2

THERMAL CYCLE RESULTS

Resin	Bond	Failure °F
1. ESM 1011 P-G-H/c-S	RTV-511	No failure*
2. ESM 1001 P-G-H/c-S	RTV-560	No failure*
3. NASA 602 G-H/c-S	RTV-560	-150
4. ESM 1004A P-G-H/c-S	RTV-560	No failure*
5. ESM 1001 P-Asb-H/c-S	RTV-560	No failure*
6. NASA 602 Asb-H/c-S	RTV-560	-180

*No failure noted down to -300° F

TABLE 3

HYPERSONIC ARC TUNNEL OPERATING CONDITIONS

Power KW	$\dot{m}$ lb/sec	Plenum ID (in.)	Throat diam (in.)	Swirl ID (in.)	$\dot{q}_{st}$ (1) (Measured)	h_s/RT_o
255	0.0013	1.5	5/32	3/8	-	503
235	0.0015	1.5	5/32	7/16	76	316
285	0.00175	1.5	5/32	7/16	-	333
77	0.0014	1.5	5/32	7/16	49	162
200	0.0010	1.5	0.099	7/16	15	-

TABLE 4

FORMULATIONS FOR ABLATION SCREENING

	Elastomer	Reinforcement	Density lb/ft^3
*	(1) ESM 1001 G-H/c	Phenolic Glass Honeycomb	54.2
	(2) ESM 1001 P-G-H/c	Phenolic Glass Honeycomb	40.4
	(3) DC 325 G-H/c	Phenolic Glass Honeycomb	57.5
	(4) NASA 602 G-H/c	Phenolic Glass Honeycomb	36.4
	(5) NASA 182 G-H/c	Phenolic Glass Honeycomb	39.4
	(6) ESM 1001 P	Unsupported	36.0
	(7) RTV-560	Phenolic Glass Honeycomb + Glass Fibers**	42.2
	(8) RTV-560	Phenolic Glass Honeycomb + Quartz Fibers	43.0
	(9) RTV-560	Phenolic Glass Honeycomb + Graphite Fibers	48.8
	(10) RTV-560	Phenolic Glass Honeycomb + Asbestos	40.2
	(11) RTV-560	Phenolic Glass Honeycomb + Zirconia Fibers	51.8
	(12) RTV-560	Phenolic Glass Honeycomb + Magnesium Fibers	50.7
	(13) RTV-560	Phenolic Glass Honeycomb + Phenolic Micro-balloons	41.0
	(14) RTV-560	Phenolic Glass Honeycomb + Silica Ecco-spheres	41.7
	(15) RTV-560	Phenolic Glass Honeycomb + Acid Leached Asbestos Low Ph	43.3
	(16) RTV-560	Phenolic Glass Honeycomb + Bone Shellac	55.3
	(17) RTV-560	Phenolic Glass Honeycomb + Al. Silicate High Ph	39.9
	(18) RTV-560	Phenolic Glass Honeycomb + Potassium Titanate	58.5
	(19) RTV-209-127-623A	Phenolic Glass Honeycomb + Asbestos	41.3
	(20) RTV-209-127-623B	Phenolic Glass Honeycomb + Asbestos	41.9

*The standards 1 to 5 were also tested in the NASA Jet Arc

**Fiber concentration in all cases = 5 percent

TABLE 5

ABLATION RESULTS OF SCREENING FORMULATIONS IN PROPANE TORCH TEST (20 - 22 BTU)

Time to Backface Temp. - $\Delta T = 200°F$

Sample	Thickness (in.)	Minutes	Density lb/ft^3
(1) ESM 1001 G-H/c	0.66	6.75	54.2
(2) ESM 1001 P-G-H/c	0.89	11.30	40.4
(3) DC 325 G-H/c	0.63	10.60	57.5
(4) NASA 602 G-H/c	0.98	16.42	36.4
(5) NASA 182 G-H/c	0.91	12.87	39.4
(6) ESM 1001 P	1.00	16.40-17.10	36.0
(7) RTV-560 + 5% Glass	0.85	10.30	42.2
(8) RTV-560 + 5% Quartz	0.83	9.30	43.0
(9) RTV-560 + 5% Graphite	0.74	17.10	48.8
(10) RTV-560 + 5% Asb	0.89	12.47	40.2
(11) RTV-560 + 5% Zirconia	0.69	10.00	51.8
(12) RTV-560 + Mg Silicate	0.71	8.57	50.7
(13) RTV-560 + 5% Mic. Bal.	0.87	11.97	41.0
(14) RTV-560 + 5% Eccos.	0.87	12.42	41.7
(15) RTV-560 + 5% Shellac	0.65	9.50	55.3
(16) RTV-560 + 5% AAH-101-OP	0.83	10.17	43.3
(17) RTV-560 + 5% Al. Sil.	0.90	12.70	39.9
(18) RTV-560 + 5% Pot. Titanate	0.61	7.50	58.5
(19) RTV-209-127-623A	0.87	12.00	41.3
(20) RTV-209-127-623B	0.85	12.17	41.9

Sample Dimension Based on 3 lb/ft^2

TABLE 6

ABLATION RESULTS OF SCREENING FORMULATIONS IN HYPERSONIC ARC TUNNEL
($\dot{q}$ = 3.4 BTU/ft^2 sec)

Model No.	Material	Back Plate Temp. at 1200 Sec (° F)	Char Thick. (in.)	Total Degradation (in.)	Weight Loss (Grams)	Heat of Ablation q*=BTU/lb (Wt. Loss)	Heat of Degradation H_d = BTU/lb (Virgin Mat. Remaining)	Density lb/ft^3
1A	ESM 1001 P-G H/c	331	0.170	0.117	9.5	12,200	10,400	40.4
B	NASA 602 G-H/c	342	0.172	0.084	15.6	7,400	16,000	36.4
2A	RTV-560 + Phen. Micro-balloons	325	0.155	0.136	9.5	12,200	8,790	41.0
B	RTV-560 + Glass Fibers	324	0.067	0.065	5.7	20,300	17,900	42.2
3A	RTV-560 + Al. Silicate Fibers	333	0.043	-----	4.5	25,700	------	39.9
B	RTV-209-127-623B + Asb Fibers	312	0.041	0.051	3.5	33,000	22,900	41.9
4A	RTV-560 + H101 OP Asb Fibers	270	0.215	0.181	7.0	16,500	6.250	43.3
B	RTV-560 + Quartz Fibers	384	0.196	0.142	7.0	16,500	8,000	43.0
5A	RTV-209-127-623A + Asb Fibers	351	0.153	0.114	6.7	17,300	10,400	41.3
B	RTV-560 + Asb Fibers	341	0.119	0.096	5.8	19,900	12,700	40.2
6A	ESM 1001 P	278	0.126	0.165	9.4	12,300	8,250	36.0
B	NASA 182 G-H/c	272	0.301	0.244	10.6	10,900	5,100	39.4
7A	RTV-560 + Zirconia Fibers	411	0.144	0.057	7.8	14,800	16,600	51.8
B	RTV-560 + Pot. Titanate Fibers	393	0.150	0.084	14.0	8,300	9,970	58.5
8A	RTV-560 + Bone Shellac	373	0.118	0.041	9.6	12,000	21,600	55.3
B	ESM 1001 G-H/c	361	0.104	0.051	6.6	17,500	17,700	54.2

1. Filler concentration is 5 percent in all cases.

2. All samples except 6A are in Phenolic Glass Honeycomb Matrix.

TABLE 6

ABLATION RESULTS OF SCREENING FORMULATIONS IN HYPERSONIC ARC TUNNEL (Cont.)
($\dot{q}$ = 3.4 BTU/ft^2 sec)

Model No.	Material	Back Plate Temp. at 1200 sec (°F)	Char Thick. (in.)	Total Degradation (in.)	Weight Loss (Grams)	Heat of Ablation q*=BTU/lb (Wt. Loss)	Heat of Degradation H_d = BTU/lb (Virgin Mat. Remaining)	Density lb/ft^3
9A	RTV-560 + Silica Ecco-spheres	293	0.239	0.214	11.4	10,100	5,500	41.7
B	RTV-511 + Asb	292	0.277	0.283	11.6	9,960	4,300	40.5
10A	RTV-209-127-623C + Asb Fibers	411	0.146	0.052	5.9	19,600	19,600	48.0
B	RTV-560 + Graphite Fibers	441	0.194	0.020	7.8	14,800	50,200	48.8
11A	RTV-560 + Mag. Silicate Fibers	402	0.089	0.039	7.2	16,100	24,800	50.7
B	DC 325 G-H/c	393	0.176	0.050	9.7	11,900	17,000	57.5
12A	ESM 1011 P-G-H/c	323	0.105	-----	3.1	37,300	------	36.0
B	Experimental RTV-518-692 + Asb Fibers	328	0.192	0.073	16.3	7,100	12,400	54.2

1. Filler concentration is 5 percent in all cases.

$$\overset{*}{q} = \frac{\dot{q}\,T}{M} = \frac{3.4 \times 1200 \times 454}{\text{wt. loss (gms)}} \times \frac{2.25 \times 4}{144} = \frac{115{,}600}{\text{wt. loss (gms)}}$$

$$H_d = \frac{3.4 \times 1200 \times 12}{\text{total degrad. (in. x den)}} = \frac{49{,}000}{\text{total degrad. (in. x den)}}$$

TABLE 7

ABLATION RESULTS OF SCREENING FORMULATIONS
IN NASA 2500 KW ARC JET

	Sample	Specimen Number	Unit Weight (lb/ft^2)	Time $\Delta T = 300°F$ (sec)	Average Cold-Wall Heat-Transfer Rate (BTU/ft^2 sec)	Effective Heat Capacity (Btu/lb)
I	ESM 1001 P-G-H/c	306	2.95	304	111	11,420
	NASA 602-G-H/c	309	3.02	374	109.5	13,350
	NASA 182-G-H/c	311	2.96	364	113	13,800
	ESM 1001-G-H/c	314	2.94	251	108.5	9.270
	DC 325-G-H/c	313	2.98	315	111	11,720
II	ESM 1001 P-G-H/c	307	2.98	320	126	13,510
	NASA 602-G-H/c	308	3.00	454	124	18,780
	NASA 182-G-H/c	310	2.96	403	128.5	17,500
	ESM 1001-G-H/c *	315	2.94	281	125.8	12,000
	DC 325-G-H/c	312	3.00	374	120	14,950

Group I:
4-Inch Nozzle
Mass Flow Rate = 0.35 lb/sec
Stream Composition - 0.30 lb/sec Nitrogen
0.05 lb/sec Air
Enthalpy 3300 Btu/lb
Shear Stress 0.5 lb/ft^2

Group II:
2-Inch Nozzle
Mass Flow Rate = 0.15 lb/sec
Stream Composition - 0.1275 lb/sec Nitrogen
0.0225 lb/sec Air
Enthalpy 3200 Btu/lb
Shear Stress 1.5 lb/ft^2

*Mass Flow Rate = 0.35 lb/sec
Enthalpy 2700 Btu/lb
Shear Stress 4.5 lb/ft^2

TABLE 8

FORMULATIONS SELECTED FOR ADDITIONAL TESTING

Material	TEST				
	Torch	Ablation 3 BTU	Ablation 40 BTU	NASA	Malta
1. ESM 1011 P-G-H/c-S	X		X	X	X
2. ESM 1001 P-G-H/c-S	X		X	X	X
3. NASA 602 G-H/c-S	X		X	X	X
4. ESM 1004A P-G-H/c-S	X	X	X	X	X
5. ESM 1001 P-Asb -H/c-S	X	X	X	X	X
6. NASA 602 Asb -H/c-S	X	X	X	X	X
7. ESM 1001 P-G-H/c-S /ESM 1001 P Composite	X	X	X	X	X

TABLE 9

BACKFACE TEMPERATURE RESPONSE OF CANDIDATE MATERIALS IN PROPANE TORCH TEST

Propane Torch Test 18 BTU

Time to Backface Temperature ΔT 200° F

Material	Thickness (in.)	Minutes (Avg. 2 runs)	Density lb/ft^3
1. ESM 1011 P-G-H/c-S	0.86	14.60	41.6
2. ESM 1001 P-G-H/c-S	0.82	11.00	44.0
3. NASA 602 G-H/c-S	0.93	17.25	38.7
4. ESM 1004A P-G-H/c-S	0.82	11.40	43.7
5. ESM 1001 P-Asb -H/c-S	0.72	7.00	50.0
6. NASA 602 Asb -H/c-S	0.86	11.00	39.5
7. ESM 1001 P-G-H/c-S / ESM 1001 P Composite	0.86	16.80	41.3

TABLE 10

ABLATION RESULTS OF CANDIDATE FORMULATIONS IN NASA 2500 KW ARC JET

Specimen Number	Material	Unit Weight (lb/ft^2)	Time $\Delta T = 300^oF$ sec	Average Cold-Wall Heat Transfer Rate (BTU/ft^2 sec)	Effective Heat Capacity (BTU/lb)
348	NASA 602 Asb-H/c-S	2.84	458	103	16,600
350	NASA 602 G-H/c-S	3.0	555	120	22,200
352	ESM 1011 P-G-H/c-S	3.0	383	119	15,200
354	ESM 1004A P-G-H/c-S	3.0	331	126.5	13,950
356	ESM 1001 P-G-H/c-S	2.97	325	120	13,100
358	ESM 1011 P-G-H/c-S (12% Asbestos Fiber)	2.98	369	115	14,200
360	ESM 1001 P-Asb-H/c-S	2.93	300	129.5	13,300
362	ESM 1001 P-G-H/c-S / ESM 1001 P (1/4 inch) Composite	2.76	300	119.5	13,000

2-Inch Nozzle
Mass Flow Rate = 0.15 lb/sec
Stream Composition - 0.1275 lb/sec Nitrogen
0.0225 lb/sec Air
Enthalpy 3200 BTU/lb
Shear Stress 1.5 lb/

TABLE 10

ABLATION RESULTS OF CANDIDATE FORMULATIONS IN NASA 2500 KW ARC JET (Cont)

Specimen Number	Material	Unit Weight (lb/ft^2)	Time $\Delta T = 300^oF$ sec	Average Cold-Wall Heat Transfer Rate (BTU/ft^2 sec)	Effective Heat Capacity (BTU/lb)
349	NASA 602 Asb-H/c-S	2.86	198	124.5	8,620
351	NASA 602 G-H/c-S	3.04	260	119	10,200
353	ESM 1011 P-G-H/c-S	2.98	59	128	2,530
355	ESM 1004A P-G-H/c-S	3.0	330	120.5	13,280
357	ESM 1001 P-G-H/c-S	2.98	163	120	6,560
359	ESM 1011 P-G-H/c-S (12% Asbestos Fiber)	2.98	116	120	4,670
361	ESM 1001 P-Asb-H/c-S	2.88	325	119	13,400
363	ESM 1001 P-G-H/c-S / ESM 1001 (1/4 inch) Composite	2.98	103	123	4,250

2-Inch Nozzle
Mass Flow Rate = 0.35 lb/sec
Enthalpy 2700 BTU/lb

Stream Composition - 0.30 lb/sec Nitrogen
- 0.05 lb/sec Air
Shear Stress 4.5 lb/ft^2

TABLE 11

ABLATION RESULTS OF CANDIDATE FORMULATIONS IN HYPERSONIC ARC TUNNEL

($\dot{q}$ = 3.4 BTU/ft^2 sec)

Density lb/ft^3	Material	Char Thick. Inches	Total Degrad. Inches	Wt. Loss Gms.	$\overset{*}{q}$ Wt. Loss	H_d Virgin Material
39.5	NASA 602 Asb-H/c	0.192	0.108	10.4	11,150	11,486
38.7	NASA 602 G-H/c-S	0.149	0.093	9.7	11,917	13,614
43.8	ESM 1001 P-G-H/c-S	0.062	0.050	6.5	17,784	22,374
43.7	ESM 1004A P-G-H/c-S	0.045	0.042	5.6	20,642	26,702
43.5	ESM 1001 P-G-H/c-S / ESM 1001 P (1/4 inch) Composite	0.070	0.042	6.8	17,000	26,819
50.3	ESM 1001 P-Asb-H/c-S	0.050	0.042	9.1	12,703	23,200
41.3	ESM 1011 P-Asb-H/c-S	0.099	0.063	7.4	15,621	18,838
40.7	ESM 1011 P-G-H/c-S	0.086	0.053	14.2	8,140	22,716

TABLE 12

ABLATION RESULTS OF CANDIDATE FORMULATIONS IN HYPERSONIC ARC TUNNEL

$\dot{q}$ = 40 BTU/ft^{2}sec

Density lb/ft^3	Material	Total Degradation (Dist. from Leading Edge) 1 in.	1.5 in.	2 in.	Avg. Heat of Degradation BTU/lb	Backface Temperature at 100 sec ^{o}F
39.5	NASA 602 Asb-H/c	0.199	0.181	0.084	8500	277
		0.198	0.192	0.121	7200	332
38.7	NASA 602 G-H/c	0.167	0.176	0.122	8000	270
43.7	ESM 1001 P-G-H/c-S	0.209	0.205	0.171	5600	288
44.4	ESM 1004A P-G/H/c-S	0.224	0.205	0.170	5400	342
41.0	ESM 1001 P-G-H/c-S/ ESM 1001 P (1/4 in.) Composite	0.194	0.175	0.161	6600	290
50.0	ESM 1001 P-Asb-H/c-S	0.169	0.170	0.136	6500	290
41.3	ESM 1011 P-Asb-H/c-S	0.212	0.205	0.150	6100	270
41.0	ESM 1011 P-G-H/c-S	0.228	0.208	0.171	5700	360

TABLE 13

ABLATION RESULTS OF CANDIDATE FORMULATIONS IN MALTA ROCKET ENGINE PIT #1 TEST

$\dot{q}$ = 150 BTU/ft^2 sec

No.	Density lb/ft^3	Material	Total Degradation (2.5 inches from edge of sample)	Heat of Degradation (BTU/lb)
1.	44.4	ESM 1004A P-G-H/c-S	0.137	4100
2.	41.3	ESM 1011 P-Asb-H/c-S	0.227	1900
3.	41.0	ESM 1011 P-G-H/c-S	-----	----
4.	43.7	ESM 1001 P-G-H/c-S	0.182	2700
5.	38.7	NASA 602 G-H/c	0.398	1300
6.	39.5	NASA 602Asb-H/c	0.267	1800
7.	50.0	ESM 1001 P-Asb-H/c-S	0.116	3100
8.	41.0	ESM 1001 P-G-H/c-S/ ESM 1001 P (1/4 inch) Composite	0.126	3400

NOTE: 1) Order of specimens are as installed on the wedge model

2) Heat flux at the centerline of the model was 150 BTU/ft^{2}sec

TABLE 14

ABLATION RESULTS OF FINAL CANDIDATE FORMULATIONS IN NASA 2500 KW ARC JET

Sample	Time $\Delta T = 300^{o}F$ Sec	Average Cold Wall Heat Transfer Rate BTU/ft^2sec	Effective Heat Capacity BTU/lb
NASA 602 G-H/c-S/ FSM 1001 P Comp.	240	123	9,800
NASA 602 G-H/c-S/ ESM 1001 P Comp.	236	124	9,700
ESM 1004A P	126	115	5,000
ESM 1004A P	124	123	5,300
ESM 1004B P	108	124	4,400
ESM 1004B P	110	117	4,400
	Test I		
NASA 602 G-H/c-S/ ESM 1001 P Comp.	401	121	16,200
NASA 602 G-H/c-S/ ESM 1001 P Comp.	390	116	15,200
ESM 1004A P	342	125	14,600
ESM 1004A P	343	117	13,800
ESM 1004B P	320	119	12,700
ESM 1004B P	338	114	13,200
	Test II		

Test I

2-Inch Nozzle
Mass Flow Rate - 0.35 lb/sec
Enthalpy - 2700 BTU/lb
Shear Stress -4.5 lb/ft^2
Stream Composition - 0.30 lb/sec Nitrogen
0.05 lb/sec Air

Test II

2-Inch Nozzle
Mass Flow Rate - 0.15 lb/sec
Enthalpy - 3200 BTU/lb
Shear Stress - 1.5 lb/ft^2
Stream Composition - 0.1275 lb/sec Nitrogen
0.0225 lb/sec Air

TABLE 15

TENSILE RESULTS FOR ESM 1001 P AND 1004B P

Sample Nomenclature and Temperature	Elastic Modulus, E_T, psi	Ultimate Strength, F_{TU}, psi	Strain at Failure, %
ESM 1004B P			
"Dog-bone" Specimens			
+77°F	268	69	--
	345	74	22
	456	81	20
Av.	356	75	21
-35°F	229	88	32
	258	80	34
	400	92	27
Av.	296	86	30
-130°F	723	268	45
	1043	346	22
	852	291	27
Av.	873	302	31
-280°F	2.07×10^5	1660	1.04
	2.10×10^5	1550	0.88
	1.98×10^5	1410	0.88
Av.	2.11×10^5	1540	0.93
ESM 1001 P			
"Dog-bone" Specimens			
-280°F	2.31×10^5	1400	0.61
	2.12×10^5	1510	0.86
	1.89×10^5	1600	1.02
Av.	2.11×10^5	1500	0.83
ESM 1001 P			
Thin Sheet Specimen			
6 in. x 6 in. x 0.25 in.			
+300°F	225	36.8	21

TABLE 16

TENSILE RESULTS FOR NASA 602 G-H/c-S

Temperature, °F	Elastic Modulus, E_T, psi	Ultimate Strength, F_{TU}, psi	Strain at Failure, %
+77°F	1450	37	5.0
	1760	30	2.8
	1740	39	5.3
Av.	1650	35	4.3
-35°F	1690	41	5.8
	1780	42	7.6
	1990	42	8.4
Av.	1820	42	7.3
-130°F	1.18×10^5	640	0.61
	1.19×10^5	760	0.72
	1.27×10^5	760	0.69
Av.	1.21×10^5	720	0.67
-280°F	3.34×10^5	1440	0.48
	3.68×10^5	1660	0.46
	3.35×10^5	1650	0.48
Av.	3.45×10^5	1580	0.47

TABLE 17

TENSILE-SHEAR RESULTS FOR ESM 1001 P (DOUBLE LAP SHEAR)

Temperature, °F	Ultimate Strength psi	Mode of Failure		
		% Adhesive		% Cohesive
+77°F	28.7	50	Side 1	50
		75	Side 2	25
+300°F	28.4	0		100
	28.8	0		100
	28.7	0		100
Av.	28.5			
-35°F	55.8	5		95
	46.8	5		95
	51.8	5		95
Av.	51.5			
-130°F	143.5	0		100
	167.5	0		100
	176.2	0		100
Av.	162.5			
-280°F	814	5	Side 1	95
		95	Side 2	5
	664	20	Side 1	80
		90	Side 2	10
	605	90		90
Av.	695			

NOTE: For ESM 1001 P (2-Square Inch Total Cross-Section: 0.25-Inch Nominal Thickness Per Section; Bonded to Aluminum with RTV-560)

TABLE 18

TENSILE-SHEAR RESULTS FOR ESM 1004B P (DOUBLE LAP SHEAR)

Temperature °F	Ultimate Stress psi	Mode of Failure % Adhesive		% Cohesive
RT	19.2	100		0
	31.0	95		5
	22.9	95		5
	24.4			
+300	36.3	5		95
	30.5	20	Side 1	80
		100	Side 2	0
	40.5	0		100
	35.8			
-35	54.0	40		60
	65.0	25		75
	75.7	5		95
	64.9			
-130	243	0		100
	210	0		100
	217	0		100
	223			
-280	850	95		5
	995	90		10
	975	85		15
	940			

NOTE: For ESM 1004B P (2-Square Inch Cross-Section; 0.25-Inch Nominal Thickness per Section; Bonded to Aluminum with RTV-560)

TABLE 19

TENSILE-SHEAR RESULTS FOR NASA 602 G-H/c-S (DOUBLE LAP SHEAR)

Temperature °F	Ultimate Stress psi	Mode of Failure	
		% Adhesive	% Cohesive
RT	31.5	15	85
	33.0	5	95
	32.5	10	90
	32.3		
+300	23.1	0	100
	18.3	5	95
	21.4	10	90
	20.9		
-35	37.3	5	95
	36.1	5	95
	36.0	5	95
	36.5		
-130	458	15	85
	503	5	95
	472	10	90
	478		
-280	1,360	35	65
	1,375	40	60
	1,180	25	75
	1,305		

For NASA 602 G-H/c-S (2 Square-Inch Total Cross-Section; 0.25-Inch Nominal Thickness per Section; Bonded to Aluminum with RTV-560)

TABLE 20

COMPRESSION RESULTS FOR ESM 1001 P AND 1004B P

Sample Nomenclature and Temperature		Elastic Modulus, E_C, psi	Stress at 25% Deflection, psi
ESM 1004B P			
1 in. x 1 in. x 1 in. Samples			
	+77°F	100	23
		97	22
		90	25
		108	24
	Av.	99	24
	+130°F	76	17
		92	21
		91	20
		94	22
	Av.	88	20
	+280°F	80	18
		80	18
		70	17
	Av.	77	18
ESM 1001 P			
1 in. x 1 in. x 1 in. Samples			
	+77°F	70	19
		84	21
		54	14
		65	15
	Av.	68	17
	+130°F	102	22
		95	22
		118	26
		105	25
	Av.	105	24
	+280°F	124	27
		95	23
		120	27
		115	24
	Av.	114	25

TABLE 20

COMPRESSION RESULTS FOR ESM 1001 P AND 1004B P (Cont)

Sample Nomenclature and Temperature	Elastic Modulus, E_C, psi	Stress at 20% Deflection, psi
ESM 1001 P Thin Sheet; 6 in. x 6 in. x 0.25 in. Samples		
-130°F	116	23
-160°F	213	43

TABLE 21

COMPRESSION RESULTS FOR NASA 602 G-H/c-S

Temperature	Elastic Modulus, E_C, psi	Ultimate Strength F_{CU}, psi	Deflection at Failure, %
+77°F	1720	108	20
	1700	112	20
	1710	108	18
	1710	110	19
+130°F	1620	96	19
	1210	94	18
	1260	94	18
	1370	95	18
+280°F	1020	80	14
	960	86	15
	960	86	15
	980	84	15

NOTE: (Split Honeycomb Reinforcement; 1 in x 1 in. x 1 in. Samples; Loaded Perpendicular to Tape Direction)

TABLE 22

THERMOGRAVIMETRIC ANALYSIS OF FINAL CANDIDATE MATERIALS

Temperature °C	Fraction of Material Remaining		
	ESM 1001 P	ESM 1004B P	NASA 602
100	1.00	1.00	1.00
200	1.00	0.99	1.00
300	0.98	0.97	0.97
350	0.97	0.96	0.95
400	0.95	0.94	0.82
450	0.91	0.91	0.40
500	0.83	0.84	0.29
600	0.55	0.56	0.28
700	0.45	0.49	0.27
800	0.42	0.46	0.27
900	0.40	0.46	0.26
1000	0.40	0.45	0.26

TABLE 23

THERMAL CONDUCTIVITY OF FINAL CANDIDATE MATERIALS

Material	Density (lb/ft^3)	Temp. (^oF)	Thermal Conductivity (BTU/ft sec ^oF)
ESM 1001 P	37.7	100	2.45×10^{-5}
		200	2.32×10^{-5}
		300	2.20×10^{-5}
		400	2.08×10^{-5}
		500	1.90×10^{-5}
		600	1.82×10^{-5}
ESM 1004B P	39.0	100	3.00×10^{-5}
		200	2.88×10^{-5}
		300	2.78×10^{-5}
		400	2.66×10^{-5}
		500	2.54×10^{-5}
NASA 602 G-H/c-S	39.5	100 to 500	2.05×10^{-5}

TABLE 24

SPECIFIC HEAT OF FINAL CANDIDATE MATERIALS

Material	Density (lb/ft^3)	Heating Rate (^oF/min.)	Temp. Range (^oF)	Specific Heat BTU/lb-^oF
ESM 1001 P	37.7	5.2	-200 to +300	0.38
			300 to 600	0.50
ESM 1004B P	39.0	3.7	-250 to +500	0.24 to 0.51
NASA 602 G-H/c-S	39.5	3.7	-200	0.11
			-100	0.36
			0 to 400	0.40

TABLE 25

Test No. 1 - MALTA ROCKET WEDGE MODEL

	Angle of Attack (degrees)	Heat Flux (Cold Wall) (btu/ft^2-sec)	Shear (lbs/ft^2)	Total Degradation* Including Char (inches)	Mass Loss* (lbs/sec)	Heat of* Degradation (btu/lb)
ESM 1001 G-H/c	0	90	10.7	0.057	0.063	1480
PN	0	90	10.7	0.027	0.042	2330
ESM 1001 G-H/c	7	461	31.2	0.148	0.131	3800
PN	7	461	31.2	0.057	0.072	6660
ESM 1001 G-H/c	11	444	32.1	0.111	0.098	4720
PN	11	444	32.1	0.056	0.070	6630
ESM 1001 G-H/c	18	690	34.8	0.157	0.174	4480
PN	18	690	34.8	0.073	0.149	6150
ESM 1001 A G-H/c	0	112	10.6	0.025	0.040	5200
PN	0	112	10.6	0.045	0.074	2000
ESM 1001 A G-H/c	9 A **	374	35.3	0.059	0.075	5720
PN	9 A **	374	35.3	0.056	0.070	5400
ESM 1001 A G-H/c	9 B **	641	49.7	0.085	0.108	5040
PN	9 B **	641	49.7	0.074	0.093	8190
ESM 1001 A G-H/c	18	845	41.4	0.089	0.144	6020
PN	18	845	41.4	0.080	0.127	6810
ESM 1001 A G-H/c	27	1075	72.2	0.175	0.283	4040
PN	27	1075	72.2	0.093	0.147	7500

*Average values of three stations.

Density - ESM 1001 G-H/c 45 lb/ft^3
ESM 1001 A G-H/c 57 lb/ft^3
PN 73 lb/ft^3

**A/B sides of 9^o wedge model

TABLE 26

Test No. 2 - MALTA ROCKET WEDGE MODEL

	Angle of Attack (degrees)	Heat Flux (Cold Wall) (btu/ft^2-sec)	Shear (lb/ft^2)	Total Degradation Including Char (inches)	Mass Loss (lb/sec)	Heat of Degradation (btu/lb)
ESM #2*	10	168	10	0.074	0.044	3700
PN	10	168	10	0.086	0.058	2810
ESM #2	20	775	37	0.143	0.086	8520
PN	20	775	37	0.145	0.099	7400
ESM #2	30	1050	43	0.265	0.148	7090
PN	30	1050	43	0.238	0.150	7000
ESM #2	45	1400	42	0.418	0.337	3890
PN	45	1400	42	0.207	0.189	6930

* Shape Stable Material No. 2

Density	ESM No. 2	68 lb/ft^3
	PN	73 lb/ft^3

TABLE 27

ABLATION HEATING RATE IN SIMULATION ABLATION TESTS

	$\dot{q}$ = BTU/ft-sec cold wall		Time[1] Integrated Flux - BTU		Shear lb/ft^2		Pressure lb/ft^2	
	Test	Flight	Test	Flight	Test	Flight	Test	Flight
Leading Edge	80-100	105	50,000	50,000	-	-	144	133
Lower Surface	20-40	15	15,000	14,000	0.25	0.23	80	20

(1) Test time was 500 seconds and was adjusted to match the time integrated flux on the leading edge.

TABLE 28

ABLATION TEST RESULTS OF SIMULATION ABLATION TESTS - LEADING EDGE

Material	Station	Heat Flux (BTU/ft^2-sec)	Char Depth (in.)	Total Degradation (in.)	Heat of Degradation (BTU/lb)	Surface Temp. (^{o}K)	Backface Temp. (^{o}F at 500 sec)
1	1	11	0.068	0.110	16,400		--
1	2	25	0.200	0.212	19,300		225
1	3	45	0.428	0.438	16,800		--
1	Stag. Pt.	88	0.766	0.735	19,600	2050	225
2	1	11	0.096	0.004	------		--
2	2	25	0.268	0.196	11,100		384
2	3	45	0.540	0.483	8,100		--
2	Stag. Pt.	88	0.876	0.809	9,500	2040	444
3	1	11	0.135	0.125	11,100		--
3	2	25	0.281	0.280	11,200		205
3	3	45	0.440	0.431	13,100		--
3	Stag. Pt.	88	0.646	0.714	15,500	2020	205

TABLE 29

ABLATION RESULTS OF COMPOSITE SYSTEMS IN PROPANE TORCH TEST (20-22 BTU)

Time to Backface Temp. - $\Delta T = 200^{\circ}F$.

Sample	Minutes	Density lb/ft^3
#1	16.3	32.5
#2	2.2	69.6
#3 (Composite)	4.2	69.6/27
#4 (Composite)	3.3	69.6/43

Sample Dimension Based on 3 lb/ft^2

TABLE 30

ABLATION TEST RESULTS OF SIMULATION ABLATION TESTS OF COMPOSITE SAMPLES

Material	Station	Heat Flux (BTU/ft^{2}sec)	Char Depth (in.)	Total Degradation (in.)	Heat of Degradation (BTU/lb)	Surface Temperature (^{o}K)	Backface Temp. (^{o}F at 500 sec)
Composite	1	11	0.099	0.080	11950	—	194
Material	2	25	0.221	0.206	10550		
#3	3	45	0.439	0.386	10100		
	Stag. Pt.	88	0.778	0.746	10250		204
Shape	1	11	0.096	0.004	—	2040	384
Stable	2	25	0.268	0.196	11100		
Material	3	45	0.540	0.483	8100		
#2	Stag. Pt.	88	0.876	0.809	9500		444

TABLE 31

DOUBLE LAP SHEAR RESULTS ON ESM SHIELD FASTENING TECHNIQUES

Sample No.	Temp. (°F)	Ultimate Stress (lb)	Type of Failure
A4	75	17	Failure in Loop and Pile
A1	150	15	"
A2	200	11	"
A3	250	8.6	"
B7	75	11.5	Cohesive failure to Aluminum at the perforations
B8	150	20	"
B9	200	13.6	"
B10	250	13.7	"
C13	75	10	Adhesive failure to Aluminum centerpiece. Fastening did not fail.
C15	150	26	"
C18	200	26	"
C14	250	34	"

6. GLOSSARY

GLOSSARY

I. SYMBOLS AND ABBREVIATIONS

B.E.	Base Elastomer
H/c	Honeycomb
Asb	Asbestos
G	(Phenolic)-Glass
S	Split
RT	Room Temperature
RTV	Room Temperature Vulcanizing
LTV	Low Temperature Vulcanizing
ESM	Elastomeric Shield Material
TC	Thermocouple
UNS	Unsupported
Comp.	Composite
P	Phenyl
PN	Phenolic Nylon

$\dot{q}$ = heat flux = BTU/ft^2 sec

H_d = heat of degradation = BTU/lb $\quad H_d = \dfrac{\dot{q} \times \text{Time}}{\text{Mass}}$

Heat of degradation is based on the amount of virgin material degraded and for reference purposes uses measured cold wall fluxes.

$\overset{*}{q}$ = heat of ablation = BTU/lb $\quad \overset{*}{q} = \dfrac{\dot{q} \times \text{Time}}{\text{Mass}}$

Heat of ablation is based on the weight of material lost in the ablation process and is calculated from cold wall heat fluxes.

h_{eff} = effective heat capacity = BTU/lb.

$$h_{eff.} = \frac{\dot{q} \times \Delta t}{\text{unit wt. (lb/ft}^2)}$$

Δt = time for back surface temperature rise of 300^{o}F

Effective heat capacity is based on the amount of thermal energy a pound of material can accommodate before experiencing a back surface temperature rise of 300^{o}F and is calculated from cold wall heat fluxes.

II. FORMULATIONS

Formulation	Resin	Filler
ESM 1001	RTV-60	4.3% asbestos 0.8% glass
ESM 1001 P	RTV-560	4.3% asbestos 0.8% glass
ESM 1011 P	RTV-511	4.3% asbestos 0.8% glass
ESM 1004A P	RTV-560	12.0% aluminum silicate
ESM 1004B P	RTV-560	6.0% aluminum silicate 3.0% asbestos 0.5% glass
NASA 602	LTV-602	10.0% phenolic microballoons 15.0% silica eccospheres
NASA 182	Sylgard 182	10.0% phenolic microballoons 15.0% silica eccospheres
DC 325	DC 325	as purchased

All formulations which contain a "P" indicate the use of the phenyl silicone base resin system. If the formulation is also designated "-G-H/c", the resin is in a phenolic-glass honeycomb matrix; "-Asb-H/c", the asbestos honeycomb matrix; and "-S" in the split honeycomb supporting matrix. Without the "H/c" or "S", the material is the free foam (unsupported) version. The letters "A" and "B" after the numerical designation indicate a change in basic filler concentration. Thus a formulation designated ESM 1004A P-Asb-H/c-S, is the foamed RTV-560 base resin containing 12 percent aluminum silicate fibers in a split, asbestos honeycomb matrix.

III. MATERIALS

A. Resins

(1) LTV-602 - Silicone Potting Compound, General Electric, Waterford, New York

(2) Sylgard 182 - Dow Corning Corp., Michigan

(3) DC 325 - Silicone, Dow Corning Corp., Michigan

(4) RTV-209-127-623A - Experimental Silicone, General Electric, Waterford, New York

(5) RTV-209-127-623B - Experimental Silicone, General Electric, Waterford, New York

(6) RTV-518-1692 - Experimental Silicone, General Electric, Waterford, New York

(7) RTV-560 - General Electric, Waterford, New York

(8) RTV-60 - General Electric, Waterford, New York

(9) RTV-511 - General Electric, Waterford, New York

B. Fillers

(1) Phenolic Microballoons - BJO-0930, Union Carbide Corp.

(2) Eccospheres Si, Emerson & Cuming, Philadelphia, Pa.

(3) Bone Shellac (pulverized), Carroll Limited Inc., Philadelphia, Pa.

(4) Quartz Fibers (Micro-quartz Bulk Fiber), Johns Manville Corp.

(5) Potassium Titanate Powder, National Lead Co.

(6) Graphite Fibers WFA, National Carbon Co.

(7) Aluminum Silicate - Spun Refractory Fiber, Johns Manville Corp.

(8) Asbestos Fiber - Acid Leached H-101-OP, American Asbestos Co.

(9) Asbestos Fiber - 7RF-1, Johns Manville Corp.

(10) Glass Fiber - 701 Cationic Milled Fibers 1/4-Inch, Johns Manville Corp.

(11) Zirconia Powder - H.I. Thompson Co., California

(12) Magnesium Silicate Powder - Mallinkrodt Chemical Works, St. Louis, Mo.

C. Reinforcements

(1) Phenolic Glass Honeycomb - HRP-1/4 GF-12-5.50, Hexcel Products, Inc., Havre de Grace, Md.

(2) Asbestos Honeycomb - HRV-1/4-ASB-5.60, Hexcel Products, Inc., Havre de Grace, Md.

(3) Owens Corning No. 116 Fiberglass - Volan Finish

D. Adhesives (other than base elastomers)

(1) HT-424 - Film Adhesive - Bloomingdale Rubber Corp., Md.